On Growth and Form and Patterning of *Drosophila* Wing Imaginal Discs

Dissertation

zur

Erlangung der naturwissenschaftlichen Doktorwürde

(Dr. sc. nat.)

vorgelegt der

Mathematisch-naturwissenschaftlichen Fakultät

der

Universität Zürich

von

Ulrike Nienhaus

aus

Deutschland

Promotionskomitee

PD Dr. Christof Aegerter (Vorsitz)

Prof. Dr. Konrad Basler

Zürich, 2013

Abstract

What determines the final size and shape of a tissue? In order to answer this question, model tissues like the wing imaginal disc of *Drosophila melanogaster*, which was used in this thesis, are analyzed. In the wing disc, factors such as gene expression patterns, cell shape changes and oriented cell divisions have been shown to play a part in the process of morphogenesis. In this thesis, a role for external mechanical forces in wing disc morphogenesis is explored using a novel method of in-vivo imaging. Several sources of mechanical stress, which act upon the wing disc at different times during development, are introduced. Evidence is presented that these sources of external mechanical stress play a role in the basic patterning and growth of the wing disc.

Zusammenfassung

Was bestimmt die Grösse und Form eines Organs? Um diese Frage zu beantworten werden Modellsysteme, wie die Flügelimaginalscheibe von *Drosophila melanogaster*, die in dieser Arbeit verwendet wurde, analysiert. In der Flügelscheibe wurde gezeigt, dass Faktoren wie Genexpressionsmuster, Zellformänderungen und gerichtete Zellteilung jeweils einen Teil zur Morphogenese beitragen. In dieser Arbeit wird eine Rolle für externe mechanische Kräfte in der Morphogenese der Flügelscheibe erforscht, mit Hilfe einer neuen Methode des 'In-vivo Imagings'. Einige Quellen externer mechanischer Kräfte, welche zu verschiedenen Zeiten während der Entwicklung auf die Flügelscheibe wirken, werden vorgestellt. Hinweise, dass diese Quellen externer mechanischer Kräfte eine Rolle in der Musterbildung und dem Wachstum der Flügelscheibe spielen, werden aufgezeigt.

Contents

1 Introduction

One of the most intriguing questions in developmental biology today asks what determines the final shape and size of a tissue. In the search for an answer, model tissues such as the wing imaginal disc of *Drosophila melanogaster* are used to study the interplay between patterning, growth and morphogenesis.

The wing imaginal disc is a tissue which constitutes the larval precursor of the adult *Drosophila* wing. In the second half of the 20th century it was discovered that this tissue is divided into different compartments, each of which is defined by the expression of a unique combination of genes and acts as a unit of growth control [1, 2]. In order to understand how and why compartments form, developmental biology has to date rested its main focus upon revealing the genes and signaling pathways which underlie wing disc patterning and growth. Although great progress has been made using this approach, a 'true understanding' of the process of morphogenesis remains elusive.

As the world of science becomes ever better connected and the boundaries between the different disciplines blur, interdisciplinary work is gaining in importance. In this context, a new approach to grasping the relationship between tissue patterning, growth and morphogenesis incorporates fundamental principles of physics, such as mechanical forces, into models of biological tissues. In recent times, mechanical forces, in addition to patterning and growth, have been shown to play a role in the morphogenesis of different organisms, such as *Drosophila*, *C. elegans* and zebrafish [3, 4, 5]. Models incorporating the idea of internal mechanical forces have also been proposed for the wing disc and have recently been supported by experimental data [6, 7, 8, 9].

What determines the final size and shape of a tissue? Although factors such as gene expression patterns, cell shapes and sizes, mitotic behavior and internal mechanical forces all play important roles, a simple list does not do the intricacy of the problem justice - not only do all of these factors change spatiotemporally, they are also complexly interlinked. Using a method of in-vivo imaging devel-

oped here, a further factor was recently indicated to be relevant to wing imaginal disc morphogenesis: external mechanical forces which act upon the wing disc in vivo. In this thesis, a role for such forces in wing disc patterning, growth and morphology, especially during the late second and early third instars, is explored. Such forces are, in all likelihood, not specific to wing disc development, but rather a basic component of general tissue morphogenesis, so that it may be possible to transfer the insight gained here to other tissues.

The theoretical background for this thesis is outlined in the following chapter. The first section is a short description of wing disc growth in terms of shape and cell numbers. In the second section, the basic patterning of the wing disc is discussed. The chain of ideas and experiments which led to the currently accepted model of wing disc patterning in respect to compartment formation is outlined. How mitotic orientations shape the wing disc as well as a possible role for mechanical forces in wing disc development are illustrated in the third and fourth sections.

The third chapter describes the experimental techniques used. A short introduction into confocal microscopy as well as the method of in-vivo imaging is given. Wing disc manipulation techniques are touched upon and the fly stocks which were utilized are introduced.

The processing of the data is described in the fourth chapter. The programs, methods and formulas used are introduced.

In the fifth chapter, the results of the experimental work are presented. Several parameters of wing disc growth were assessed as well as the development of wing disc patterning, especially in relation to the formation of the compartment boundaries. Possible sources of external stress are also pointed out.

The experimental results are discussed in separate sections concerning wing disc growth, patterning and the observed sources of external stresses in the first part of the sixth chapter. An attempt to unify the results is made in the latter part

of the chapter before a short outlook on possible future work is given in the final chapter.

2 Theoretical Background

The wing imaginal disc is a tissue, which is set aside during the embryonic stage of *Drosophila* development, destined to become the adult fly's wing and mesonotum [10, p. 358], [11].

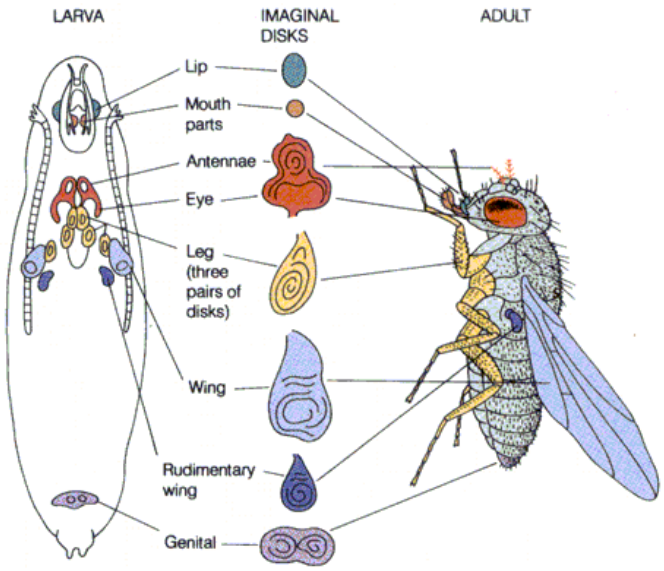

Figure 1: Overview of the imaginal discs of *Drosophila* adapted from [12].

Upon hatching, a larva goes through three larval stages separated by molts [10, p. 49] during which the wing disc becomes patterned and grows to reach a characteristic, as well as disc-autonomous, size and shape [13]. By the end of the third instar, the wing disc is made up of two distinct cell layers, the peripodial membrane and the disc proper. It is also divided into three cell lineages which will become the future notum, hinge and wing, as well as into four compartments, divided by the anterior-posterior(AP) and dorsal-ventral(DV) compartment boundaries (see Fig. 2).

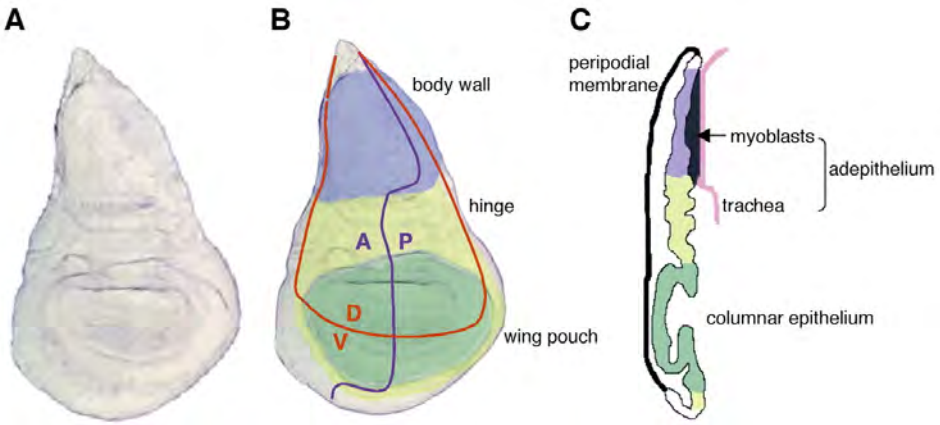

Figure 2: The wing imaginal disc. A: Morphology. B: Fate map showing the wing pouch, hinge and notum (body wall) as well as the AP and DV compartment boundaries. C: Side view showing the peripodial membrane and the disc proper (columnar epithelium). Adapted from [14].

In the following sections, growth of the wing disc as well as patterning of the disc proper will be described, especially in respect to compartment formation. Factors which play a part in determining the wing disc's final shape and the role of mechanical forces in wing disc development will be discussed as well.

2.1 Wing Disc Growth

The wing imaginal disc is formed during embryogenesis as an invagination of the embryonic ectoderm [10, p. 350] as early as 9-10 hours after egg laying (AEL) [15]. In the newly-hatched larva it appears as a hollow oval sac [16], consisting of 20-30 [15] cells and measuring about 12 µm by 6 µm [16], which is connected to the larval epidermis by the so-called peripodial stalk [17]. In the ensuing larval stages, called instars, the wing disc grows to its characteristic size and shape [13], thereby integrating cell proliferation and cell shape changes.

During the greater part of the first larval instar the cells of the wing disc grow without dividing, increasing their volumes six-fold before mitosis resumes at about 15 hours after hatching. At the same time the cells become flatter and elongated resulting in an elongation of the wing disc along the anterior-posterior axis [16].

In the second larval instar cell numbers increase at a rapid rate [13], accompanied by a decrease in cell volume [16] as well as considerable changes in cell shape: while all the cells of the first instar wing disc are cuboidal, they form two distinguishable layers, the disc proper and the peripodial membrane [16], in the second instar. The disc proper forms at around 60 hours AEL when the cells on one side of the disc become columnar, a process which has been shown to be driven by Dpp-signaling [18]. Slightly later, at about 72 hours AEL, the cells on the other side of the disc become squamous and form the peripodial membrane which may play a role in wing disc patterning [19, 20].

The cells of the wing disc continue to divide at a high rate until the middle of the third larval instar when proliferation rates begin to decrease. They steadily decrease throughout the latter half of the third instar until growth ceases when the wing disc has reached its final size of 30-50,000 cells [13, 21]. Throughout the entire third instar, cell volumes continuously decrease as well [16, 22].

Although overall wing disc growth, in terms of cell numbers, may be described as asymmetrically sigmoid [13], a closer look shows that different regions of the wing disc do not, in fact, always grow at the same rate. This was recognized in 1970 when Bryant saw that despite the fact that the number of mesonotum cells makes up about one third of the total number of cells in the wing disc until the end of the second larval instar, this number decreases to a value of only one sixth during the third instar, indicating that the mesonotum grows more slowly at this stage [11]. Other examples of non-uniform growth include higher proliferation rates in cells of the posterior compartment of the wing between 36 and 60 hours AEL [23], a zone of non-proliferating cells which forms at the future wing margin around the middle of the third larval instar [24] and lower cell doubling times in the hinge in comparison to the wing pouch at around 48 hours and 115 hours AEL [25].

Some of these inhomogeneities have been linked to patterning events [26], indicating that patterning controls growth. An overview over the basic patterning of the wing disc is given in the next section with a special focus on boundary formation.

2.2 Wing Disc Patterning

Patterning in the most general sense successively divides a tissue initially made up of identical cells into ever smaller regions, each containing cells of a different fate. One of the first steps in the patterning of the wing imaginal disc is compartment formation, whereby the tissue is divided into two compartments by the permanent activation of a selector gene which is expressed in only one of the two compartments. The different cell lineages then interact along the compartment boundary, leading to the induction of morphogens which regulate the further patterning and growth of the tissue [27].

The next chapter will look at the basic patterning of the wing imaginal disc by discussing the formation of the anterior-posterior(AP) and dorsal-ventral(DV) compartment boundaries as well as the wing-notum(WN) boundary in detail. This will be done in a historical fashion leading from the first experiments which studied cell lineage patterns in the wing to what is known today.

2.2.1 Boundaries in general and the AP compartment boundary

Cell lineage patterns in the wing and mesonotum of *Drosophila* were originally studied in the late 1960's using x-ray induced somatic crossing over [11, 28, 29, 30], a method which utilizes flies that are genetically designed such that an event of mitotic recombination leads to one cell which is phenotypically different. In this way, a random cell can be genetically marked with a non-interfering marker during the embryonic or larval stage. Since this marker is then inherited by all the daughter cells of the marked cell, information about mitotic behavior can be obtained [31]. Using this method, it was discovered that, in the wing, descendent cells remain coherent, forming so-called clones. The size and number of such clones is dependent on the developmental time point of irradiation, with earlier irradiation leading to fewer, larger clones [11, 32]. The shapes of the clones were generally found to differ, establishing that cell fates are not predetermined [32]. In the wing, for example, clones tend to form longitudinal stripes and yet clones found in the same region of different wings are not identical [11, 32].

A significant discovery made at the time was that certain boundaries exist which clones do not cross if they are induced after the formation of the respective boundary has taken place [11, 33]. This led to the idea of compartments [33], regions of the wing which were originally defined by lineage restrictions [34] before the definition was expanded to include that compartments are controlled by certain unique combinations of activated genes [1] which make the cells of one compartment fundamentally different from those of another.

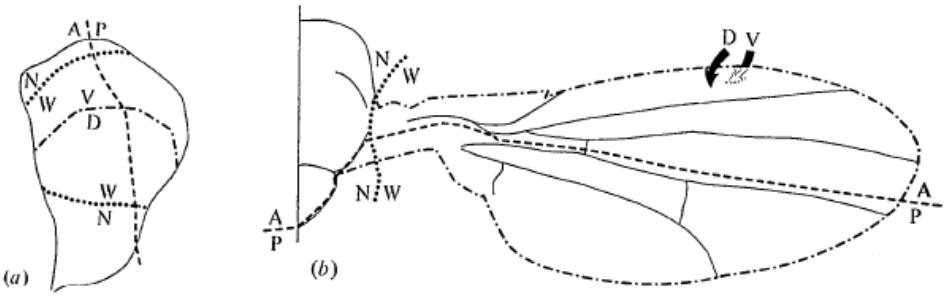

Figure 3: Boundaries in the A: wing disc. B: adult wing [35].

To learn more about compartment boundaries, the so-called Minute technique was used in the 1970's [2, 36]. This technique uses flies that are heterozygous for dominant lethal mutations (Minutes) which lead to decreased developmental rates. Irradiation and the resulting mitotic recombination results in homozygous wild-type, and thus faster-dividing, cells which can form larger clones in the slower growing organism, thereby better defining compartment boundaries [2]. Using this technique, it was found that the so-called anterior-posterior boundary, which divides the wing into an anterior and a posterior compartment, is present from at least the first larval instar on [36].

According to the compartment hypothesis, the division of the wing into an anterior and a posterior compartment is maintained by a selector gene which is activated in only one of the two compartments [1]. It was discovered that the gene *engrailed* defines the posterior compartment since it is indispensable to its normal development - *engrailed* expression is needed during the entire larval instar to keep the compartment boundary straight and positioned correctly. This has been

proposed to be due to a difference in adhesive properties between the cells of the two compartments, which causes them to minimize their area of contact [23, 37].

Besides the AP boundary, two further boundaries were seen if clones were induced at the end of the first larval instar [11, 33]. At this point in development, clones could no longer cross from the the ventral to the dorsal wing surface, defining the DV compartment boundary, or from the dorsal wing surface to the mesonotum, defining the NW boundary, though it was not clear which restriction was established first [11, 36].

Using the Minute technique, it was also found that despite the higher division rate of the wild-type cells, wing size and shape remained constant [2]. This suggests that compartments act as units of growth, indicating a role for compartments in growth control.

Up to the early 1980's, clones were studied solely in the adult wing, limited by the available genetic markers [38]. Results from the wing were transfered to the wing disc with the help of so-called fate mapping experiments. In such experiments defined fragments of wing discs were implanted into late third instar larvae, where they differentiated during metamorphosis, forming recognizable structures of the adult wing. In this way, each region of the wing could be assigned to the according region in the wing disc, defining a fate map [39] .

In 1981, a marker was discovered which allowed clonal analysis directly in the wing imaginal disc [41]. Using this new genetic marker, it was confirmed that, as in the adult wing, clones in the wing disc are restricted to certain compartments. The location of the anterior-posterior boundary could also be defined more exactly than in the fate mapping experiments. It was seen that a line of tissue belonging to the posterior compartment runs down along the posterior side of the notum (see Fig. 4). The AP boundary was thus not entirely straight but featured a kink, indicating that factors other than cell affinities must play a role in its establishment [38].

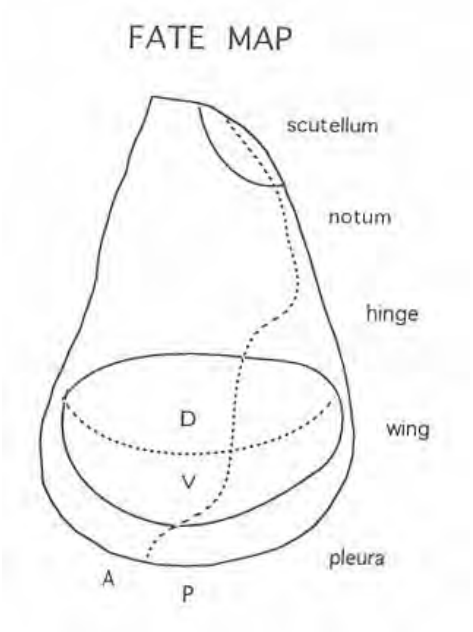

Figure 4: Fate map showing the kink in the AP boundary [40].

In subsequent decades, a lot of effort went into understanding which genes and signaling pathways play a role in the establishment of the compartment boundaries, aided by new methods such as antibody staining [42] and fluorescent markers [43]. It was thus found that the AP boundary of the wing disc is established during embryogenesis, about one to two cell divisions after the blastoderm stage [44, 45]. AP patterning in the wing disc is hence a consequence of AP patterning in the embryo, which begins during oogenesis with the maternal effect genes that define the polarity of the developing organism. When the egg is fertilized, the proteins encoded by the maternal effect genes are translated and form concentration gradients, thus defining a coordinate system in the embryo, in respect to which other genes are sequentially activated at certain threshold levels. This gene cascade, which patterns the embryo, ranges from the gap genes over the pair-rule genes to the segment polarity genes, one of which is *engrailed*. In the embryo, *engrailed* is expressed in the anterior part of each embryonic parasegment,

corresponding to the posterior part of the larval and adult segments. The wing disc originates in the T2 segment [46] and is divided by a parasegment boundary. This is why *engrailed* is expressed in its posterior compartment (see Fig. 5) [10, ch. 5/p. 353].

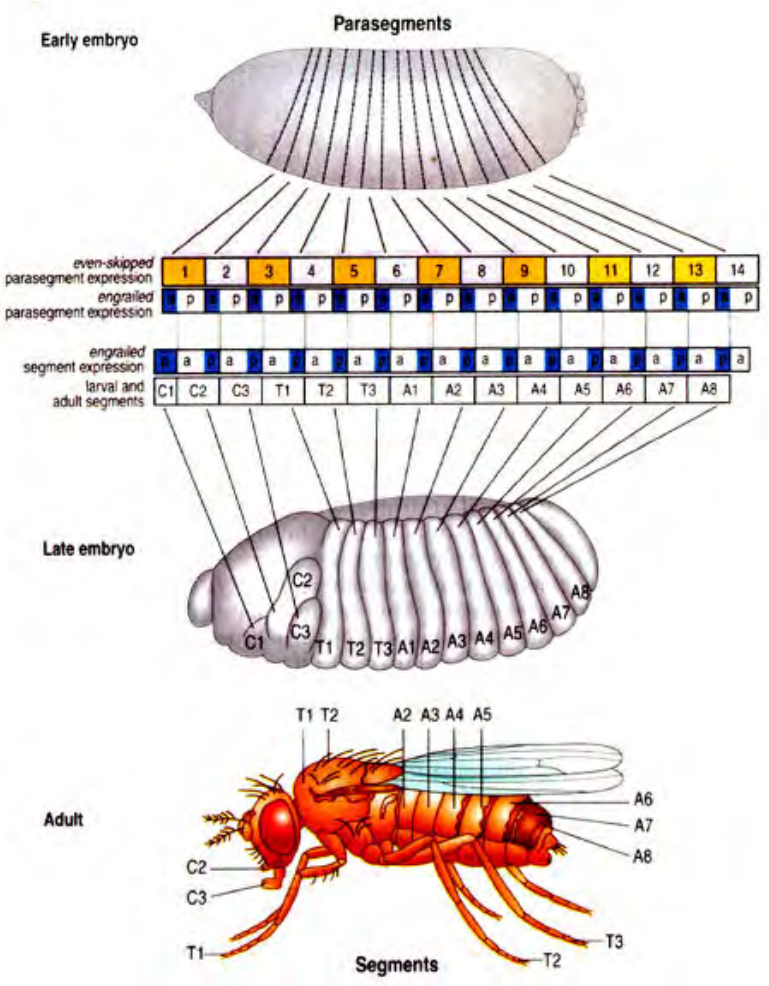

Figure 5: *Engrailed* expression in embryonic parasegments and larval/adult segments [47], [10, p. 166].

The AP compartment boundary is stabilized in the basic manner mentioned above. Cells in the posterior compartment express the selector gene *engrailed*(*en*) as well as a segment polarity gene called *hedgehog*(*hh*). The Hedgehog protein, which only the anterior en^- cells can respond to, acts as a short-range inducer, diffusing only several cell diameters into the anterior compartment, where it effects the expression of the gene *decapentaplegic*(*dpp*). The Dpp protein, which is a growth factor [49], acts as a long-range morphogen [50], forming a gradient which plays a fundamental role in the further patterning and growth of the wing disc [10, p. 351], [51] (see Fig. 6).

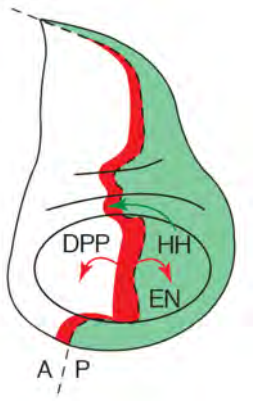

Figure 6: Signaling at the AP compartment boundary, adapted from [48].

2.2.2 The DV compartment boundary

The other compartment boundary of the wing imaginal disc is the dorsal-ventral boundary. It is defined by the selector gene *apterous* [40, 52, 53], which is first expressed in the future dorsal compartment in the late first instar [54]. Signaling at the DV boundary is shown in Fig. 7. The particulars are explained further down.

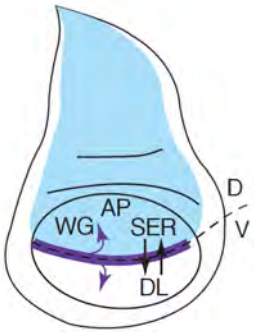

Figure 7: Signaling at the DV compartment boundary, adapted from [48].

That *apterous* is a likely candidate for the selector gene of the dorsal compartment was first indicated by experiments using genetic mosaics in the early 1990's, in which the boundaries of induced clones were compared to the boundary of the *apterous*-expressing area. These experiments showed that dorsal as well as ventral clones respected the boundary of *apterous* expression. It was also discovered that *apterous* is required throughout wing disc development for the specification of dorsal cell fate: when ap^- clones were induced in the dorsal compartment any time during larval development, the cells in the clones cell-autonomously took on a ventral identity, while loss of *apterous* function from ventral cells showed no effect [40]. Also, when *apterous* function was lost from dorsal cells after the dorsal-ventral boundary had formed, they sorted into the ventral compartment [52], again indicating that *apterous* specifies dorsal identity. Furthermore, it was seen that ectopic wing margins formed where *apterous*-expressing cells came into contact with ap^- clones, indicating that the interaction of dorsal and ventral cells leads to the formation of the wing margin [40], and that *apterous* regulates PS integrin expression [52] in the larval stage [55], ensuring that the dorsal and ventral surfaces of the wing later adhere to each other [55, 56].

The experimental results above indicate that *apterous* is not only required to specify dorsal cell fate and maintain the DV lineage restriction, it also plays a role in wing disc patterning by regulating the expression of downstream genes [40, 52], which explains why the loss of *apterous* expression leads to the loss of the entire wing despite the fact that *apterous* is only expressed in the dorsal wing pouch [53]. These results imply that *apterous* is indeed the selector gene for the formation of the dorsal and ventral compartments [52].

There is considerable debate over the exact point in time of the establishment of the DV boundary as a lineage restriction. The early work of Bryant and Garcia-Bellido et al. indicated that the boundary is formed between the mid-first and mid-second instars [11, 32]. Considering the nature of the method of x-ray induced somatic crossing over and the fact that these studies, being done before the employment of the Minute technique, only looked at small clones and sample sizes, these results are not necessarily very reliable. Using Minute mutants and allowing for the ensuing delay in development, especially after the second instar

[57], indicates that the DV boundary is not established as a lineage restriction until after the second instar, possibly as late as the middle of the third instar [34, 36, 58]. The fact that the DV boundary does not become smooth until the middle of the third instar when bond tension has been shown to increase may also support this idea [59, 60].

The patterning of the DV boundary is more complex than the patterning of the AP boundary, a fact which has been attributed to the fact that the two compartments need be identical in size and shape to form a functioning wing [48]. The establishment of the DV organizer will be described in the next few paragraphs.

Around the turn of the millennium, Vein/Epidermal Growth Factor Receptor (Vn/EGFR) signaling was shown to be significant to the establishment of both the DV boundary and the NW boundary in that it is required for the development of both the notum and the wing [61, 62, 63]. The gene *vein*, which encodes the molecule Vein that is permissive in the activation of EGFR signaling [63], was proposed to be restricted to the proximal region of the wing disc by distally expressed *wingless* [61], a gene that specifies ventral cell fate and is needed for wing formation [64, 65] in early wing disc development (see Fig. 8). Cavodeassi et al. could not confirm this proposition. They showed that the expression domain of *vein* did not expand distally in *wingless* mutants, but rather, that a second, distal domain of *vein* expression was formed [66]. Baonza et al. showed that EGFR signaling in the notum represses *wingless* expression in that region [67].

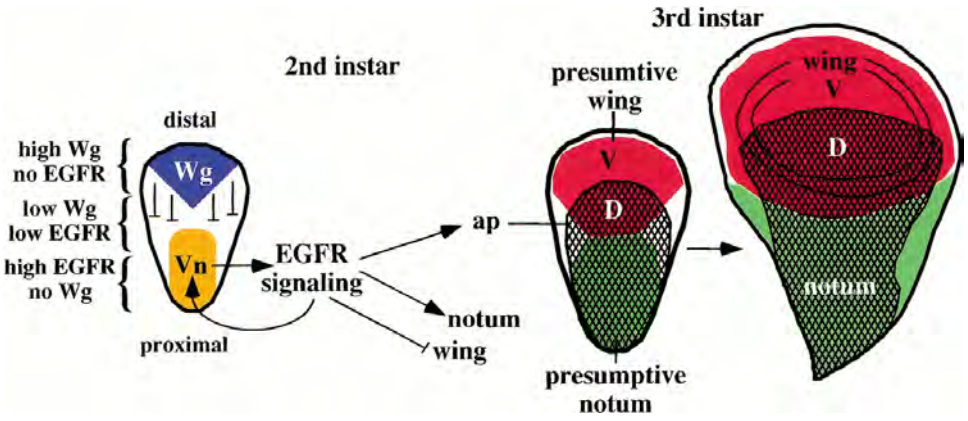

Figure 8: Model for the part EGFR signaling plays in the development of the wing and notum [61].

EGFR signaling is essential to wing formation only between the mid-first and mid-second instars, as was discovered by Wang et al. using a temperature-sensitive allele. They provide evidence that this is due to the fact that EGFR signaling acts transiently to activate *apterous* [61], a result which was confirmed by Zecca and Struhl [62], although the exact mechanism is not understood as EGFR is also active both before and after *apterous* induction [62].

Once *apterous* has been activated, cells maintain their status of *apterous* expression, independent of EGFR signaling, throughout the rest of wing disc development, passing this status on to all their descendants [62, 63]. As the *apterous*-expressing cells proliferate, some move out of the region of high EGFR expression, a prerequisite for the establishment of the future DV organizer as high levels of EGFR signaling inhibit this process [63] (see Fig. 9).

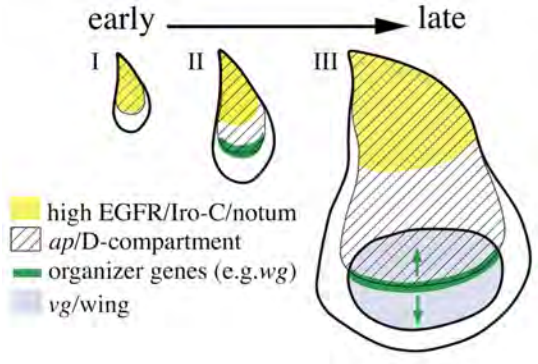

Figure 9: The role of EGFR signaling in wing disc development [63].

The establishment of the DV organizer is initiated in the second larval instar when *apterous*(*ap*) triggers a cascade of gene expression, beginning with the activation of *fringe*(*fng*) [68] in the cells of the dorsal compartment. This leads to the expression of *serrate*(*ser*) [69] in dorsal cells [70]. Serrate, in turn, activates its receptor Notch(N) [71], as well as Delta(Dl) [72] in ventral cells [73]. Delta, in turn, induces Wingless(wg) and maintains Serrate in dorsal cells [55] (see Fig. 10). Wingless and Notch are proposed to maintain the expression of *serrate* and *delta* in a positive feedback loop at the DV boundary [74, 75].

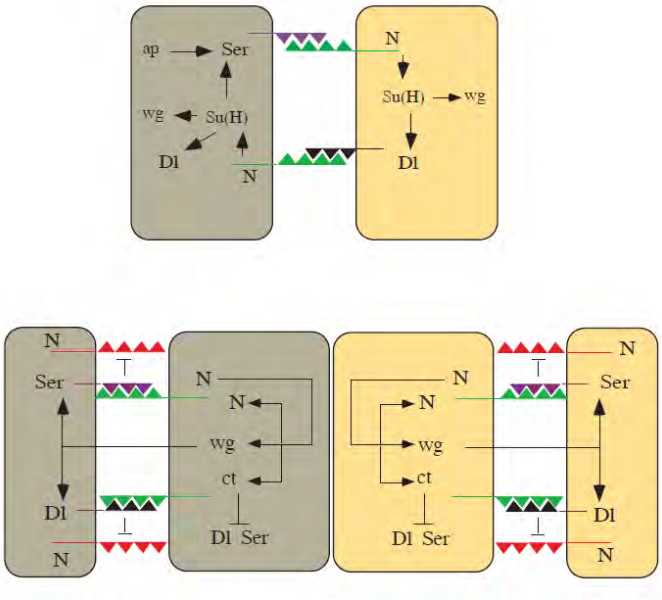

Figure 10: Model for signaling at the DV boundary. Top: early third instar, bottom: late third instar. Brown: dorsal cells, yellow: ventral cells [75].

Later in development [76], apterous induces the expression of the competitive inhibitor dLMO, which negatively regulates its activity [77], thus restricting the time during which it can maintain the asymmetric expression patterns of *serrate*, *fringe* and *delta* needed to induce the DV organizer [55]. Over the course of the first half of the third instar, apterous activity, and accordingly, the expression of apterous-dependent *serrate* and *fringe* is strongly reduced due to increasing dLMO levels, with the *serrate* expression domain gradually becoming confined to cells near the DV boundary.

By the middle of the third instar, *serrate*, *fringe* and *delta* are expressed in the symmetric apterous-independent patterns needed for normal development of the wing. Signaling at the DV boundary thus becomes independent of apterous, involving only the short-range signals Serrate and Delta, as well as the long-range signal Wingless [55, 78, 79].

2.2.3 The NW boundary

Besides activating apterous, EGFR signaling also induces the expression of the Iroquois complex (Iro-C) genes, which are specific to the notum [81], during the late first to second larval instar [54, 61, 62, 63]. Thus, EGFR signaling also plays a role in the establishment of the WN boundary.

The precise location of the WN boundary is given by the extent of Dpp signaling, which represses Iro-C expression and is found only in the distal wing disc in the second instar [66]. *Msh*, which is activated by apterous in the dorsal hinge, has also been shown to play a part [80] (see Fig. 11). Experiments with clones which could not receive Dpp showed a normal Iro-C border in the anterior compartment, as opposed to the posterior compartment where the Iro-C domain expanded distally, indicating that additional factors play a role in maintaining the NW boundary [66], especially in the anterior compartment.

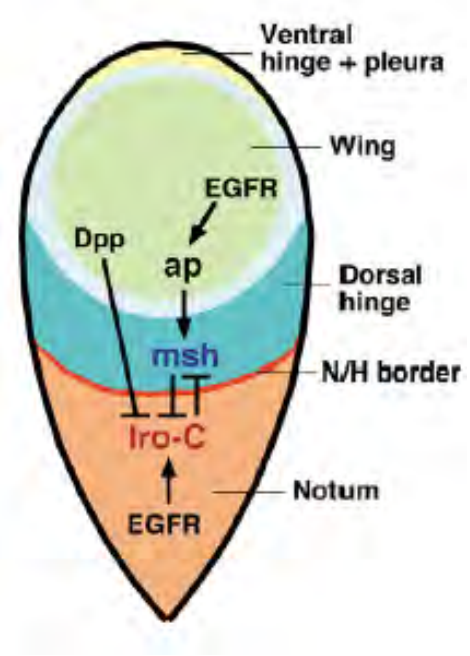

Figure 11: Second instar wing disc showing interactions that define and/or maintain the WN boundary, adapted from [80].

On a side note, EGFR signaling independently represses *wingless* expression and maintains *engrailed* expression in the posterior notum from 55 to 72 hours

AEL [67], as is shown in Fig. 12. This may be the reason why Wingless can only reprogram cells from notum to wing fate in the early second instar [65].

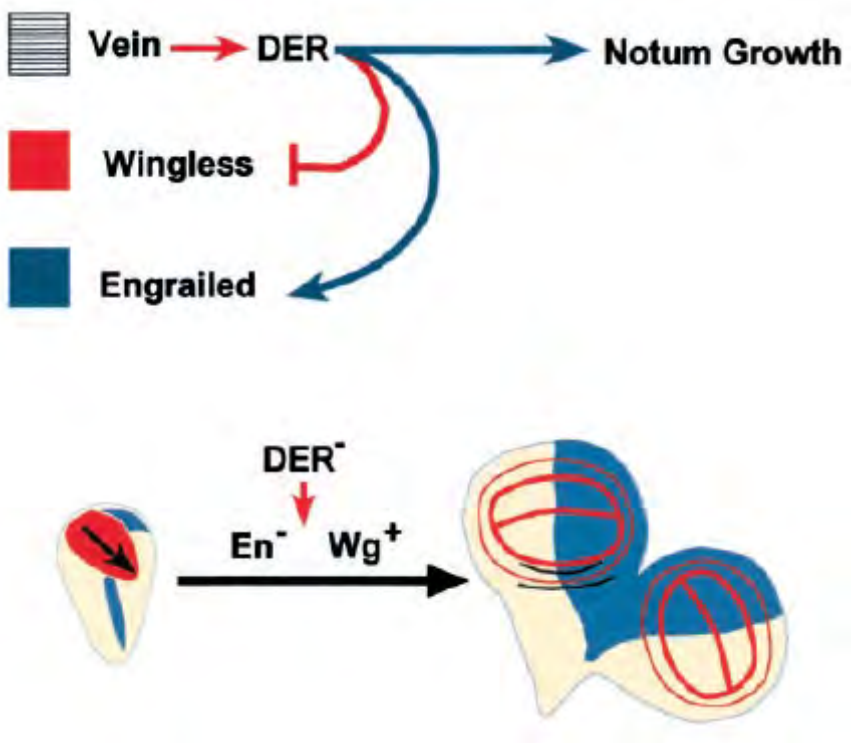

Figure 12: EGFR (DER) represses *wingless* expression and maintains *engrailed* expression in the posterior notum, adapted from [67].

It is unclear whether this third prominent boundary of the wing disc is indeed a compartment boundary in the sense of the AP and DV boundaries. Although Iro-C$^+$ cells do not mingle with Iro-C$^-$ cells [62], the boundary does not appear to be well-defined since clones induced between 72 and 96 hours AEL seem to cross it [62, 81]. This implies that cells which are excluded from, or included in, the expression domain of the Iro-C genes through proliferation can change their fates respectively [81]. Furthermore, unlike the other two boundaries, the WN boundary is not sharply defined, meaning that the expression of Iro-C genes does not end abruptly from one row of cells to the next, but rather decays over a span of several cell diameters. Interestingly, the expression pattern of *apterous* is divided into two parts by this boundary in the late third instar - high levels of expression are found in the dorsal wing pouch and hinge, while low levels are found in the

notum [40, 82, 83].

The patterning of a tissue has been shown to drive morphological changes. The general morphology of the wing imaginal disc, as well as a role for gene patterns in controlling it, is discussed in the next section.

2.3 Wing Disc Morphology

The general morphology of the wing disc becomes increasingly complex during the course of larval development. The wing disc begins as a simple oval structure, before the peripodial membrane and disc proper form [16] in the second instar. Anisotropic growth with lower effective growth rates along the anterior-posterior axis in the second and third instars give the wing disc its characteristic shape [84]; a morphological groove at the DV boundary [85], as well as a series of folds, begins to form around the middle of the third instar [11].

The shape of a growing tissue generally depends on the shape of the newly formed cells as well as their spatial arrangement which is, in turn, dependent on cell rearrangements and oriented cell divisions [86, 87].

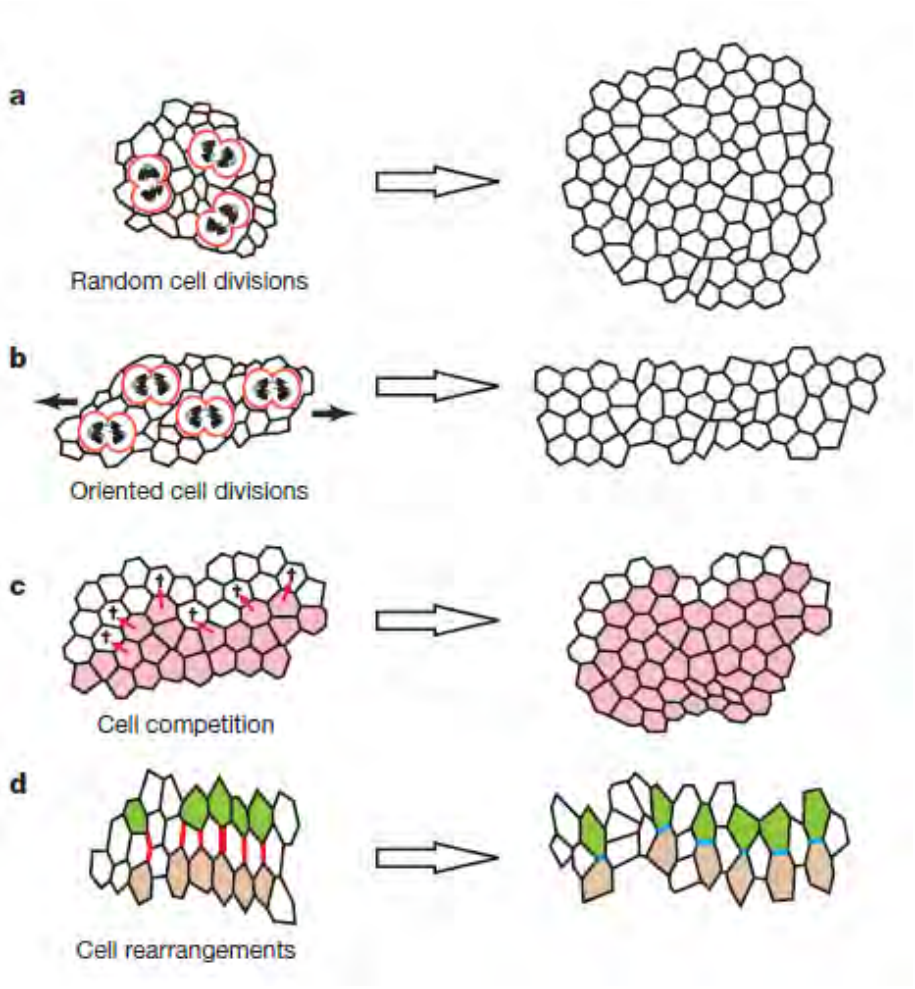

Figure 13: Cellular mechanisms which influence tissue shape and size [86].

Oriented cell divisions have been shown to play a part in the development of different organisms. In *Drosophila* embryos, for example, elongation of the posterior germband during the fast phase of germband extension is driven by cell divisions which are predominantly oriented longitudinally [88]. Furthermore, in zebrafish embryos, elongation along the anterior-posterior axis is driven in part by oriented cell divisions parallel to the animal-vegetal axis (see Fig. 14). This process has been shown to be under the control of non-canonical Wnt/PCP signaling [89, 90], indicating that morphogenetic processes are under the control of genes. The patterning of a tissue thus directly affects the behavior of its cells, which in turn determines the tissue's shape.

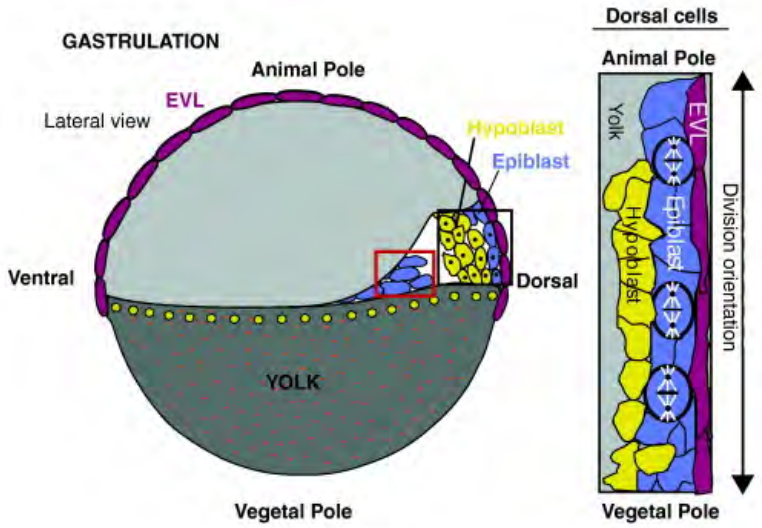

Figure 14: Oriented cell divisions during zebrafish gastrulation, adapted from [90].

As early as 1970, Bryant mentioned the possibility that the longitudinal shape of clones in the wing disc might also be due to oriented cell divisions [11]. In 2005, Baena-López et al. found that the shape of a clone in the wing is indeed related to the orientation of the cell divisions which form it. After mitosis, the daughter cells maintain the positions dictated by the oriented cell division and subsequently divide along the same axis. In second instar wing discs, cell divisions in the wing region are mainly oriented proximal-distally. In the notum, cell divisions show no preferential orientation [87]. This is in agreement with twin clone experiments done by Resino et al. which show that, in the wing, exponential and intercalary growth leads to clones that are compact and longitudinal, whereby the ratio of length to width decreases during the second instar indicating that later growth becomes more isodiametric, while clones in the notum are generally more isodiametric [91].

In 2011, Mao et al. discovered that the planar polarization of Dachs, an atypical myosin, is needed to orient cell divisions in the wing disc. Dachs changes the shapes of cells by constricting cell-cell junctions, thus indirectly orienting the mitotic spindle and therefore cell divisions. Since Dachs is polarized by the Dachsous gradient this directly shows that patterning plays a role in wing disc

morphogenesis [92].

Other steps in the morphological development of the wing disc have also been shown to be influenced by gene expression patterns. For example, wing discs which overexpress *dpp* form a wider wing pouch [49], while the fold which separates the notum from the hinge probably forms due to the juxtaposition of cells which express Iro-C and cells which do not, since ectopic folds form around clones of cells which do not express Iro-C in the notum [81]. As a general rule, the complexity of the morphology of the wing disc seems to scale with the intricacy of the gene expression patterns.

Although patterning plays an crucial role in morphogenesis, actual changes in the shape of a tissue must be induced by mechanical forces. Such forces have attracted great interest in the last decade and some of the results arrived at will be discussed in the next section.

2.4 Mechanical Forces

Morphogenesis is a mechanical process, so it may not be remarkable that mechanical forces have been shown to play a role in the shaping of various organisms. During dorsal closure of the *Drosophila* embryo, for instance, both the amnioserosa and the lateral epidermis have been shown to be under tension, with the leading edge of the lateral epidermis acting as a purse-string [3] (see Fig. 15A).

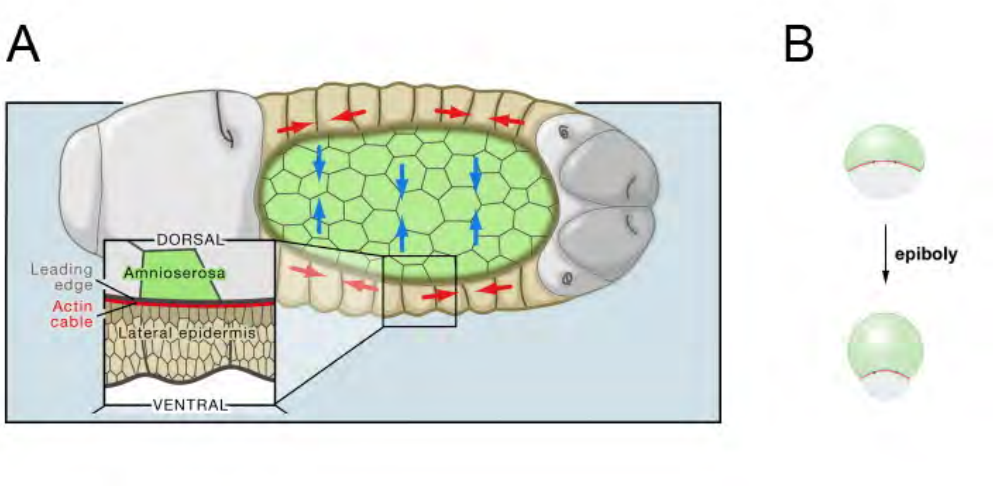

Figure 15: The purse-string mechanism as a simple model for A: dorsal closure in the *Drosophila* embryo, adapted from [93]. B: zebrafish epiboly, adapted from [5].

A similar process plays a role in zebrafish epiboly [5] (see Fig. 15B), representing a conserved mechanism, and has also been proposed to close the ventral pocket during ventral enclosure in *C. elegans* embryos [4] (see Fig. 16).

In the past, morphogenesis of a tissue was shown to be intimately linked to patterning and yet patterning alone could not explain all the observed behavior. In the third instar wing disc, for example, growth is spatially uniform despite the fact that growth factors form gradients. To resolve this contradiction a role for mechanical forces in tissue growth and patterning was proposed by Shraiman in 2005 [95], supported by an experiment which demonstrated that the gene *twist* could be induced ectopically in the *Drosophila* embryo by deforming it mechanically [96]. Based on this idea,

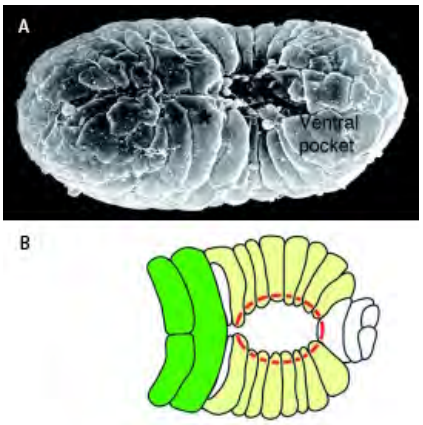

Figure 16: *C. elegans* ventral enclosure. A: Scanning electron micrograph. B: Schematic diagram, adapted from [94].

different models incorporating mechanical forces were presented. These models were not only able to explain the existence of uniform growth, but also how the cessation of growth upon reaching the correct size is regulated [6, 7], a behavior which was shown to be disc-autonomous in experiments by Bryant and Levinson in 1985 [13].

The model of Aegerter-Wilmsen et al. proposes that growth factors as well as stretching induce growth, while compression inhibits it. During wing disc growth, the model shows an increase in compression in the center of the wing pouch, where growth factor levels are highest, which eventually leads to the cessation of growth when compression is strong enough to inhibit the growth induced by the growth factors [6]. This model is supported by experimental evidence in that birefringence measurements show that compression does indeed increase in the wing pouch during wing disc development [8] and that mechanical stretching leads to an increase in cell proliferation [9].

This model was recently augmented and now also takes into account signaling pathways. Growth is terminated when two conditions are fulfilled: besides compression exceeding a certain threshold level at the center of the disc, the compression gradient must also be below a different threshold level in the remainder of the disc. One of the predictions of this model is that an apical cell area gradient forms during growth, whereby apical cell areas decrease towards the center of the disc, which becomes more shallow over time [97]. This has been confirmed experimentally [85, 97].

In this thesis, several sources of external mechanical forces which act upon the wing disc are described, indicating a possible role for external mechanical forces, in addition to internal mechanical forces, in wing disc development. These sources include *twist*-expressing cells which appear to make up the peripodial stalk, and may be identical to the persistent *twist*-expressing cells described in [98], as well as so-called mini threads and a muscle fiber which has been shown to exert considerable force on the wing disc around the time of the second larval molt [60].

This muscle fiber was first described by Dambly-Chaudière et al. in 1986.

Having previously found the muscle proteins tropomyosins and actin I in several imaginal discs, the authors used an antiserum against tropomyosin to investigate how the protein is distributed in these discs. Surprisingly, they found that the protein was not located in the discs, but in connections between the wing, third leg and haltere discs, indicating that these discs are linked by muscles [99].

These findings indicate that it may not suffice to consider merely the isolated wing disc as such in order to understand growth control. Instead, it may be essential to take into account its surroundings, for instance in tackling the problem of in-vivo culturing.

How a tissue knows when it has reached its final size and shape is one of the most interesting questions in developmental biology today. The final size of a tissue appears to be determined by an intricate interplay between factors such as gene expression, internal mechanical forces, oriented cell divisions and cell shape changes. The exact parameters differ for different tissues, and even spatiotemporally in a single one, but it is intriguing to suppose that a common mechanism underlies all tissue morphogenesis. In this thesis, results will be presented which support the idea that another factor, namely external mechanical forces, must also be considered. The experimental methods used to obtain these results will be discussed in the following chapter.

3 Experimental Methods

Most of the results in this thesis were obtained using a combination of in-vivo imaging and dissection. More details concerning these methods and the fly stocks used are introduced in this chapter, following a short section on confocal microscopy.

3.1 Confocal Microscopy

In confocal microscopy, light is scanned across a specimen point by point, whereby all scattered light is rejected, leading to images of high resolution and allowing for thick and highly scattering specimens. The basic concept is as follows: a bright source of light (10 in Fig. 17), nowadays usually a laser, passes through a pinhole(16) followed by a beamsplitter(17), before passing through a lens(11) which focuses the light onto one point of the specimen(22). In the original patent filed by Minsky in 1957 [100], the light was then reflected by a mirror(15), which is not common in today's microscopes, before passing back through the lens and being reflected by the beamsplitter to converge at the second pinhole(26). Any light which does not come from the focal point inside the sample will not pass through this pinhole. The intensity of the light which does pass through the pinhole is measured using a photomultiplier. The sample is thus scanned point by point and the intensity for each point plotted, generating the final image [100].

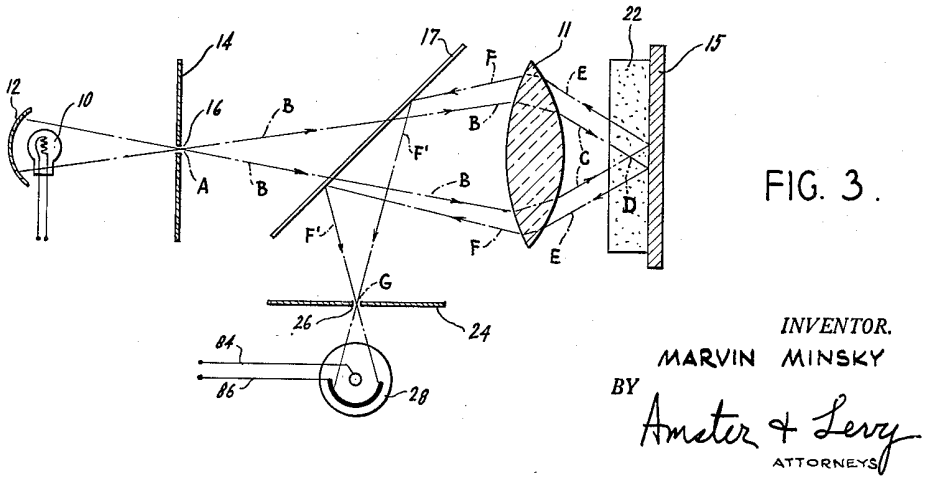

Figure 17: Optical system used in confocal microscopes, adapted from [100].

Today, confocal microscopy is often used to image fluorescent specimens. In this case, excess light from the excitation light ray may pass through the sample, allowing the simultaneous acquisition of a non-confocal transmission image, as well as a confocal image gained from the light emitted by the fluorescent sample.

3.2 In-vivo Imaging

In order to image larvae in vivo, they need to be immobilized. This was done as follows: a clean larva was placed into a drop of water or phosphate buffered saline (PBS) on a cover slip which had been attached to a microscope slide with water using the capillary effect (see Fig. 18). Since the refractive indices of the solution and the cuticle of the larva are similar, the cuticle became almost transparent at this point. A second cover slip, again of a similar refractive index, with a thickness of 170 µm and of a size appropriate to the size of the larva (18 x 18 mm^2 for first and second instar larvae, 24 x 50 mm^2 or 24 x 60 mm^2 for third instar larvae) was then placed on top of the larva. Next, the larva was carefully rolled until the, usually left, main tracheal branch was directly below the upper cover slip, allowing optimal imaging of the left wing and/or haltere discs. Once the larva was correctly oriented, the force upon the larva resulting from the capillary effect could be increased by removing excess liquid from between the cover slips

until the larva was sufficiently immobilized.

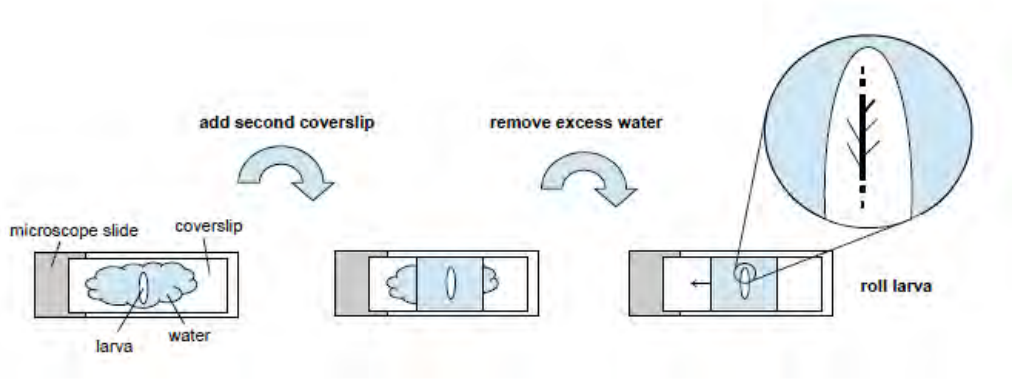

Figure 18: Schematic of the process for imaging the larvae and locating the wing and haltere discs [60].

Immobilized larvae were imaged using an upright Leica SP1 confocal microscope, utilizing one or more fluorescent channels, as well as the transmission channel, simultaneously with a resolution of 512 x 512 pixels. The wing disc was located on the second thoracic lateral tracheal branch; the haltere disc on the third lateral tracheal branch. A 40x immersion objective was used to image cell outlines and entire wing discs until about the third instar. The wing discs of older third instar larvae were imaged using the 20x immersion objective or the 5x objective. If the wing disc moved out of the z-range of the stack during imaging due to residual larval motion, this was corrected manually when possible. Imaging times were generally kept to a minimum and did not exceed 5-10 minutes as this greatly reduced larva survival rates.

After imaging, water or PBS was added between the cover slips to decrease the pressure until the larva could move freely. Larvae which immediately resumed normal feeding activity at this time were likely to survive - survival rates were generally lower for younger larvae. The larva was then returned to its respective petri dish containing standard fly medium until the next imaging session (either about 8 or about 16 hours later). The larvae were kept at room temperature (22(1)°C). Larvae which died after one or two imaging sessions or did not develop normally, usually developing too slowly, were not evaluated. Larvae which pupated and eclosed showed normal wings.

In-vivo imaging offers a way to obtain temporal data on wing disc growth and patterning. Although there are drawbacks, such as low larval survival rates and larger errors due to a certain lack of influence on the exact positioning of the wing disc, this method does have its advantages. To date, temporal data has usually been gained by dissecting wing discs from different larvae at different stages [84, 101]. This method necessarily takes into account a certain error due to variation between individual larvae which can be avoided using in-vivo imaging. Another alternative technique for obtaining temporal data is in-vitro culturing which has been used successfully [102, 103], though as yet during a rather limited time span. Possibly the greatest advantage of in-vivo imaging lies in the fact that the wing disc remains in its natural environment - if external mechanical forces play a role in wing disc development, these are removed upon dissection and may need to be generated artificially for methods such as in-vitro culturing to be effective for times spanning all of larval development.

3.3 GAL4/UAS System

The GAL4/UAS system allows gene expression to be controlled both temporally and spatially [104]. The technique makes use of two transgenic lines of flies and is illustrated in Fig. 19. One line, termed the responder line, contains the target gene under the control of a UAS (Upstream Activation Sequence) element which is GAL4-dependent. The other lines, the driver, expresses the transcriptional activator GAL4 in a certain temporal and spatial pattern. When these lines are crossed, the resulting line expresses the target gene in the temporal and spatial pattern given by the driver line.

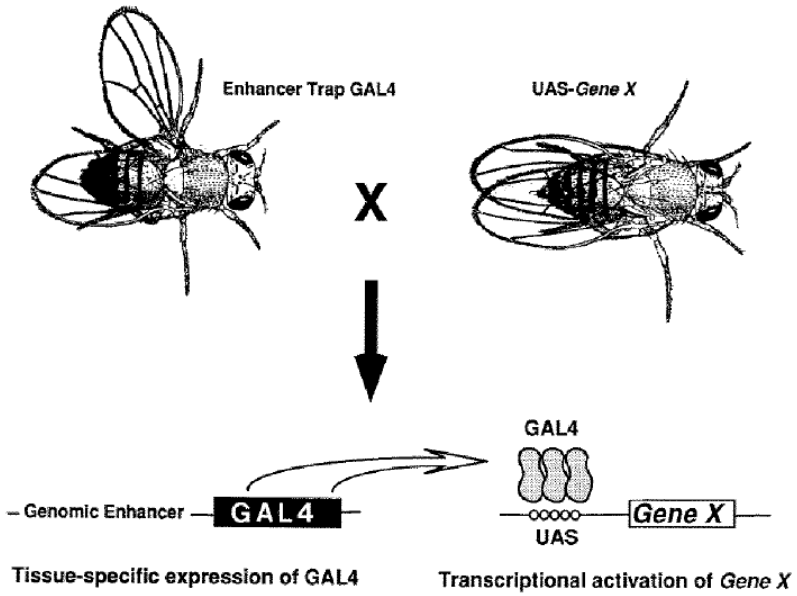

Figure 19: GAL4/UAS system in *Drosophila* [105].

This technique has several advantages. Since the driver line is missing the target gene while the responder line lacks the activator protein, both lines are viable even if the target gene leads to toxic or lethal gene products. This system is also extremely versatile in that a certain target gene can be expressed in a variety of patterns, only limited by the availability of the correct driver lines [104, 105].

In this thesis, the GAL4/UAS system was mainly used to fluorescently label cells which expressed a certain gene in order to follow the spatial and temporal development of the gene expression pattern. The stocks used are introduced in the following section.

3.4 Fly Stocks

3.4.1 E-Cadherin-GFP III Flies

To assess the increase in apical area of the wing disc during larval development, **E-Cadherin-GFP III** larvae [106] were imaged in-vivo. Flies of this stock, in which GFP is fused to E-Cadherin, meaning that the apical cell outlines are fluorescently labeled, will be called 'E-Cadherin-GFP III flies' in the following.

Larvae were imaged twice a day, usually with about 8(1) hours between sessions. In all 18 larvae were imaged.

Fluorescent and transmission stacks of the whole wing disc were taken using the 40x immersion objective until the wing discs grew larger than the field of view. At this point, the 20x immersion objective was used.

After taking stacks of the whole disc to quantify the increase in disc area, stacks of cell shapes were taken using the same larva to determine how apical cell areas change during larval development. Such stacks were taken using the 40x immersion objective with an appropriate zoom in an area of the wing discs where the cell outlines were well-recognizable.

3.4.2 Engrailed Flies

To observe the development of the anterior-posterior compartment boundary, a fly strain in which the membranes of *engrailed*-expressing cells were labeled with GFP was generated by crossing **y w f;** $\frac{\textbf{en GAL4}}{\textbf{CyO}}$ virgin females and **y[1] w[*]; P{w[+mC]=UAS-mCD8::GFP.L}LL5** males. Flies of this strain will be named 'engrailed flies' in this thesis. Engrailed larvae were imaged twice a day, with about 8 hours between sessions, beginning in the first larval instar. Images of whole wing discs with a resolution of 512 x 512 pixels were taken using the fluorescent and transmission channels. As before, the 40x and 20x immersion objectives were used.

3.4.3 Apterous Flies

In order to assess the development of the dorsal-ventral compartment boundary, the *apterous* expression pattern was observed in **y w, UAS-CD8-GFP; ap-GAL4(CyO); TM6B** flies, in which the membranes of *apterous*-expressing cells are labeled with GFP. Due to the TM6B balancer chromosome, these larvae are more squat than wild-type larvae [107]. 'Apterous larvae' were imaged twice a day, with about 8 hours between sessions. Imaging was begun in the late first or early second instars, in order to observe the initiation of *apterous* expression. Images of wing discs with a resolution of 512 x 512 pixels were taken using the

fluorescent and transmission channels. The 40x and 20x immersion objectives were used, as well as the 5x objective for late third instar larvae.

3.4.4 Raeppli Flies

By crossing **Raeppli:Ras9; Raeppli:Ras3 homozygous** and $\frac{\textbf{apGAL4, UASFLP}}{\textbf{CyO}}$ flies, a strain was generated with which the mitotic behavior of single *apterous*-expressing cells could be observed. These 'Raeppli flies' have the ability to express several different fluorescent proteins, namely TagBFP, TFP, m-Orange2 and mKate, attached to a membrane marker. When a cell begins to express *apterous*, it also begins to express a random combination of two of these proteins, whereby the double expression of one protein is a possibility.

3.4.5 Single Cell Clone Flies

To observe mitotic behavior over time **ywhsF; CyO/Sp; Act>CD2>GAL4 (w+) UAS-GFP(y+)/TM6B** virgins were crossed with **y[1] w[*]; P{w[+mC]= UAS-mCD8::GFP.L}LL5** males, leading to a strain of flies in which GFP expression could be induced in single cells by a heat shock ('single cell clone flies'). Tubes were heat shocked for 12 minutes at 37°C once the first larvae had hatched. The first round of imaging using early second instar larvae took place about 24 hours later to allow for sufficient fluorescence. Images of complete wing discs were taken with the 40x and 20x immersion objectives using the fluorescent and transmission channels with a resolution of 512 x 512 pixels.

3.4.6 Twist Flies

In order to image the expression of the gene *twist*, larvae of the **w*; rib(P7) dp cn bw/CyO, twi-GAL4 UAS-2xGFP** [108] stock were used. In this stock (henceforth called 'twist flies') the cytoplasms of cells expressing *twist* are labeled with GFP. The expression pattern of the endogenous *twist* gene does not appear to be represented completely by the twi-GAL4 transgene used, since adepithelial cells in the wing disc, which are known to express *twist* [98], are not fluorescently labeled.

3.5 Wing Disc Dissection and Stretching

Imaginal discs were dissected in PBS using Dumont tweezers (Biology and Microscopy #5 and #7). To image the wing disc, or other sample, a microscope slide was prepared by sticking a ring of electrical tape to it, forming a kind of well to hold the medium for the sample. Poly-L-Lysine(PLL) (Sigma-Aldrich) solution was applied to the slide inside the ring; the excess was removed after about a minute. In the next step, the respective medium, for example PBS, was added to the well and the wing disc transferred to it. The wing disc was subsequently maneuvered toward the microscope slide using the tweezers, where it adhered electrostatically due to the positively charged PLL. Depending on whether a cover slip was placed upon the sample to prevent evaporation of the medium, whereby the ring of electrical tape acted as a spacer, or the sample was imaged as is, either the 40x or 20x immersion objectives or the 40x water immersion objective were used, respectively. Images were attained using the fluorescent and/or transmission channels with a resolution of 512 x 512 pixels.

To image stretched wing discs, part of the wing disc was first attached to a microscope slide using PLL as described above. The wing disc was then stretched manually using tweezers by pulling on, for instance, the trachea. These trachea were then stuck to the microscope slide coated with PLL, thus maintaining the stretched configuration of the wing disc.

4 Data Processing

Different programs and procedures were used to process the data. Some of these are described in this chapter.

4.1 Determination of Apical Wing Disc Areas

To determine the apical wing disc area, the in-vivo data gained from the E-Cadherin-GFP III larvae was processed as follows. After removing any images that were distorted, due to occasional strong movements of the larva, from the fluorescent stack, an image was chosen which showed a large portion of the fluorescent apical wing disc area. The stack was aligned with respect to this image using the StackReg plugin (affine transformation) of ImageJ [109], allowing for the correction of slight residual movement of the larva. A z-projection (Average Intensity or Sum Slices) of the newly aligned stack was then taken, possibly despeckled, and the brightness and contrast adjusted. The area obtained in this way was compared to the images of the stack. If the alignment did not appear to be correct, the process was repeated after choosing a different reference image and/or removing further slides.

The apical area of the disc proper $A_{d,pix}$ was measured in pixels for each time point using the 'Polygon selections' tool in ImageJ. This area was converted into square micrometers using the following formula:

$$A_d = A_{d,pix} \ \frac{(250\mu m)^2}{(512 \cdot \text{zoom})^2} \tag{1}$$

512 x 512 pixels correspond to 250 µm^2 when the 40x objective is used with a zoom of 1. Correspondingly, the zoom was multiplied by 0.5 when the 20x objective was used.

The apical wing disc areas for each larva were filled into the columns of a table, whereby each row represented eight hours. A time of 80 hours was arbitrarily chosen as the beginning of the third larval instar and the columns adjusted accordingly, whereby the larval instar was determined from the morphology of

the trachea. This introduces a systematic error of several hours into the timing for each larva since the exact time of entry into the third instar is not known. The average apical cell area could then be calculated for each point in time by averaging over the respective row. The standard error for each point in time was determined as well.

4.2 Determination of Apical Cell Areas

The apical cell outlines gained from imaging E-Cadherin-GFP III larvae in vivo were processed in an analogous way to the apical wing disc areas: after removing any distorted images from the fluorescent stack, an image with well recognizable cell outlines was chosen, the StackReg plugin used, and a z-projection made.

Apical cell areas were then determined using Packing Analyzer [110]. The cells were outlined manually in the z-projection with the help of the stack to ensure that only cells of the disc proper were outlined once this layer was distinguishable. Cells at the edge of the wing disc were usually avoided since the visible apical cell area in that region may not represent the entire apical cell area. This was sometimes difficult in first instar wing discs due to the small number of cells. An example for z-projections with superimposed cell outlines, in red, is shown for the development of one larva in Fig. 20. Once the cells had been outlined, the Packing Analyzer software calculated the areas of the cells, as well as other data such as the number of vertices for each cell.

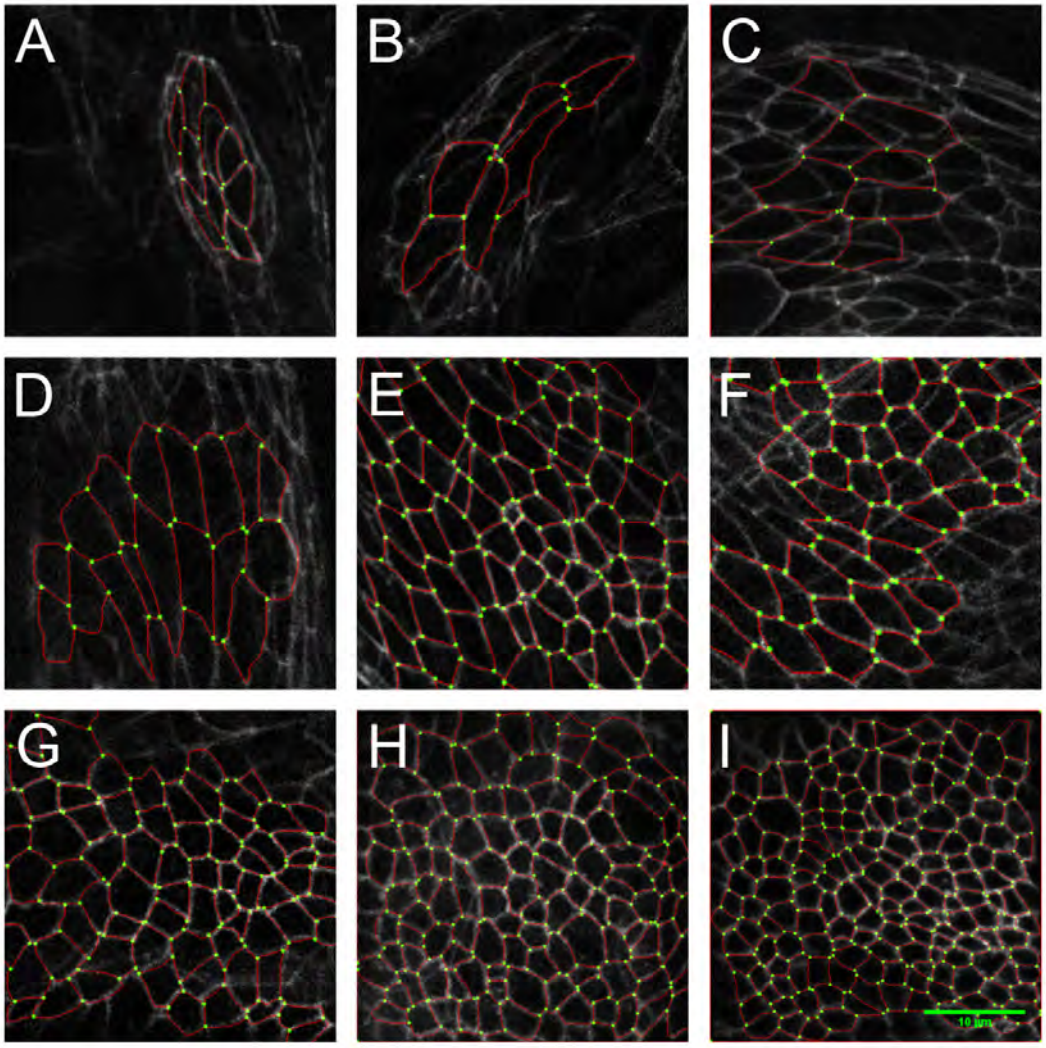

Figure 20: Apical cell outlines in one larva over time. A: First instar wing disc (24 h). B: The larva has molted (32 h). C: 48 h. D: 56 h. E: 72 h. F: The larva is now in the third instar (80 h). G: 96 h. H: 104 h. I: 120 h. The scale bar denotes 10 µm.

Histograms were plotted using all the apical cell areas, converted into μm^2, at the given point in time. Apical cell areas were assessed in steps of 2 μm^2.

The apical cell areas obtained using Packing Analyzer were averaged for each larva and the average apical cell area in pixels again converted into μm^2. These average apical cell areas for each time point and larva were filled into a table analogous to the one used for the apical wing disc areas. The areas were again

averaged over the different larvae for each point in time and the standard errors calculated.

Dividing the area of a wing disc by the respective average apical cell area at a given time t gives the approximate number of cells in the wing disc, $N(t)$, at that point in time. Averages over all the larvae for each point in time were again calculated.

The number of cells as a function of time can be used to calculate the proliferation rate $g(t)$ of the cells for each larva and at each point in time t:

$$g(t) = \frac{d\ln(N(t))}{dt} = \frac{\ln(N(t_+)) - \ln(N(t_-))}{t_+ - t_-} \tag{2}$$

The latter term describes the proliferation rate as a function of discrete time steps whereby t_+ and t_- are the points in time after and before t, corresponding to ± 8 hours. Averages over all the larvae for each point in time were also calculated.

To calculate the strain ellipses for all the apical disc proper cells of one wing disc, the peripodial membrane was first 'digitally removed' by making collages from the fluorescent data stacks: the z-projections gained using aligned data from different parts of one or several stacks was merged using the respective zooms, to get an overall picture of the apical cell areas. Packing Analyzer was then used to process the data and the output data generated by Packing Analyzer, in turn, used to calculate strain ellipses with the help of a Matlab program [97, 111, 112].

4.3 Engrailed Flies

Raw confocal data from the in-vivo imaging of the engrailed flies was also processed using ImageJ. First, a reference slice was chosen which showed a clear picture of the wing disc in the transmission channel as well as ample fluorescence in the fluorescent channel. The StackReg plugin was then used to remove residual larval movement from the fluorescent channel before a z-projection (Average Intensity) was produced. If this process did not result in an accurate reproduction of the fluorescent channel, a different reference image was chosen, taking into

account a poorer transmission image. The z-projection gained in this way was combined with the according transmission image, resulting in a composite image displaying information from both channels. Brightness and contrast were then adjusted in both channels and an RGB image made. If the wing disc was too large to fit into the field of view, two stacks were taken using the same microscope settings and 'patched' together. To better recognize the wing disc it was roughly outlined and the 'Lightness' increased using Adobe Photoshop.

In order to follow the development of the AP boundary the outlined wing discs were cut out and opened as new images with two new layers added - one in grayscale showing the entire wing disc area and one in green showing the area of *engrailed* expression. The wing discs for each larva were then scaled, aligned along the presumptive NW boundary using the attachment point of the muscle fiber as a fixed point and stacked on top of each other. The grayscale layers were hidden for all except the oldest disc, so that the final image showed the growth of the *engrailed*-expressing region against the area of the oldest wing disc.

4.4 Apterous Flies

For the apterous flies, in-vivo images were acquired and processed in the same way described in the previous section. Additionally, the wing disc area and the area of the *apterous*-expressing domain were measured for each wing disc using the 'Polygon selections' tool in ImageJ.

The images showing a possible role for mechanical forces in the induction of *apterous* are RGB images of composite images made up of a Min Intensity z-projection of the transmission channel stack as well as an Average Intensity z-projection of the fluorescent channel stack. One of the two images was flipped horizontally for better comparison.

4.5 Single Cell Clones

Images of single cell clones were again acquired and processed in the way described in the section on engrailed flies, with the addition that slices showing

the peripodial membrane were sometimes removed from the fluorescent stacks before producing the z-projection. In order to assess mitotic behavior, a clone was chosen and an assortment of recognizable points selected, whereby each point was assigned a different color. The same points were thereupon selected in all of the following images of the developing wing disc and given their respective colors. The images of the wing discs were again scaled, stacked and aligned as described above. All the points of one color were then connected, giving a so-called 'growth trail' for that point. Some growth trails are made up of fewer elements than others. These derive from points which were first defined at later time points, since the number of recognizable points increases as the wing disc grows.

5 Experimental Results

In the following chapter the experimental results are presented, divided into sections on wing disc growth, wing disc patterning, growth anisotropies, as well as a section on the different sources of external stresses which act upon the wing disc. These results are then discussed in Chapter 6.

5.1 Wing Disc Growth

In order to quantify wing disc growth, the temporal development of the apical area of the disc proper, as well as the average apical cell area, were assessed. This allows the calculation of the number of disc proper cells as a function of time, which, in turn, can be used to calculate the proliferation rate as function of time. These results are presented in the following.

The apical wing disc area as a function of time was determined by imaging E-Cadherin-GFP III larvae in-vivo. When the apical wing disc area is plotted semilogarithmically as a function of the time for each larva, whereby 80 hours represents the beginning of the third instar (and 20 hours represents the beginning of the second instar), Fig. 21 is obtained. The growth curve for each of the 18 larvae is represented by a line of a different color. Depending on when in development imaging was started, and how long the larva lived, the lines have different starting and end points. The error in the time is about 1h between time points; a systematic error of several hours for each larva is linked to the normalization process. The first and second molts are represented by the two dashed gray lines.

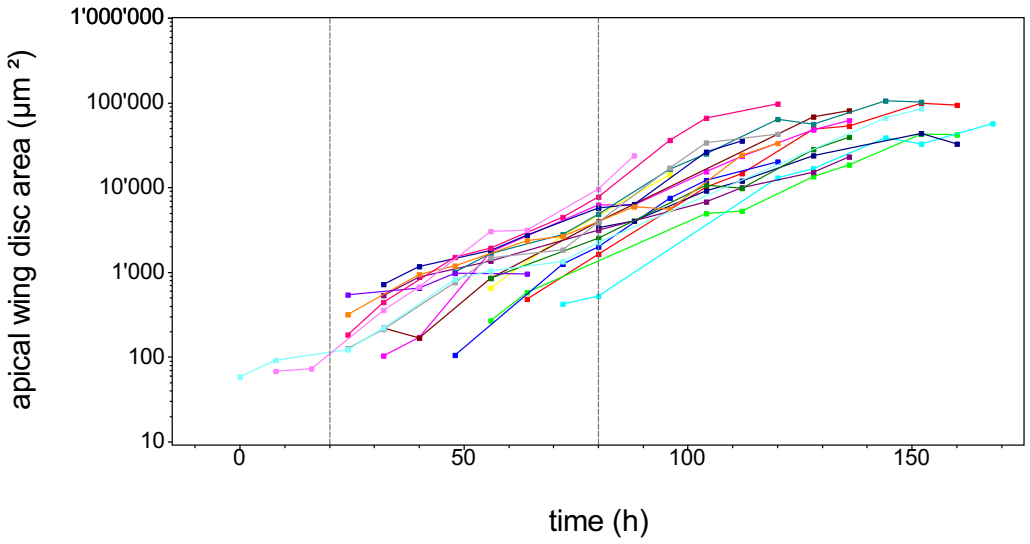

Figure 21: Growth curves for wing discs of different larvae.

In this plot, the slope of a curve at a certain point in time is equal to the growth rate at that time. It can be seen that the different larvae shows individual growth rates over time, and yet the curves have a few attributes in common: the growth rate is low during the first instar, roughly exponential during the second and early third instars and decreases in the second half of the third larval instar.

Averaging over the areas for each time point gives Fig. 22. The apical wing disc area is $6(1) \cdot 10^1$ µm^2 in the first larval instar and grows to become $6(2) \cdot 10^4$ µm^2 in size before pupation. The error bars give the standard error for each time point (whereby a relative error of 0.2 was assumed when only one value was available).

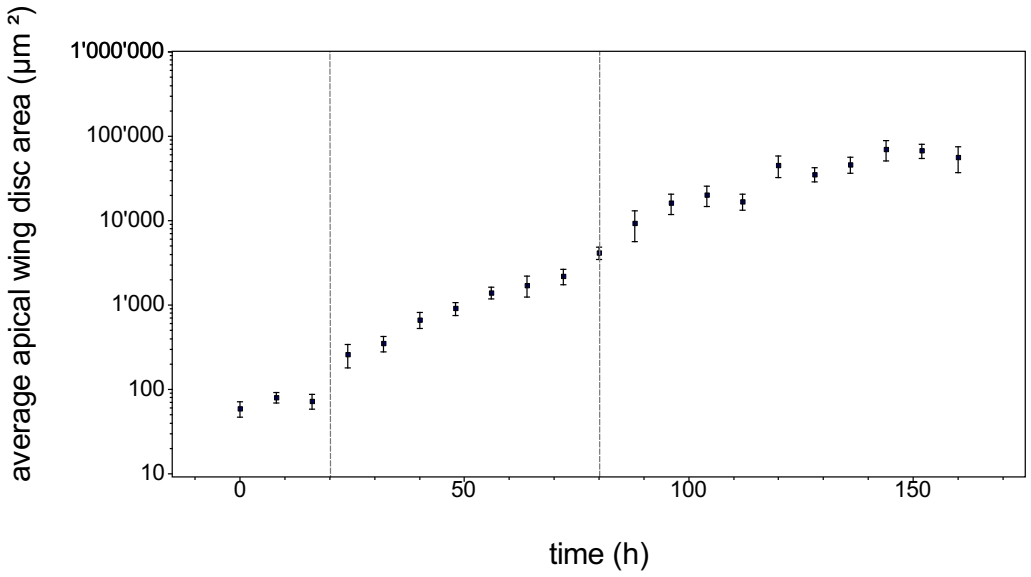

Figure 22: Average growth curve of the wing disc during larval development.

Using data from the same larvae, the average apical cell area was determined for each point in time - first for each larva, then averaged over all the larvae. Plotting the average apical cell area as a function of time gives Fig. 23. The three instars are again separated by the dashed lines. On a side note, averaging over all the cells of all the larvae for each point in time leads to the same results, within errors.

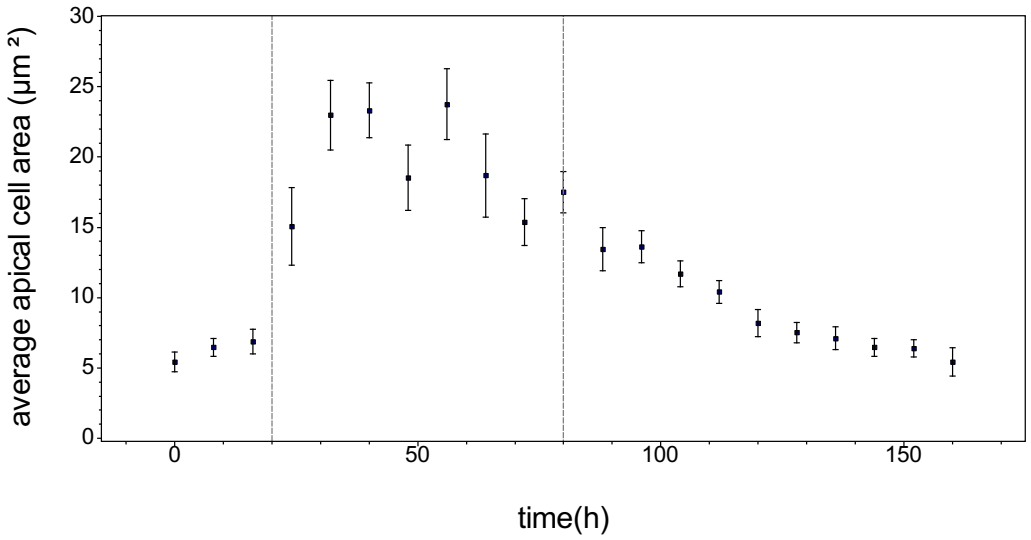

Figure 23: Average apical cell area in the wing disc as a function of time.

The apical cell area is about 5(1) µm^2 in the first larval instar, increasing to a peak size of 24(3) µm^2 around the mid-second larval instar, before it begins to decrease, reaching an area similar to the area at the beginning of the first larval instar by the end of the third instar (5(1) µm^2). The error bars again give the standard error for each time point (the standard error for the average over the respective cells was used when only one average apical cell area was available).

The following histograms show the probabilities for a certain apical cell area at different representative times during wing disc development. The red bars were calculated from the cells of all first instar larvae (n = 26). The cells are all of similar size with a peak in the distribution at about 5 μm^2. In the mid second instar (56 hours, green bars), cell areas are not only significantly larger, but also show more variance. In the late third instar (152 hours, blue bars), the distribution of the apical cell areas is again similar to the distribution found in the first larval instar. These results are in agreement with the error bars in Fig. 23, which are largest in the second instar.

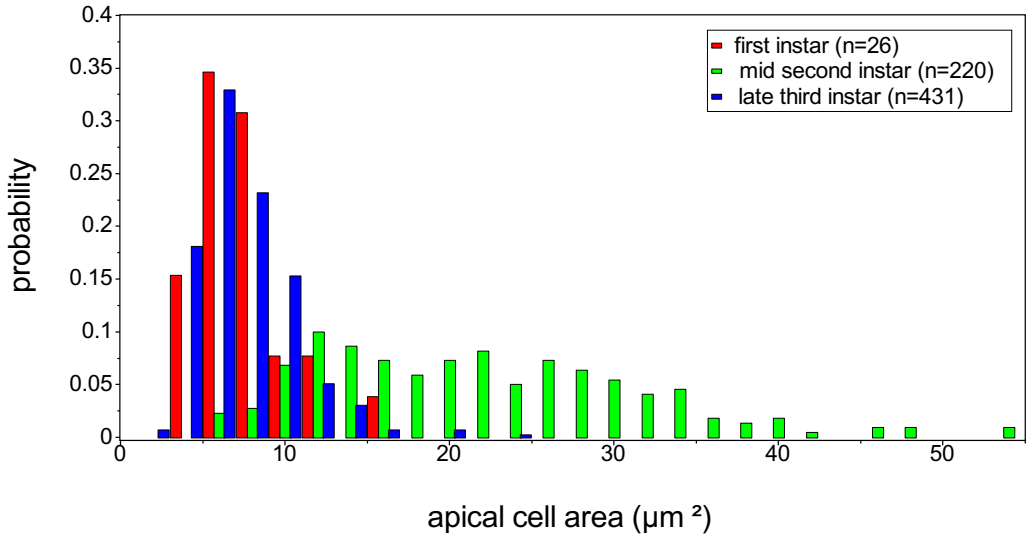

Figure 24: Histogram of the apical cell areas at representative times.

Plotting the average apical cell area as a function of the respective apical wing disc area for all larvae and all time points gives the following log-log plot. Data for first, second and third instar larvae is represented by red, green and blue points, respectively. Data from larvae which did not develop normally was included under the assumption that slower development does not interfere with the relationship between the apical wing disc area and the average apical cell area.

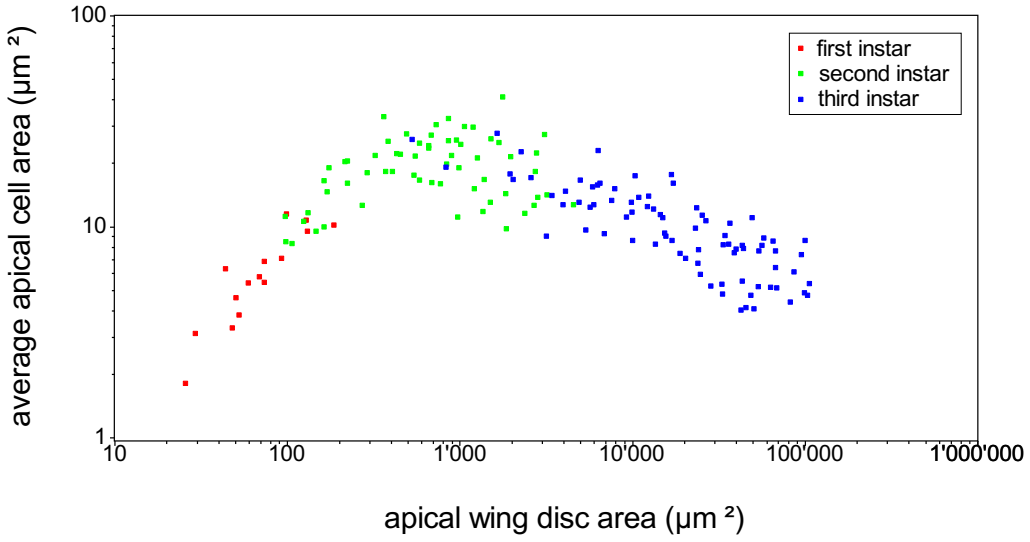

Figure 25: Apical wing disc area as a function of the average apical cell area.

The data for the first larval instar has a slope of one, indicating a linear relationship between the average cell area and the wing disc area - in other words, the increase in wing disc area is not due to cell divisions, but to an increase in the average apical cell area during the first instar. Once the maximum apical cell area has been reached, the spread in the data points increases. Due to the logarithmic scale this spread decreases in absolute terms until the end of the third instar, confirming the results shown in Fig. 24 and giving an idea of how histograms for intermediate points in time would look.

Dividing the apical area of the disc proper by the average apical cell area for each point in time gives an estimate for the number of cells in the disc proper at that time. Averaging over all the larvae and plotting the number of cells as a function of time gives the following semi-logarithmic graph:

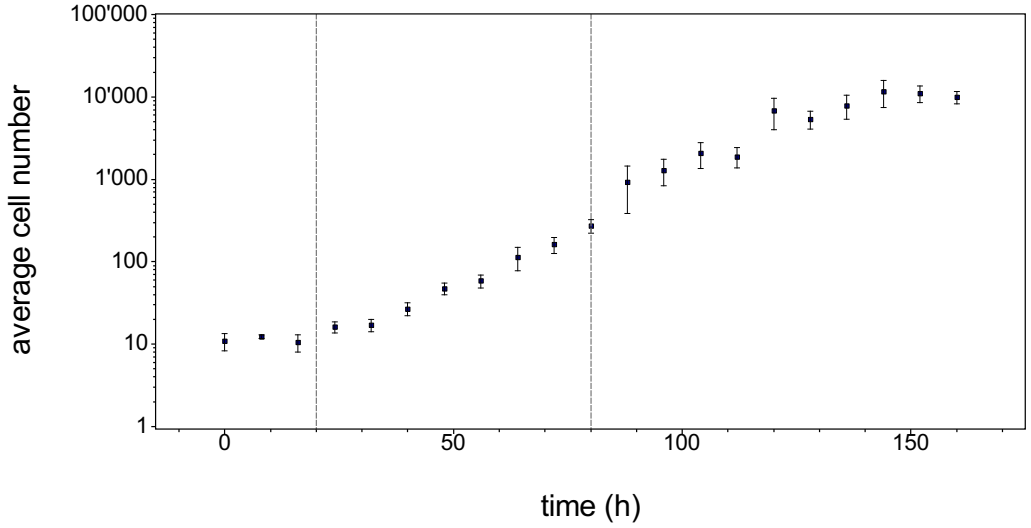

Figure 26: Average cell number as a function of time.

The number of cells remains at around 12 cells during the first larval instar, then increases exponentially until the middle of the third instar after which cell proliferation slows down. Cell proliferation ceases in the late third instar at a cell number of about $12 \cdot 10^3$. The error bars give the standard error for each time point (error propagation was used to calculate the errors if only one value was available).

Using the cell numbers at different times, the proliferation rate for each point in time could be calculated using (2). The proliferation rate was averaged over all the larvae and is shown as a function of time in Fig. 27.

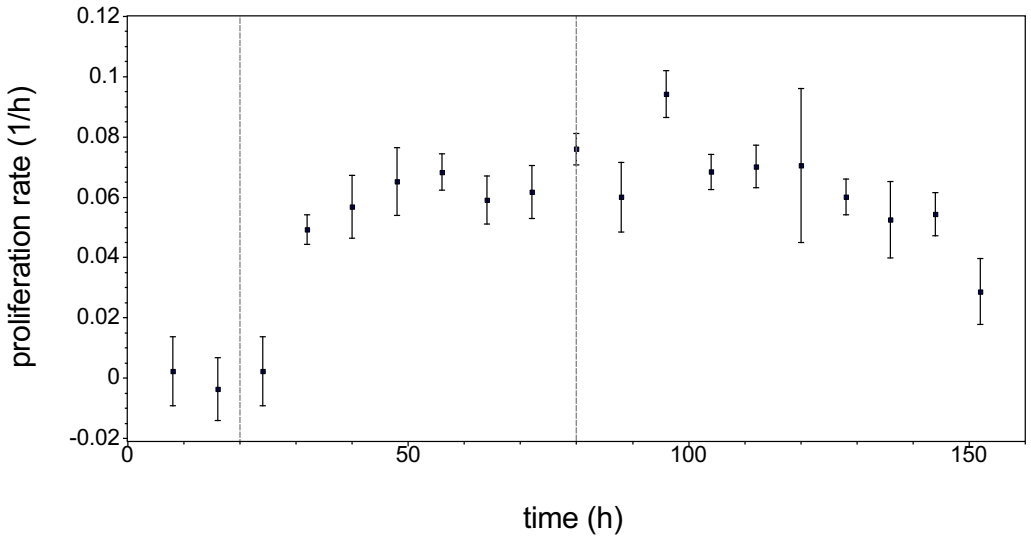

Figure 27: Average proliferation rate as a function of time.

The proliferation rate is zero, within errors, during the first instar. It increases sharply to around 0.06(1) h^{-1} after the first molt, then peaks at 0.09(1) h^{-1} shortly after the second molt, before decreasing again until wing disc growth ceases. The error bars shown indicate the standard error (the maximum error was calculated when only one value was available).

Plotting the proliferation rate as a function of the average apical cell area leads to Fig. 28. A correlation is observed between the proliferation rate and the average apical cell area in the third instar. Calculating the Spearman's rank leads to a value of 0.8, which corresponds to a p-value of 0.01.

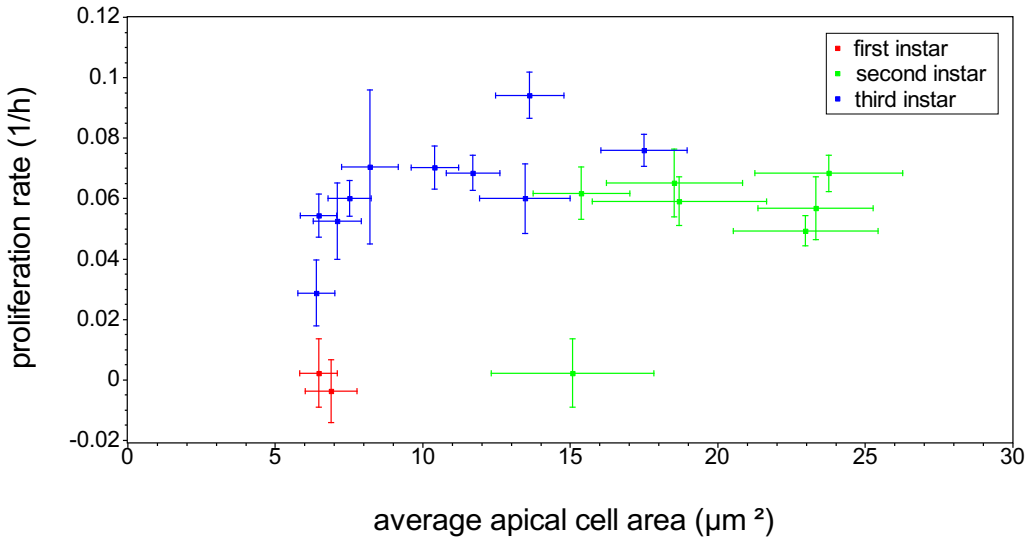

Figure 28: Average proliferation rate as a function of the average apical cell area.

5.2 Wing Disc Patterning

In-vivo imaging was also used to study the patterning of the wing disc, especially in respect to the formation of the AP and DV compartment boundaries. The expression domains of the selector genes *engrailed* for the posterior compartment, as well as *apterous* for the dorsal compartment, were imaged during larval development. The results are presented in this section.

5.2.1 Development of the AP compartment boundary

The development of the AP compartment boundary was assessed using larvae in which the GAL4 gene under the control of the driver gene *engrailed* was used to express CD8-GFP under UAS control. Figure 29 shows a representative series of images taken of the left wing disc of a single larva over time. The scale bars are 50 µm. Image A was taken while the larva was in the late first instar, as can be recognized by the outlines of the second instar trachea surrounding the dark first instar trachea - *engrailed* is already being expressed in the posterior compartment. Images B and C show the same wing disc 16(1) and 24(1) hours after the first image (AFI). The larva is in the second instar and, as can be recognized by the different orientations of the wing disc, the disc is still rather ellipsoid in shape. Image D (40(1) hours AFI) shows a second instar larva shortly before the second molt as is indicated by the morphology of the trachea. In Image E (48(1) hours AFI), the larva has entered the third instar and shows the characteristic wing disc shape and *engrailed* patterning, including the 'kink' which forms near the WN boundary. Images H (88(1) hours AFI) and I (96(1) hours AFI) show mid to late third instar wing discs, exhibiting the folds characteristic of this developmental stage. The *engrailed* boundary in the peripodial membrane has shifted anteriorly, in accordance with [20].

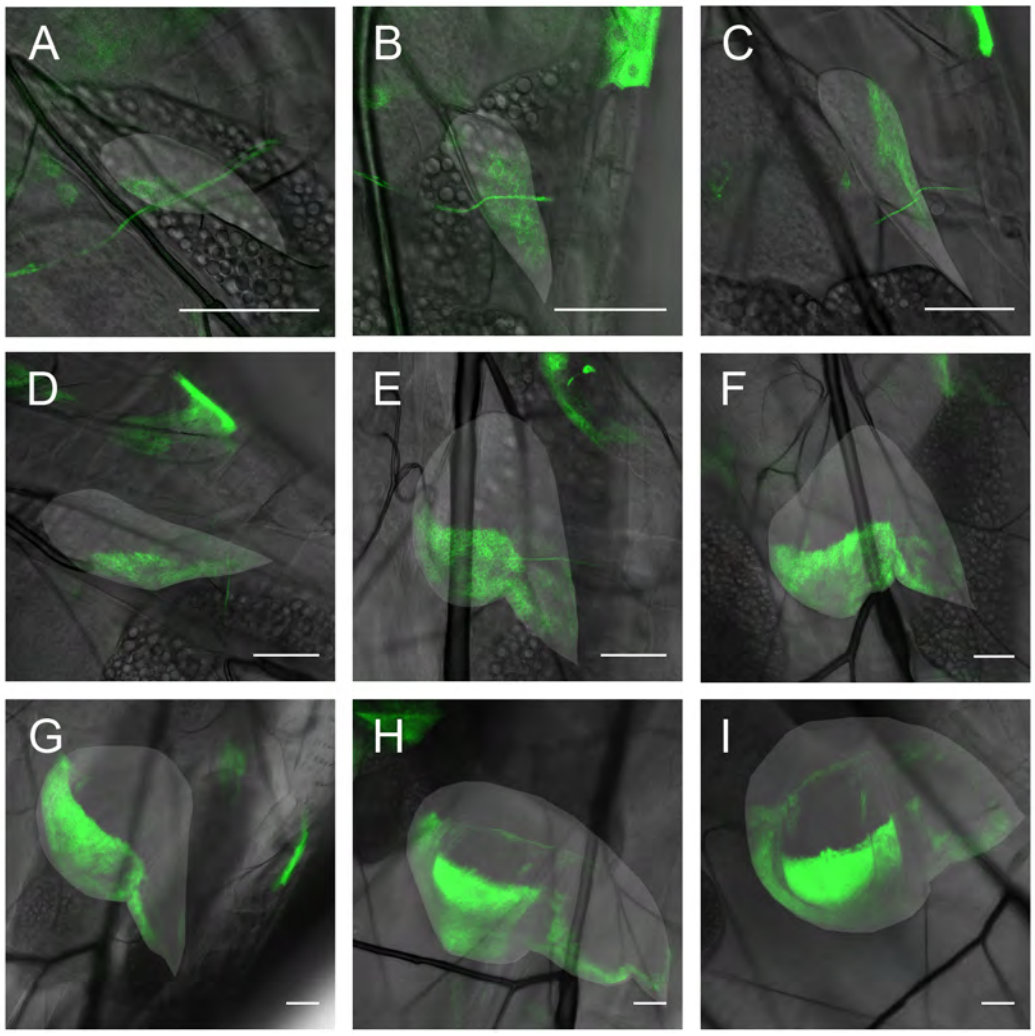

Figure 29: Temporal development of the *engrailed* expression pattern in a left wing disc. A: Late first instar larva. B: 16(1)h AFI. C: 24(1)h AFI. D: 40(1)h AFI. E: 48(1) h AFI. F: 64(1)h AFI. G: 72(1)h AFI. H: 88(1)h AFI. I: 96(1)h AFI. Scale bars: 50 µm.

Fig. 30 shows the development of the AP boundary over time between the second and mid-late third instars of a different larva. The time between two consecutive *engrailed*-expressing areas alternates between 8 and 16 hours. The third smallest *engrailed*-expressing area appears to have a straight border - this is due to the fact that the wing disc is deformed by the trachea next to it. At this point, the larva has just entered the third instar. The neighboring smaller wing disc was imaged 8 hours earlier, while the neighboring larger one, which first shows the characteristic kink, was imaged 16 hours later. The scale bar is 50 µm, the dashed

line indicates the WN boundary.

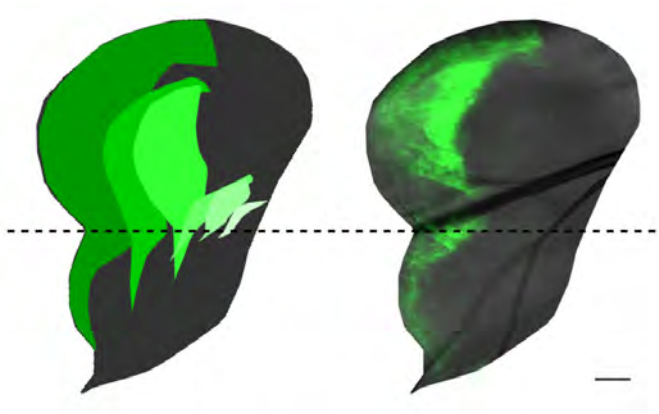

Figure 30: Development of the AP compartment boundary. Scale bar: 50 µm.

5.2.2 Development of the DV compartment boundary

The development of the DV compartment boundary was observed using larvae in which the GAL4 gene under the control of the driver gene *apterous* was used to express CD8-GFP under UAS control. Figure 31 shows a representative temporal series of the expression pattern of apterous in a left wing disc over time, beginning with an image of a second instar wing disc in which only a few cells express *apterous*. In the following images, *apterous* is induced in the cells proximal of the region of first expression. In Image D, at 40(1) hours AFI, the larva has entered the third instar. The DV boundary is still rough, whereby the roughness appears to be the result of non-oriented cell divisions. By 64(1) hours AFI (Image F), the D/V boundary has smoothened and looks well-defined. The scale bar is again 50 µm in all the images.

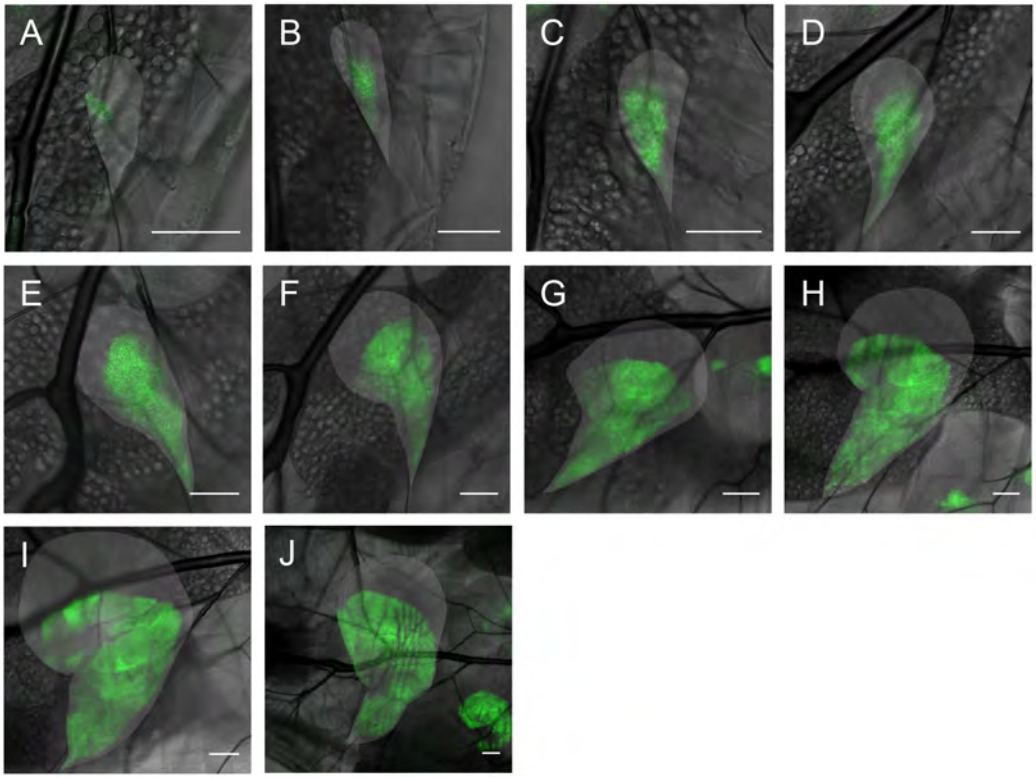

Figure 31: Temporal development of the *apterous* expression pattern in a left wing disc. A: Second instar wing disc. B: 16(1)h AFI. C: 24(1)h AFI. D: 40(1)h AFI. E: 48(1)h AFI. F: 64(1)h AFI. G: 72(1)h AFI. H: 88(1)h AFI. I: 96(1)h AFI. J: 112(1)h AFI. Scale bars: 50 µm.

Fig. 32 shows the development of the DV boundary over time for the larva shown in Fig. 31. The dashed line indicates the WN boundary and the scale bar is 50 µm.

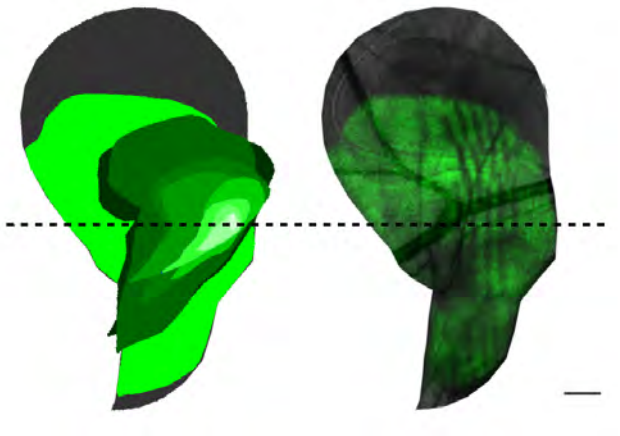

Figure 32: Development of the DV compartment boundary. Scale bar: 50 µm.

Figure 33 shows the typical development of the *apterous* expression pattern in a haltere disc, beginning with a first instar left haltere disc which does not yet express *apterous*. By Image B, at 16(1) hours AFI, the larva is in the second instar and *apterous* is being expressed. In Image F (64(1) hours AFI), the larva has entered the third instar while in Image G (72(1) hours AFI) it can be recognized that the D/V boundary is not yet smooth. By the middle of the third instar (Image H: 88(1) hours AFI), the D/V boundary has smoothened and looks well-defined. The scale bar is 50 µm in all the images.

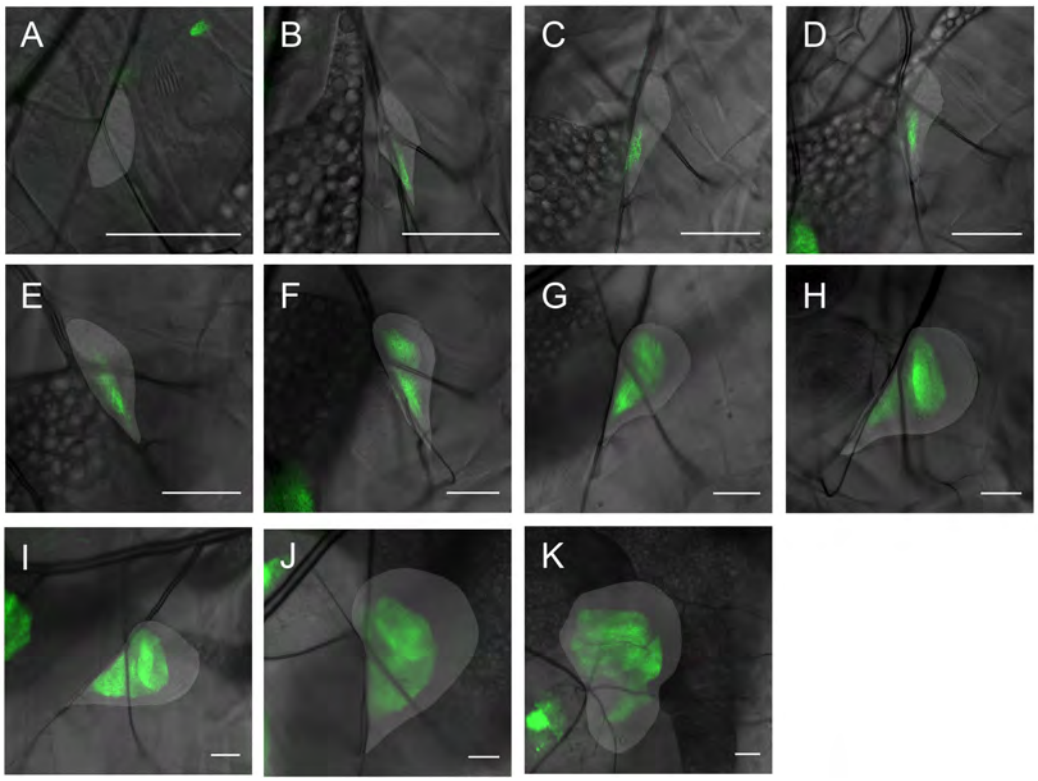

Figure 33: Temporal development of the *apterous* expression pattern in a left haltere disc. A: First instar haltere disc. B: 16(1)h AFI. C: 24(1)h AFI. D: 40(1)h AFI. E: 48(1)h AFI. F: 64(1)h AFI. G: 72(1)h AFI. H: 88(1)h AFI. I: 96(1)h AFI. J: 112(1)h AFI. K: 120(1)h AFI. Scale bars: 50 µm.

Apterous appears to be induced independently in the wing and haltere discs, as well as in the right and left wing discs, as can be seen from Figs. 34 and 35. Fig. 34 shows the wing and haltere discs of the larva imaged in Fig. 31, whereby only the wing disc shows expression of *apterous*. Both images were taken with the same gain settings within one minute. Fig. 35 shows the right and left wing discs of a different larva. In this case, only the right wing disc shows *apterous* expression. The two images were again taken with the same gain settings, the time difference was about 10 minutes, albeit other images taken within a time span of three minutes show the same result.

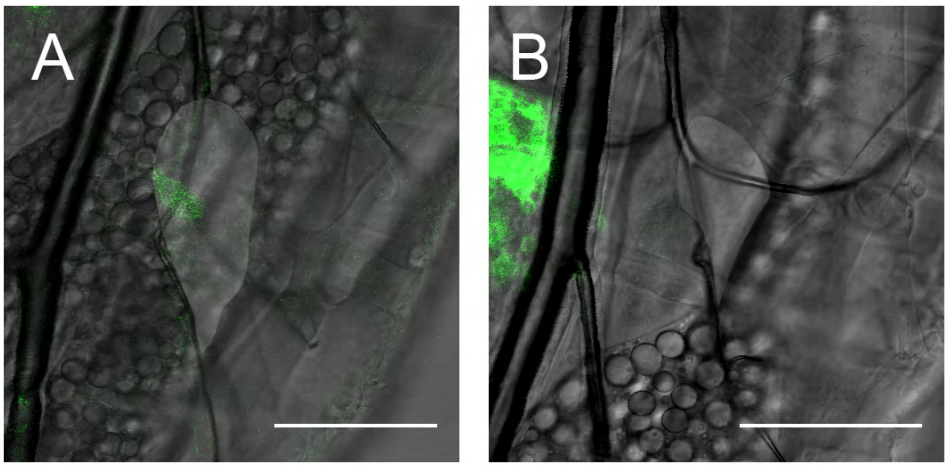

Figure 34: *Apterous* expression is induced independently in wing and haltere discs. A: Second instar wing disc showing *apterous* expression. B: Haltere disc of the same larva still lacking *apterous* expression. The scale bars are both 50 µm.

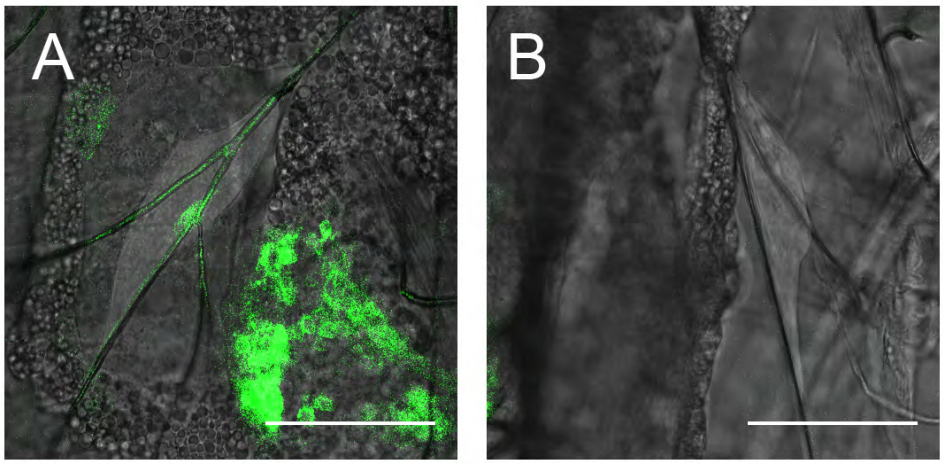

Figure 35: *Apterous* expression is induced independently in the left and right wing disc. A: Second instar right wing disc showing one cell expressing *apterous*. B: Left wing disc of the same larva still lacking *apterous* expression. Scale bars: 50 µm.

When *apterous* is first expressed, it is only observed in one or two cells (see Figs. 35 and 36). Oftentimes it is expressed in a posterior region near the tracheal fork and WN boundary.

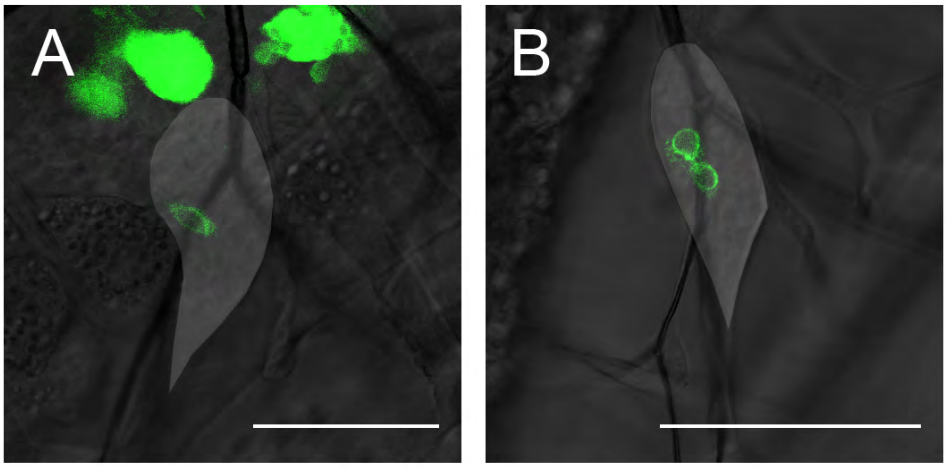

Figure 36: Early apterous expression.

The domain of *apterous* expression then increases, first mainly filling out the proximal region (see Fig. 32). Plotting the area of the entire wing disc against the area of *apterous* expression for many different wing discs in a log-log plot leads to Fig. 37. Data for the three larval instars is indicated in red, green and blue. The black data points indicate dissected discs for comparison, whereby the third instar data is from Raeppli wing discs. The in and ex vivo data is in agreement. The turquoise data points show the sizes of single cells in wing discs which showed *apterous* expression in 1-2 cells. Wing discs lacking *apterous* expression were assigned an area of *apterous* expression of 1 µm in order to appear in the log-log plot. It can be seen that the *apterous*-expressing region grows faster, in comparison to the wing disc area, until the second molt.

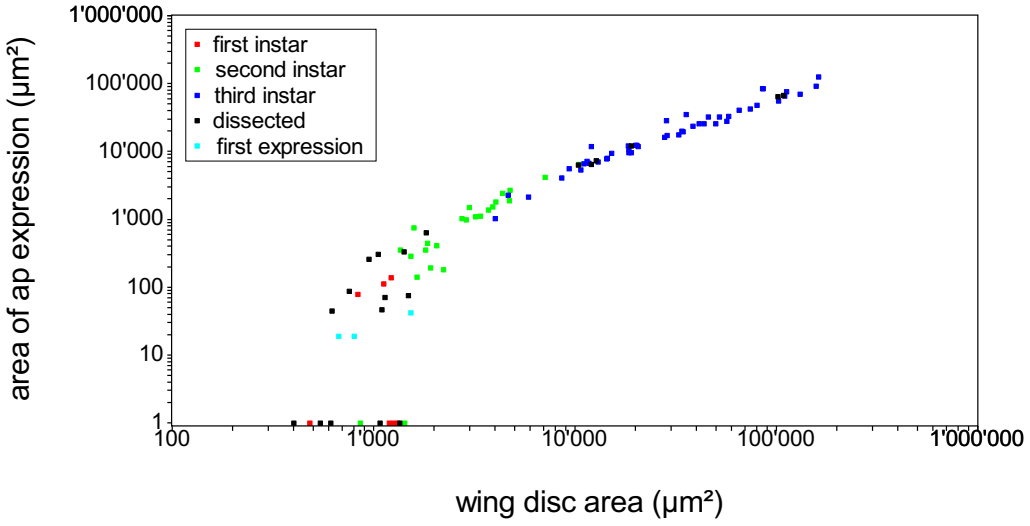

Figure 37: Wing disc area as a function of the area of *apterous* expression, by instars.

Fig. 38 shows some of the same data as Fig. 37, except that the data is not shown by instars, but by larvae. This figure illustrates that each larva individually shows the change in growth rate after the second molt.

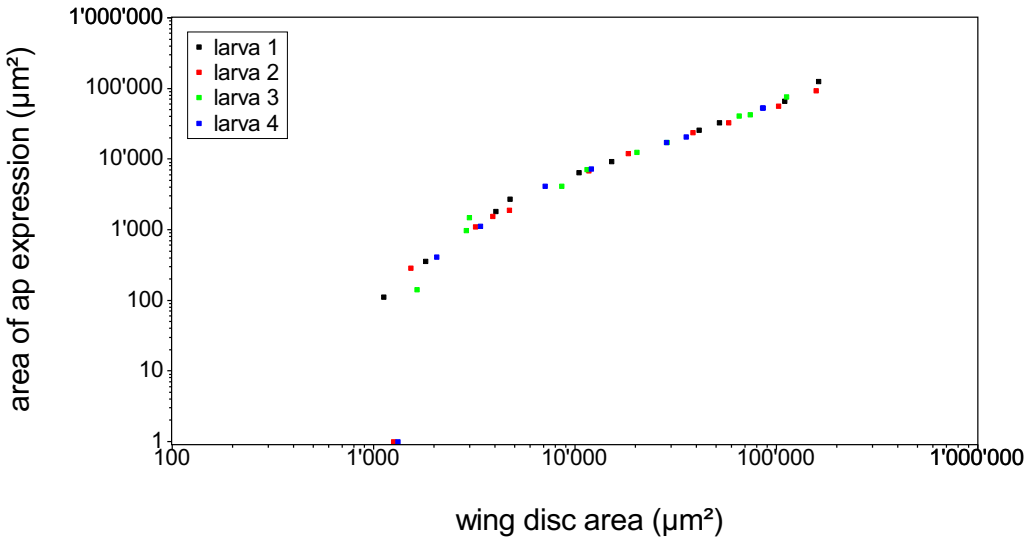

Figure 38: Wing disc area as a function of the area of *apterous* expression, by larvae.

Generally, *apterous* appears to be induced in the late first or early second instar when the wing disc has an area of about $10(1) \cdot 10^2$ µm^2. Once *apterous* expression has been induced, the area of *apterous* expression grows faster than the wing disc area until the disc reaches an area of about 10,000 µm^2 at around the time of the second molt. This can be seen by the slope of the graph at this time (> 1). In the greater part of the third instar, both areas grow at the same rate, as can be recognized by the slope of one found at this time, with the area of apterous expression making up around 60% of the entire wing disc area (see Fig. 39).

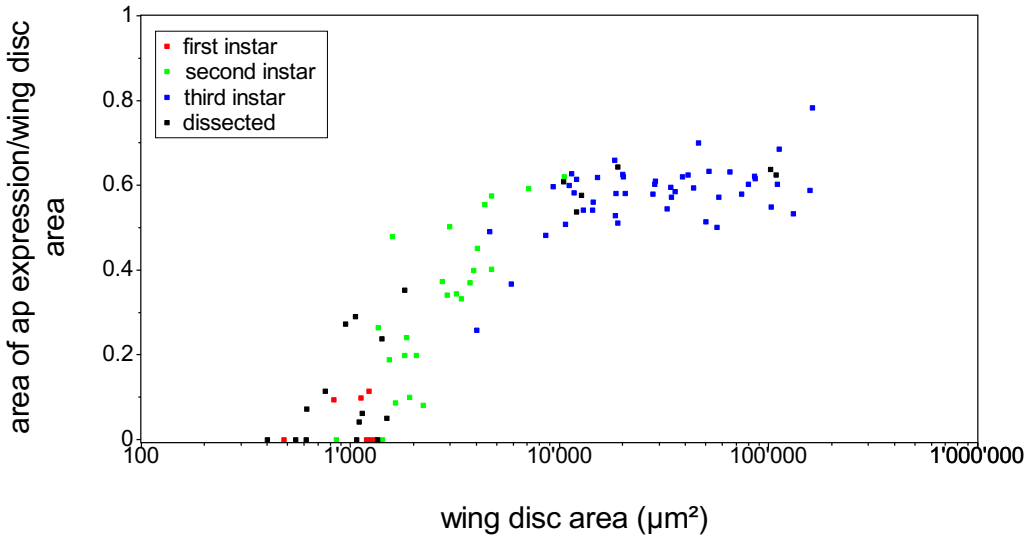

Figure 39: Wing disc area as a function of the ratio of the area of *apterous* expression to the wing disc area.

Apterous is oftentimes first induced in only one or two cells, in an area of the disc which is prone to mechanical stress, at a time shortly before the maximum in cell area is reached. This may indicate that *apterous* induction is linked to mechanical forces. To assess this possibility, wing discs with little *apterous* expression were dissected, imaged, stretched and imaged once more, typically about 5 minutes later, using the same gain settings and number of slices.

Figs. 40 and 41 show results for two wing discs manipulated in this way. The wing disc in Fig. 40A shows one brightly fluorescing cell, indicating *apterous* expression. Fig. 40B shows the same wing disc with considerably more fluorescence after being stretched, including at least two newly fluorescing cell outlines (white arrow), near the remains of the trachea (black arrow). The trachea likely adhered to the microscope slide during the stretching process, leading to the exertion of additional stretch on the cells in its vicinity.

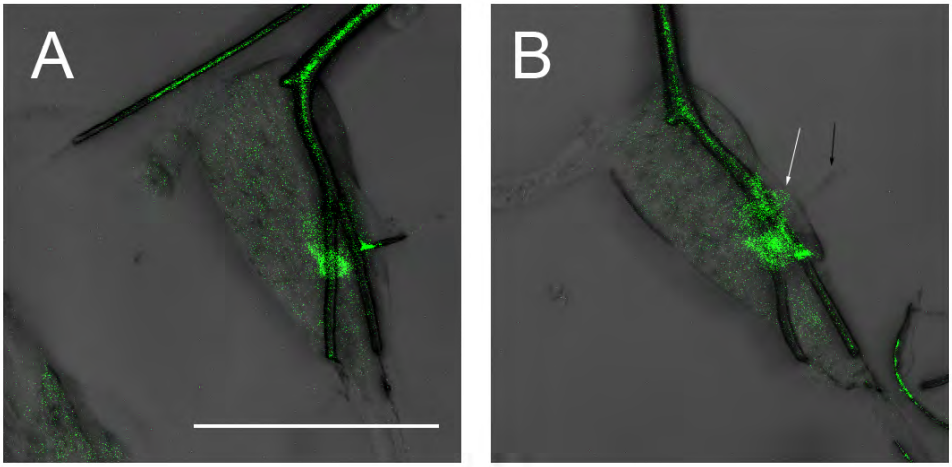

Figure 40: Increase in fluorescence upon stretching. A: Wing disc showing one cell expressing GFP. B: The same wing disc after being stretched, showing an increase in the area of GFP expression (white arrow). The black arrow indicates the tracheal remains. The scale bar denotes 50µm and applies to both images.

Fig. 41A shows a wing disc (right) and a haltere disc (left) with first *apterous* expression. Fig. 41B shows the wing disc after stretching, showing additional fluorescence (white arrow) near the trachea (black arrow) which may have exerted additional stretch on the cells in its vicinity.

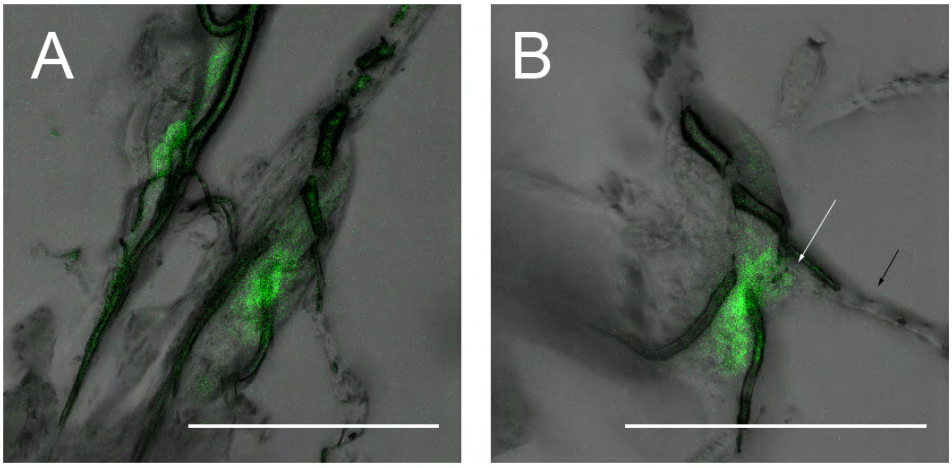

Figure 41: Increase in fluorescence upon stretching. A: Wing (right) and haltere (left) discs showing GFP expression. B: The wing disc after being stretched, showing an increase in the area of GFP expression (white arrow). The black arrow indicates the trachea. The scale bars denote 50µm.

Raeppli Flies

To gain further insight into the development of the dorsal compartment, Raeppli wing discs were imaged. Fig. 42 shows wing discs which were dissected from Raeppli larvae. Blue indicates the expression of TFP, green the expression of m-Orange2 and red the expression of mKate. The other colors result from overlaying these channels and indicate cells which express two different fluorescent proteins. Areas which remain black most likely express TagBFP, which could not be excited since the necessary laser line was not available.

Images A and B show two different younger wing discs with larger, possibly longitudinal, clones in the notum and smaller clones in the hinge. M-Orange (green) cannot yet be detected, probably due to a longer maturation time. The late third instar wing discs in C and D confirm these observations: the clones appear larger in the notum and smaller closer to the wing margin.

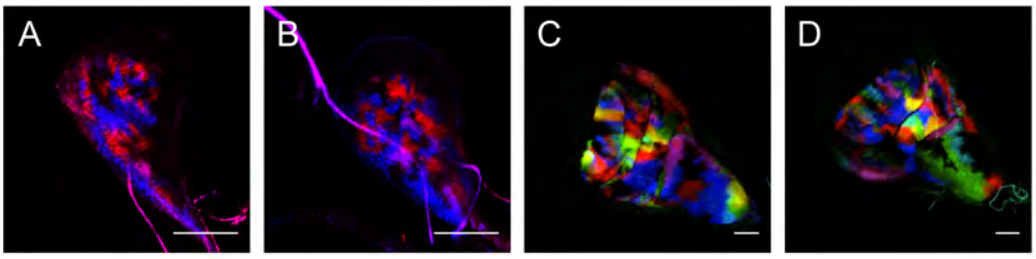

Figure 42: Raeppli wing discs showing larger clones in the notum. Red: mKate, green: m-Orange2, blue: TFP, black: TagBFP or unlabeled. The scale bars are 50 µm.

5.3 Growth Anisotropies

The wing disc does not grow uniformly in time, as was seen above. In this section results concerning spatial growth anisotropies are presented. While the published results pertaining to spatial growth anisotropies mentioned above assess growth in terms of cell numbers, areas are looked at here.

5.3.1 Single Cell Clones

To asses the mitotic behavior of wing disc cells, clones were induced in the early stages of wing disc development. Figs. 43 and 44 show the development of altogether three disc proper clones from the second instar to the third instar.

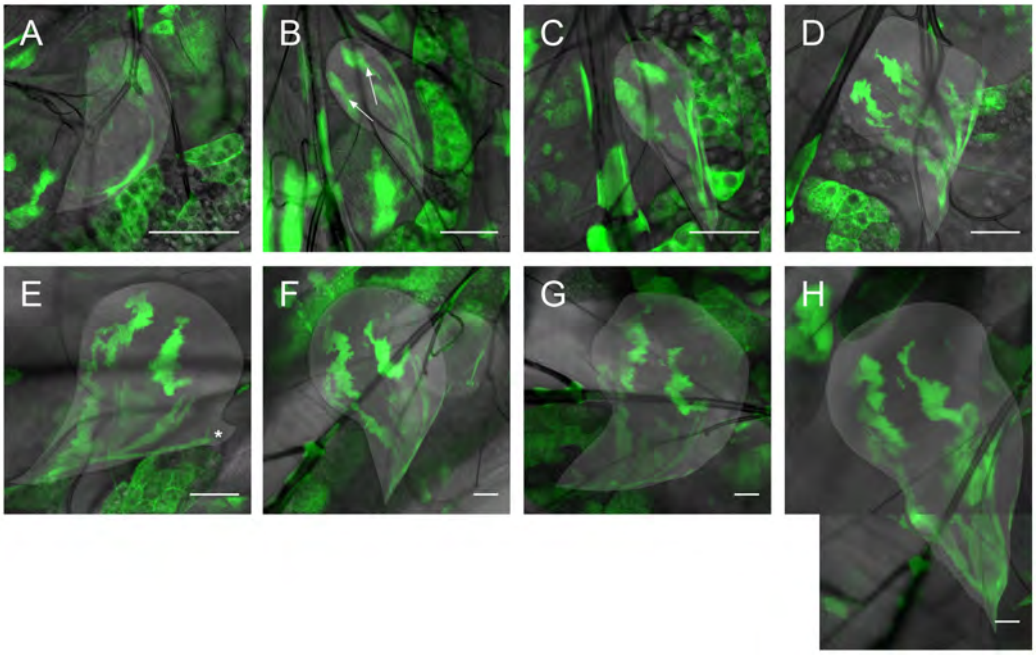

Figure 43: Temporal development of single cell clones in the pouch region of a left wing disc. A: Second instar wing disc. B: 16(1)h AFI. C: 24(1)h AFI. D: 40(1)h AFI. E: 48(1)h AFI. F: 64(1)h AFI. G: 72(1)h AFI. H: 88(1)h AFI. Scale bars: 50 µm.

The wing disc shown in Fig. 43 exhibits two clones in the wing pouch of the disc proper, indicated by the white arrows in Image B. The clones in the notum are not considered in the following since they are part of the peripodial membrane. Image A shows the wing disc with early fluorescence, the clones are not yet readily identifiable. On a side note, the long time span until GFP expression was sufficient is the reason why clones could not be followed from the first larval instar on. It may be possible to overcome these difficulties by keeping the flies at 29°C after heat shocking. In Image B, the clones are discernible. Conspicuously, the clones in both the peripodial membrane and the disc proper are longitudinal in shape. In Image C, the larva is near the second molt as can be recognized by the trachea. In the next image, the larva has molted and is in the third instar; the

wing disc is deformed by its proximity to the trachea. The attachment point of the muscle fiber, which exerts a pulling force on the wing disc in the early third instar, can be recognized in Image E (*). The scale bar is 50 µm in all the images.

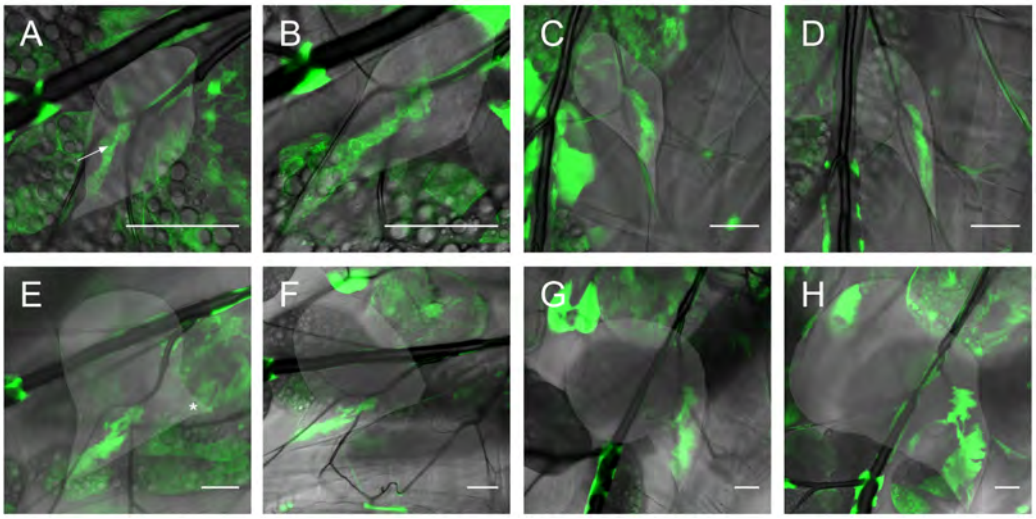

Figure 44: Temporal development of a single cell clone in the notum of a left wing disc. A: Second instar wing disc. B: 6(1)h AFI. C: 24(1)h AFI. D: 32(1)h AFI. E: 48(1)h AFI. F: 57(1)h AFI. G: 79(1)h AFI. H: 96(1)h AFI. Scale bars: 50 µm.

The second instar wing disc shown in Fig. 44 exhibits one, again strikingly longitudinal, clone in the notum of the disc proper, indicated by the white arrow. Slides showing the peripodial membrane were removed before making z-projections of the fluorescent channel because a clone in the peripodial membrane overlapped the disc proper clone shown. In Image D, the larva is near the second molt. In Image E, it has molted and the attachment point of the muscle fiber is again recognizable (*). Image F shows a slightly deformed wing disc - it was most likely held in an unnatural position by the immobilization process. The scale bar is again 50 µm in all the images.

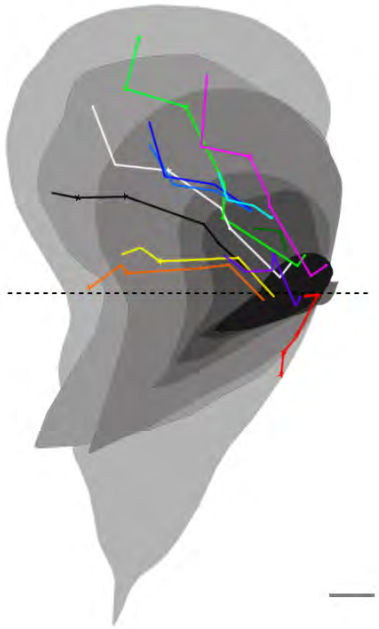

Figure 45: Growth trails. The dashed line indicates the WN boundary; the scale bar is 50 µm.

In Fig. 45 the growth trails for several recognizable points of the single cell clones in Fig. 43 are shown. The dashed line indicates the WN boundary.

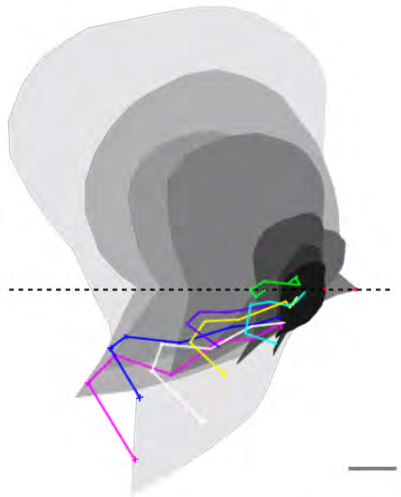

Figure 46: Growth trails. The dashed line indicates the WN boundary; the scale bar is again 50 µm.

Fig. 46 shows the growth trails for several recognizable points of the single cell clone in Fig. 44. The dashed line again indicates the WN boundary.

Common to both images is the fact that cells appear to maintain their positions in respect to the WN boundary. Cells which are proximal of the WN boundary in the second instar, remain proximal of it until pupation; cells which are distal of it in the second instar, remain so until the end of larval development.

Concerning the notum, both images have in common that this region appears to grow in width more than in length in the third instar. Furthermore, most of this growth seems to take place in the anterior compartment (see Fig. 30). Also, the notum increases in area more slowly than the disc as a whole until at least the third instar as can be seen from Figs. 47 and 48.

In Fig. 47 the area of the notum is plotted as a function of the area of the wing disc for the two single cell clone larvae as well as for five engrailed larvae. The slope of the curve is below one until the second molt.

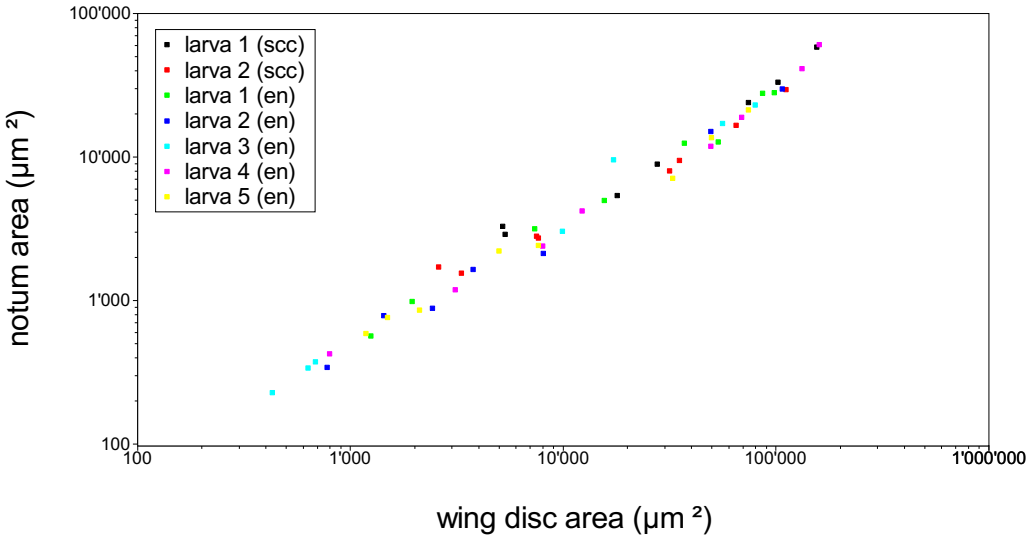

Figure 47: Area of the notum as a function of the wing disc area.

In Fig. 48 the ratio of notum to wing disc area as a function of the wing disc area is plotted. The ratio is about 0.55 in the mid to late first instar and decreases to about 0.3 by the beginning of the third larval instar. During the third instar, the ratio remains nearly constant, indicating that the notum grows at the same rate as the entire wing disc at this time.

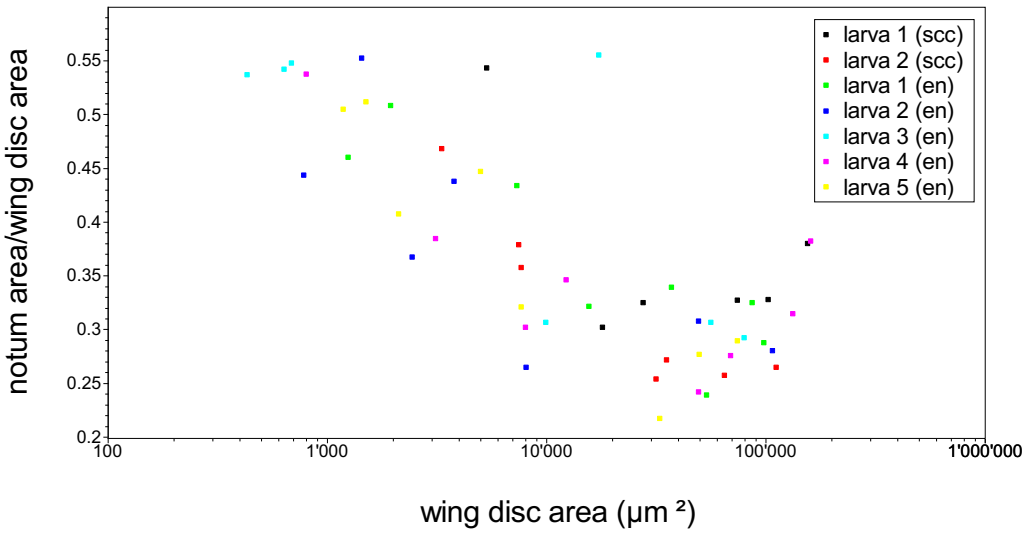

Figure 48: Ratio of notum to wing disc area as a function of the wing disc area.

Another growth anisotropy in the wing disc concerns the ventral compartment and the wing pouch region. The ventral compartment does not appear to grow significantly in area until the early mid-third instar when the pouch also begins to increase in area, growing out in a radial fashion. This is depicted in Fig. 49 which shows the approximate location of the wing pouch at each point in time (white areas), as estimated by the shapes of the clones, working back from Image H.

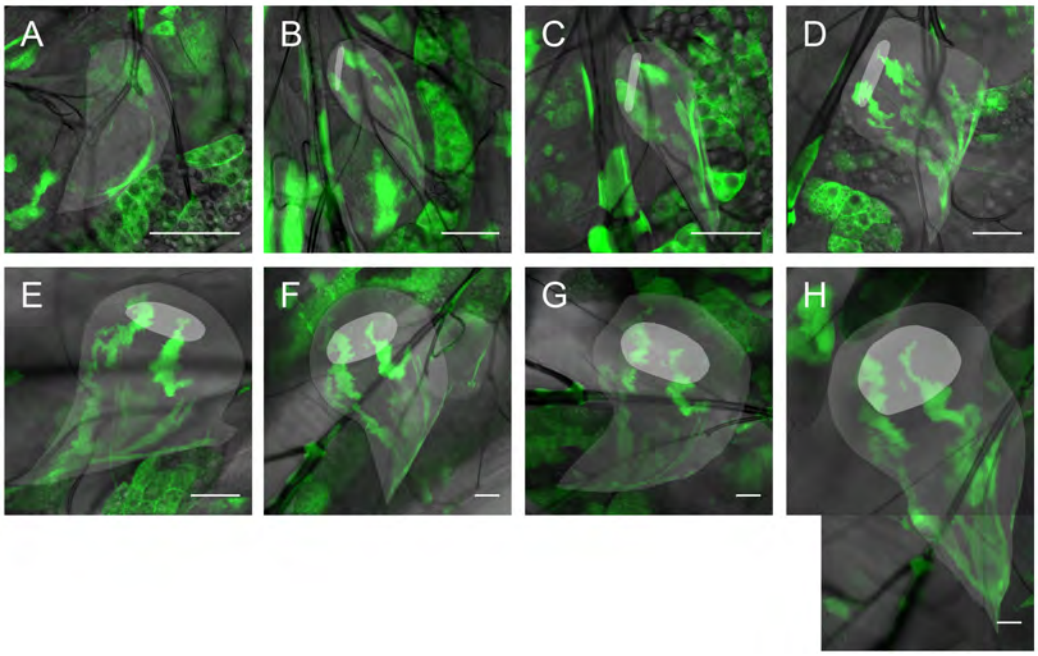

Figure 49: Growth of the wing pouch. The wing pouch is indicated by the white areas. The scale bars denote 50 µm.

5.4 External Stresses

The wing imaginal disc develops as part of the drosophila larva and, as such, is necessarily connected to it by tissues such as trachea or muscle fibers. Such external tissues may well play a role in the growth of the wing disc by exerting external forces upon it. In the following section the connective tissues observed during this thesis are presented.

The wing disc is most distinctly attached to the second thoracic lateral tracheal branch. Throughout larval development, the same characteristic part of the tracheal branch is in contact with the wing disc. This part is illustrated by the green dotted line in Fig. 50. It ranges from the 'knee' (black arrow) along the trachea shown, whereby it is possible that stretches of trachea in the central region are not in (permanent) contact with the wing disc, and was determined from a combination of in-vivo imaging results and dissection experiments. The distal end of first and early second instar wing discs begins below the knee. Since opposite ends of these early wing disc are in contact with the trachea, growth of the trachea likely has large effects on early wing disc growth.

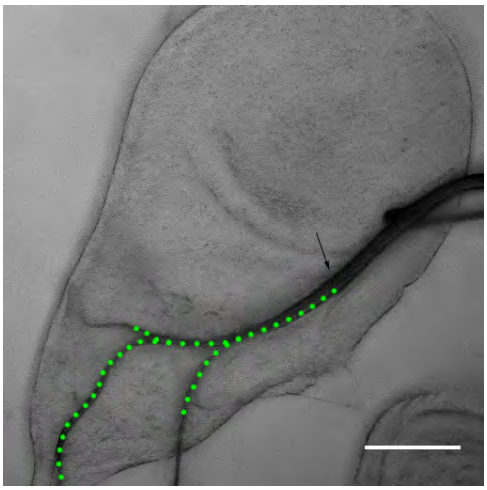

Figure 50: The part of the tracheal branch which is attached to the wing disc throughout the entire larval stage is indicated by the green dotted line. The scale bar is 50 µm.

Besides being connected to the trachea, the wing disc is connected to the cuticle by *twist*-expressing cells which probably make up the peripodial stalk and may be attached to, or surround, the trachea at the proximal end of the wing disc. Fig. 51 shows the fluorescent *twist*-expressing cells, indicated by the white arrow, which attach the wing disc (wd) to the larval cuticle.

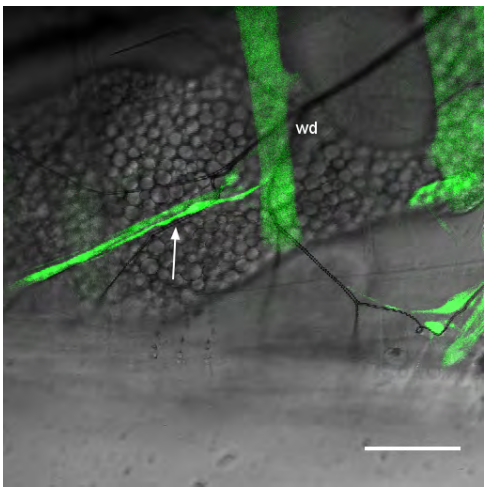

Figure 51: *Twist*-expressing cells (white arrow) connect the wing disc (wd) to the larval cuticle. Scale bar: 50 µm.

The *twist*-expressing cells, possibly in conjunction with the trachea, appear to exert a pulling force on the proximal end of the wing disc, since dissected first and early second instar wing discs tend to become rounder in comparison to wing discs in vivo. Fig. 52A shows a dissected wing disc (right) with a few *apterous*-expressing cells. It is round in shape. Upon stretching (Image B), the wing disc takes on the shape it characteristically shows in vivo. The same behavior is seen in the haltere disc (left) on the neighboring tracheal branch.

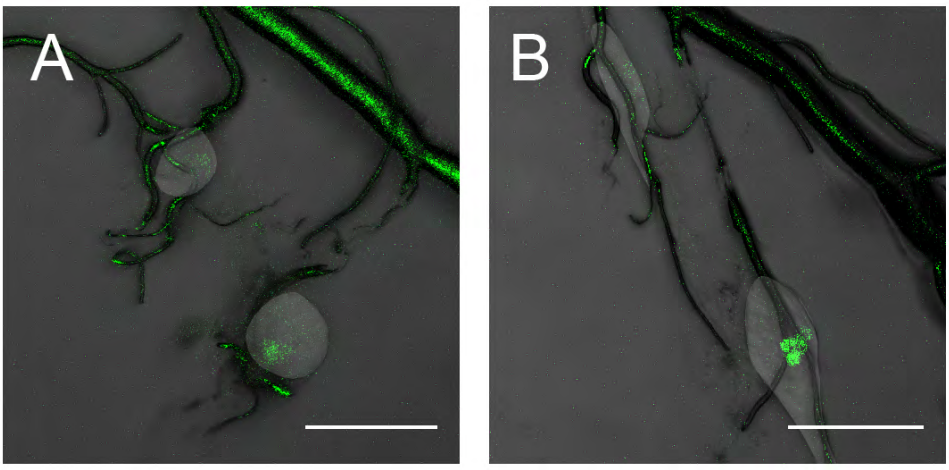

Figure 52: *Twist*-expressing cells exert a pulling force on the wing disc (right). A: Round dissected wing disc. B: The same wing disc when stretched. Scale bars: 50 µm.

The distal end of the wing disc is also connected to several fibers. One or two fibers are attached to the tracheal knee, outline the distal anterior segment of the wing disc and appear to be spanned down to the cuticle (white arrows in Fig. 53).

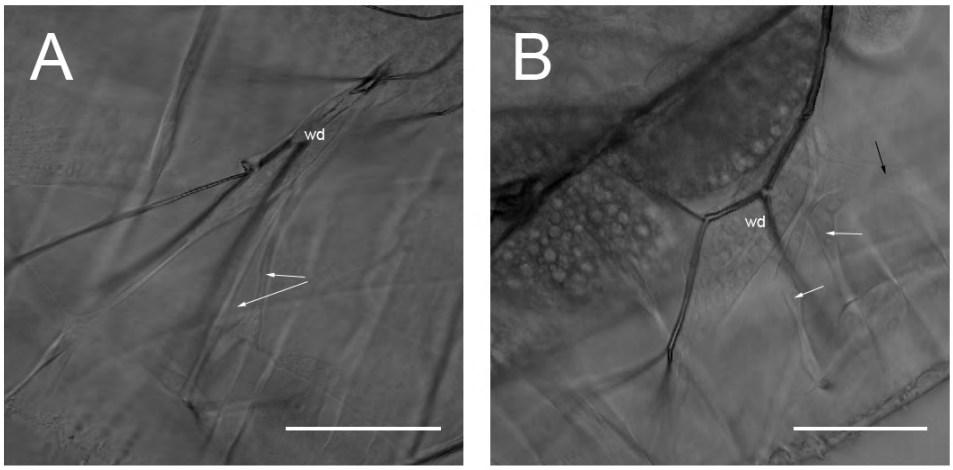

Figure 53: Fibers which attach the wing disc to the cuticle (white arrows) and the muscle fiber which attaches it to the leg and haltere discs (black arrow). Scale bar: 50 µm.

A muscle fiber, which is not observed until the second instar, attaches the wing disc(wd) to the leg(ld) and haltere(hd) discs (black arrow in 53). This muscle fiber most likely also begins at the knee and appears to be located closer to the cuticle than the other fibers, as can be seen in Fig. 54, which shows two consecutive slices of a z-stack. In Image A, the muscle fiber can be seen exerting a force on the wing disc (black arrow). Image B, which is slightly further into the larva, shows a fiber (white arrow) which starts at the knee, outlines the distal wing disc and is spanned to the cuticle (compare Fig. 53).

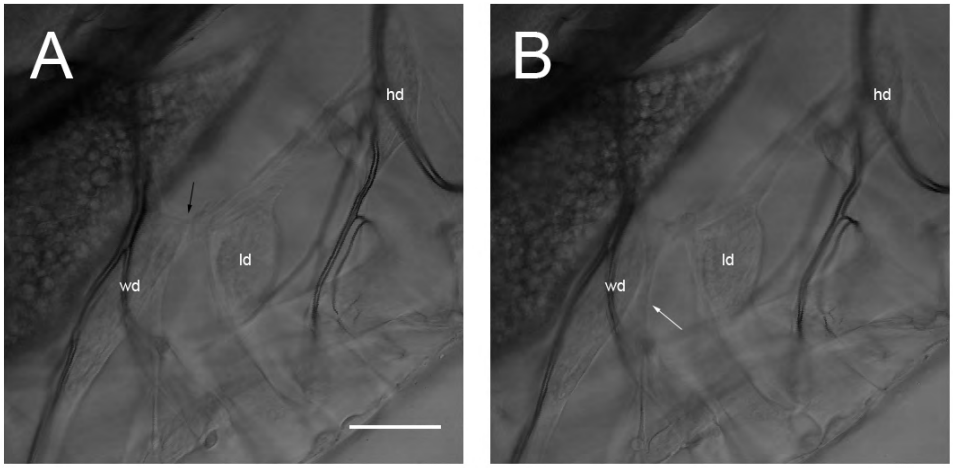

Figure 54: A muscle fiber (black arrow) attaches the wing disc(wd) to the leg(ld) and haltere(hd) discs. A: The wing disc is stretched over the fiber shown in B. B: Single slice showing an outlining fiber. Scale bar: 50 µm.

The muscle fiber which connects the wing, leg and haltere discs attaches to the wing disc at the WN boundary as can be seen in Fig. 55. In these z-projections (Min Intensity) of transmission stacks the muscle fiber is indicated by the white arrows, the knee by the black arrows. The scale bar is 50µm and applicable to both images. In the right image the wing disc was stretched far beyond its natural state for clarification. The area inside the rectangle shows data from only the most basal slice to explicitly show the fiber which outlines the first and early second instar wing discs and is later covered by wing disc tissue. It is possible that the rest of the anterior edge of the wing disc is also outlined by a fiber. This is supported by the fact that the proximal tip of dissected third instar wing discs faces anteriorly, contrary to what is observed in vivo, which it would if this area was stretched in vivo.

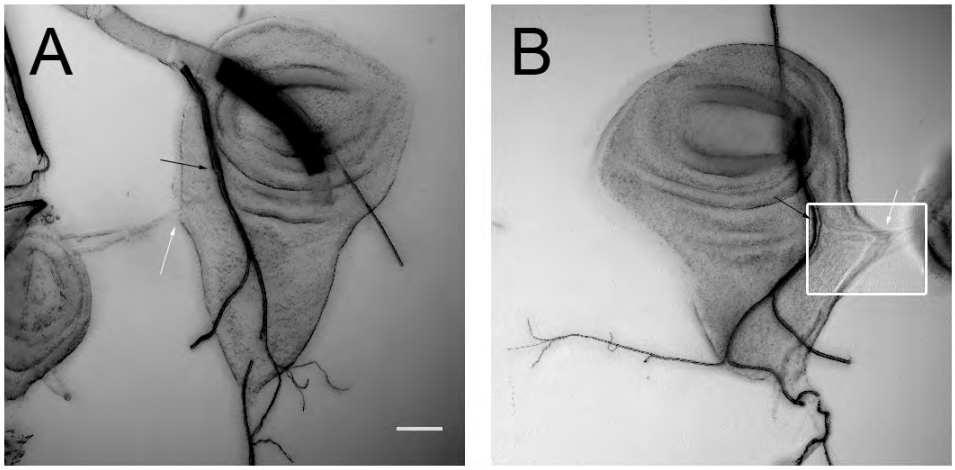

Figure 55: Attachment point of the muscle fiber in late third instar wing discs. A: Right E-Cadherin-GFP III wing disc. B: Left twist wing disc. Scale bar: 50 µm.

In order to assess the stretching of the wing disc due to the muscle fiber, the apical cell areas were studied. Fig. 56 shows three collages of different left third instar E-Cadherin-GFP III wing discs arranged by size. The scale bar is 50µm and applicable to all three images. The red asterisks indicate the attachment point of the muscle fiber.

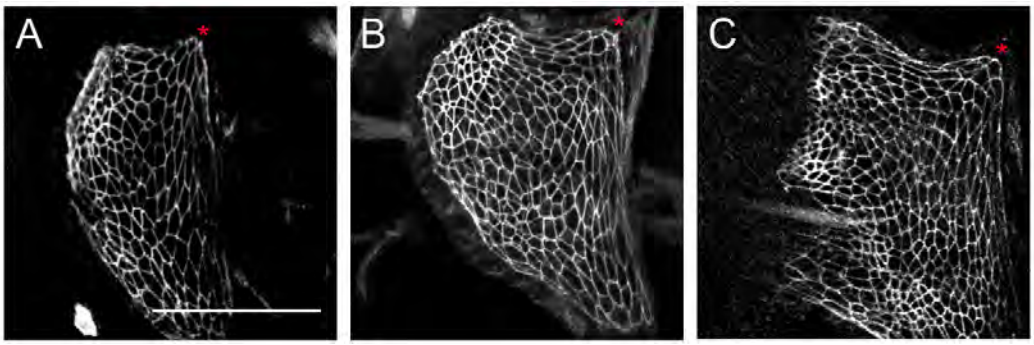

Figure 56: Cell outlines in different third instar wing discs. A-C: The attachment point of the muscle fiber is labeled by the red asterisks. Scale bar: 50 µm.

The wing disc from Fig. 56B is shown again in Fig. 57A as a composite image made up of the fluorescent and the transmission channels (and turned clockwise by 90°). The scale bar is again 50µm. In Fig. 57B, the apical cell areas, which range from 2µm^2 to 33µm^2, are coded in grayscale with lighter shades of gray indicating larger cell areas. Fig. 57C shows the strain ellipses for each cell.

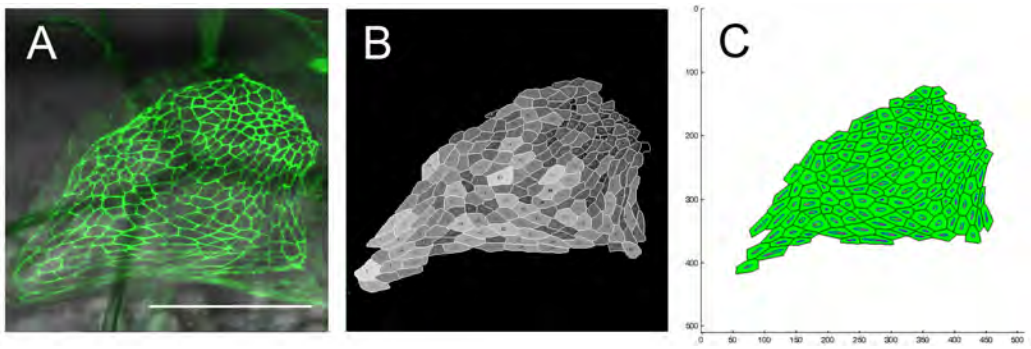

Figure 57: Early third instar wing disc. A: Composite image. B: Cell areas coded in grayscale - lighter shades of gray indicate larger cell areas. C: Strain ellipses. Scale bar: 50 µm.

Cell areas appear to be larger and under more strain between the attachment points of the muscle fiber and the *twist*-expressing cells. The cells with the smallest apical cell areas and lowest strain are found at the distal tip of the wing disc. This data indicates that the muscle fiber exerts a pulling force on the disc. This can also be observed in vivo. Fig. 58 shows two consecutive slices of a z-stack - the distal end of the wing disc points downwards in these images. In the time it took to take the images, the configuration of the muscle fiber, indicated by the white arrow, changed from contracted (Image A) to relaxed (Image B). Image C shows an overlay of the fluorescence of the fiber at the two time points. The contraction can be recognized in the different overall lengths of the fiber as well as the shortened distance between the ridges. The same behavior was also observed ex vivo.

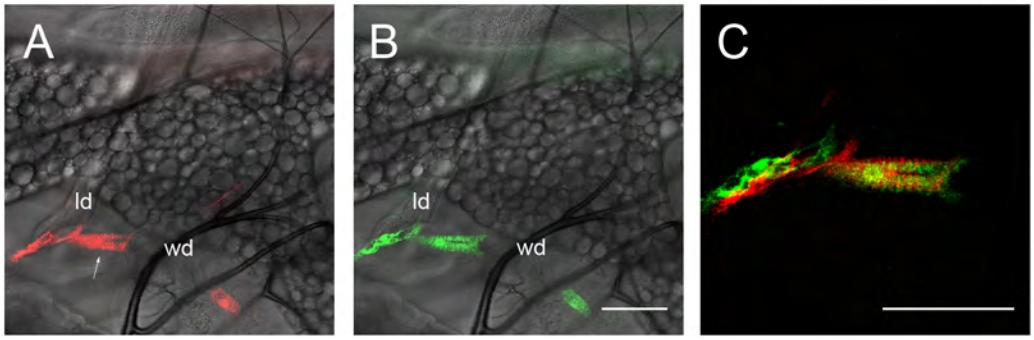

Figure 58: A: Fluorescent muscle fiber (white arrow) between the wing(wd) and leg(ld) discs the distal end of the wing disc points downwards. The fiber is contracted. B: The fiber is more relaxed. C: Overlay of the fluorescent fibers indicating the difference in the configurations. Scale bars: 50 µm.

In order to confirm that the muscle fiber does indeed exert a pulling force on the wing disc, wing discs were first imaged in-vivo, then dissected. Fig. 59 shows the same early third instar E-Cadherin-GFP III wing disc in vivo and after dissection - some slices showing the peripodial membrane were removed for clarity. Image B shows a clear relaxation of the entire disc; this relaxation is also seen in the cell outlines. The scale bar in the right image is 50µm and applies to both images. The red x marks the same spot in both images for comparison. The white arrow in the upper right-hand corner of Image A indicates the muscle fiber which attaches the wing disc to the leg and haltere discs while the arrow in the lower left-hand corner points to a 'mini thread'.

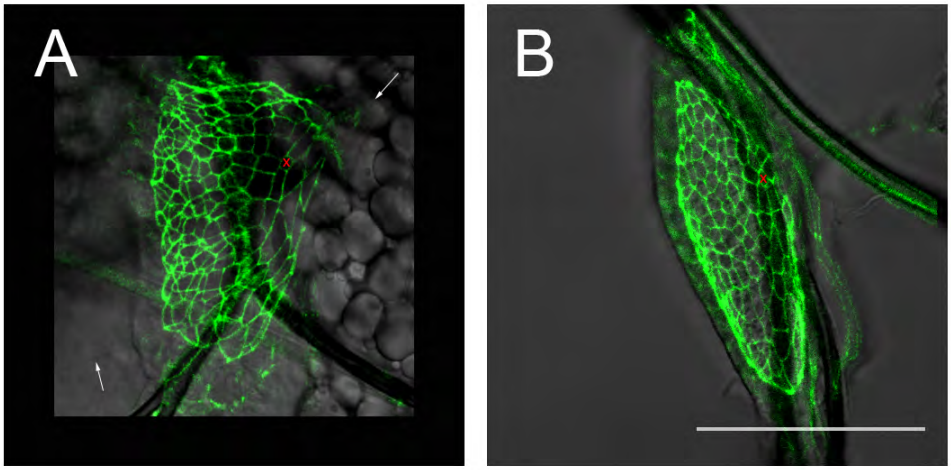

Figure 59: E-Cadherin-GFP wing disc. A: In vivo, stretched. The muscle fiber (white arrow, upper right) and a 'mini thread' (white arrow, lower left) are indicated. B: After dissection, relaxed.

A further source of external mechanical stress on wing discs are 'mini threads'. Mini threads are filaments which appear to attach to the edge of the wing disc during early development, especially in the posterior proximal region, although it cannot be excluded that they are found at later times and in other areas as well. Fig. 60 shows examples of mini threads in apterous larvae, indicated by the white arrows. In Image A, *apterous* is just beginning to be expressed, interestingly, in the region where the mini thread is pulling. The wing disc in Image B is being stretched by several mini threads.

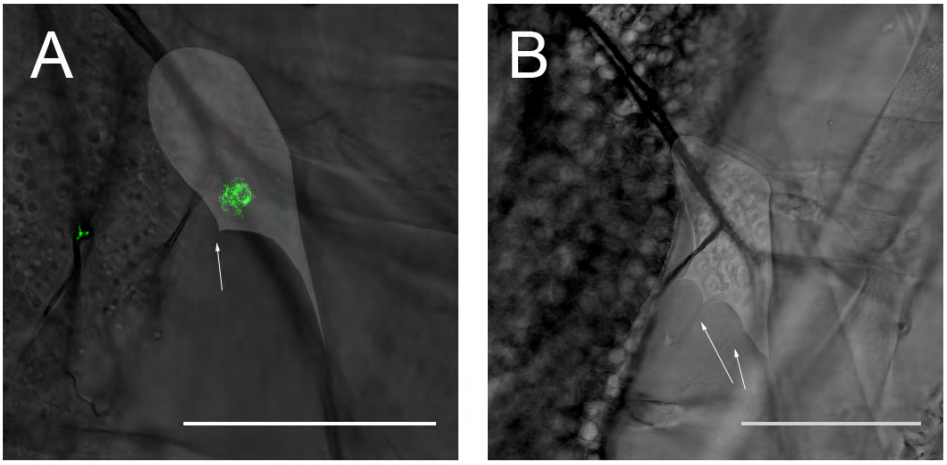

Figure 60: Examples of mini threads (white arrows) attached to wing discs. Scale bar: 50 µm.

6 Discussion

In this chapter the experimental results which were presented in the last chapter are discussed. Wing disc growth, wing disc patterning and external stresses will be examined separately before an attempt is made to unify the results.

6.1 Wing Disc Growth

Wing disc growth was directly assessed in terms of wing disc and average apical cell areas using in-vivo imaging. These parameters were then used to calculate cell numbers and proliferation rates as functions of time. These results are discussed in this section.

In order to assess whether larvae developed normally, despite being imaged in-vivo, apical wing disc growth was evaluated. It was seen that growth rates differ between larvae as well as temporally for single larvae, findings which indicate a role for external factors in wing disc growth. At the same time, the temporal variations observed were found to follow a general pattern: there is little growth in the first instar, exponential growth during the second and early third instars, before growth decreases in the second half of the third larval instar. A case for normal development is supported by the fact that, upon taking into account the longer larval stage due to the lower temperature and incorporating how the apical and total wing disc areas differ, the data for the temporal development of the average apical wing disc area (see Fig. 22) is in agreement with published data for the mid-second to late third instars [84], within errors.

Besides the temporal development of the apical wing disc area, the temporal development of the average apical cell area was assessed. The data in Fig. 23 shows that the average apical cell area increases by a factor of about five in the first and early second instars. The average thickness of the epithelial layer, in the central region of the wing disc where most early apical cell areas were determined, is approximately constant at this time, within errors - although individual values may differ by a factor of about two. The increase in apical cell area thus

necessitates an increase in cell volume. This in agreement with Madhavan and Schneiderman who found that wing disc cells increase in volume by a factor of six before mitosis resumes and cell volumes decrease [16], although there are certain discrepancies regarding the exact timing.

Apical cell areas appear to be similar in size in the first instar (see Fig. 24), yet only few cells located in the centers of different wing discs were taken into account, so that this statement should be treated with caution. In the second instar, the average apical cell area peaks before beginning to decrease, possibly in connection with the columnarization of the disc proper cells. The larger error bars at this time are most likely linked to the larger variance in cell areas in the second instar (see Fig. 24). In the third instar, the average apical cell area, as well as the variance, decrease with more cells becoming hexagonal [103] due to increasing internal growth regulation.

When the average apical cell area is plotted as a function of the apical wing disc area (see Fig. 25), it is seen that these parameters appear to be linked. In the first instar the plot has a slope of one, indicating a linear relationship between the two parameters. This means that the increase in wing disc area at this time is due merely to an increase in apical cell areas, as opposed to mitosis, and is in accordance with Madhavan and Schneiderman [16], at least for the first 15 hours of the first instar. This is shown more clearly in the data on the temporal development of the number of cells in the wing disc, which is constant within errors in the first instar. Beginning in the second instar, especially once the maximum cell area has been reached, the distribution of average apical cell areas becomes wider, as might be expected considering the larger variance in apical cell areas at this time. Differences in development between larvae may also have to be taken into account. In the third instar, the average apical cell area decreases as the apical wing disc area increases. Interestingly, wing disc development follows this curve, to a certain extent independently of instars, indicating that wing disc development and larval development are strongly linked, yet allow for a certain flexibility.

From the apical wing disc area and the average apical cell area of the disc

proper, the number of cells in the disc proper was calculated as a function of time. The cell number in the first instar was found to be about 12. Taking into account that cell areas from both future layers of the wing disc were used to calculate the average cell area at this stage when the cells are still indistinguishable, the cell number calculated here represents only half of the cells in the entire disc at this developmental stage. The total cell number is in accordance with [15] and [113].

The temporal development of cell numbers in the wing disc area could be described as asymmetrically sigmoid (see Fig. 26), in agreement with [13], again indicating that larvae imaged in-vivo develop normally. A comparison of these results with the histological analysis done by Madhavan and Schneiderman [16] and the cell numbers arrived at by Bryant and Levinson using dissociated discs [13] shows that the cell numbers calculated here are substantially lower. Reasons for this discrepancy may include the following:

- In the histological analysis by Madhavan and Schneiderman and the analysis using dissociated discs by Bryant and Levinson all the cells in the wing disc were counted [13, 16], while only the cells in the disc proper were calculated here. This argument plays more of a role in the second instar when peripodial membrane cells make up about one third of wing disc cells, as opposed to later development, when only one twentieth of the wing disc's cells belong to the peripodial membrane [20]. Martín et al. found a value of only 30,000 cells in late third instar wing discs [21], which is closer to the result arrived at here and also indicates that there is large uncertainty in the final number of wing disc cells.

- Until the early second instar, the wing disc appears to be an ellipsoid, as opposed to a flat structure. Calculating the number of cells using the projected wing disc area thus necessarily leads to a smaller number of cells. This remains a problem for cells at the edge of the wing disc throughout wing disc development, yet becomes ever less significant.

- Calculating the cell number using an average apical cell area only gives an estimate for the number of cells. In the second instar, cell areas vary

strongly (see Fig. 24) so that the number of cells calculated is quite dependent on the sample area which was chosen to calculate the average cell area.

- The apical wing disc area was oftentimes difficult to determine exactly. Errors due to deformations of the wing disc inside the larva or insufficient imaging may play a role, although they are likely within the given errors. Also, since wing discs were rarely imaged right before pupariation, they may not have reached their maximum size. Along the same lines, Aegerter-Wilmsen et al. found that the cells at the center of the pouch have an area of only about 3 μm^2 in the late third instar [97], again indicating the importance in the region chosen to measure the cell areas. The combination of these errors would suffice to explain the lower cell numbers.

The proliferation rate as a function of time shown in Fig. 27 was calculated the cell numbers at consecutive time points. It is zero, within errors, during the first instar, as would be expected from the results discussed above. The proliferation rate increases in the second instar, in agreement with [32], reaching its peak after the second molt, before decreasing during the remainder of the third instar, in accordance with [20].

The proliferation rate is correlated with the average apical cell area during the third instar (see Fig. 28), indicating that mechanical compression, which has been determined to be related inversely to the apical cell area [114], may negatively influence cell proliferation rates [9, 97]. Along the same lines, it was recently shown experimentally that mechanical stretching leads to higher proliferation rates [9] - the higher proliferation rate during the middle of larval development may thus be due, at least in part, to the stretching of the wing disc by the *twist*-expressing cells and the muscle fiber.

In summary, many published results on wing disc growth could be reproduced, although there are certain discrepancies concerning the exact timing and cell numbers. Overall, the results show that in-vivo imaging does not severely interfere with normal wing disc development.

6.2 Wing Disc Patterning

Wing disc patterning, especially in respect to compartment boundary formation, was assessed using in-vivo imaging of larvae showing fluorescence in cells expressing the selector genes *apterous* or *engrailed*. The results are discussed in the following section.

6.2.1 Engrailed Pattern

In order to assess whether in-vivo imaging has an effect on wing disc patterning, flies with fluorescence in cells expressing *engrailed* were imaged, since the development of the *engrailed* expression pattern is well documented. The data in Fig. 29 shows that the pattern of *engrailed* expression develops in the characteristic fashion, indicating that in-vivo imaging does not have an effect on wing disc patterning.

A conspicuous characteristic of the *engrailed* expression pattern is a kink found at the WN boundary, which appears to form in the early third instar. This kink indicates that factors besides a difference in adhesive properties [23, 37] play a role in the establishment of the AP boundary [38]. It is possible that one of these factors is the muscle fiber which is located at the WN boundary and pulls on the wing disc, most noticeably around the time of the second molt. While the wing disc mainly grows parallel to the second thoracic lateral tracheal branch until about the mid second instar, the hinge and wing pouch then begin to grow at an angle to this tracheal branch. This is underlined by the fact that the centroid of the wing disc, which remains in a rather constant position near the tracheal fork during the first and second instars, begins to move distally at this time. On a side note, the centroid may coincide with the region where regenerative ability switches its polarity, published by Bryant in 1975 [39]. The change in the direction of growth is possibly due to a combination of the growth factor Dpp, which is expressed in this region in an asymmetric fashion from the mid-second instar on [54, 66], as well as the pull of the muscle fiber. Fig. 61 illustrates this possibility. The two wing discs overlaid were outlined in Figs. 29D and E; the orange line shows where *dpp* is expressed. The red arrow in the bottom left-hand corner

represents the stress caused by the *twist*-expressing cells, while the three arrows on the right indicate the stress due to the muscle fiber, which possibly changes its angle as shown as the leg disc grows away from the cuticle - this is supported by the change in the tilt of the wing discs in Figs. 30 and 32. The forces exerted by the muscle fiber may lead to oriented cell divisions, causing cells to divide in directions radiating out from the attachment point of the muscle fiber. In this way, the posterior compartment forms half of the wing pouch in the third instar.

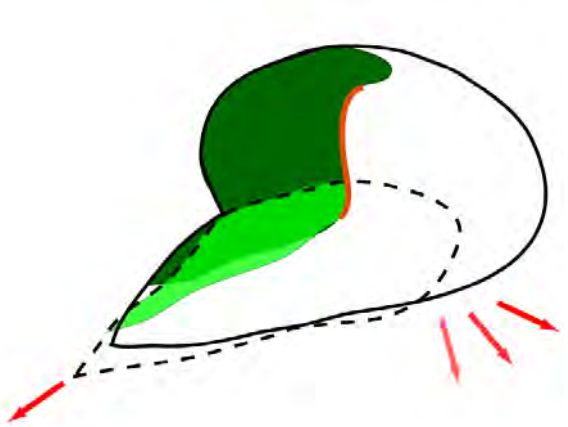

Figure 61: Illustration of a possible role for the muscle fiber in the formation of the kink in the AP compartment boundary.

6.2.2 Apterous Pattern

Having established that in-vivo imaging does not interfere with the patterning of the wing imaginal disc, the method was used to study the development of the DV compartment boundary. The results arrived at are discussed in this subsection.

The induction of *apterous* appears to be disc-autonomous, taking place independently in each wing and haltere disc of a larva at some time between the late first and mid second instars (see Figs. 34 and 35). This is a difficult statement to make since it can depend strongly on the gain settings as well as the angle of imaging chosen whether weak *apterous* expression becomes visible or not. Yet, first expression is oftentimes found in the same region, which would not be expected if it was only a question of choosing a high enough gain. Assuming that *apterous*

is indeed induced disc-autonomously implies that *apterous* is not induced via an external signal such as a hormone pulse, in agreement with the opinion arrived at by [62].

Wing discs appear to begin to express *apterous* in one or two cells when they reach an area of about 1,000 μm^2, as is shown in Fig. 37. On a side note, although wing disc areas are generally more difficult to determine without fluorescent labeling, this does not tend to be much of a problem in the first two instars. *Apterous*-expression begins at around this area, independent of the instar the larva is in, again supporting the idea that the induction of *apterous* is not linked to external factors such as ecdysone pulses. Since the apical disc and average cell areas are correlated (see Fig. 25), *apterous* induction at a certain wing disc area, and therefore average cell area, could indicate a role for mechanical forces in *apterous* induction, especially since it appears that *apterous* is first expressed near the peak in cell area. A role for mechanical forces in *apterous* induction is also suggested by the fact that the first *apterous*-expressing cells are oftentimes located in a distinct region of the wing disc which appears to be especially stress prone, lying between two tracheal branches and the *twist*-expressing cells (see Fig. 36). The stretching experiments which led to more GFP expression (see Figs. 40 and 41) also support this idea, although these results are difficult to interpret since the time span between the stretching and the increase in fluorescent signal is so short. It is thus possible that EGFR signaling, which is essential to wing formation between the mid first and mid second instars [61], is only permissive to *apterous* induction, while mechanical stretch is necessary. This would explain why EGFR is also active both before and after *apterous* induction [62].

Considering that the wing disc is already divided into an anterior and a posterior compartment when *apterous* is induced, *apterous* needs to be expressed in at least one cell of each compartment in order to be able to fill the entire future dorsal compartment. This speaks in favor of growth of the *apterous*-expressing area, at least partly, by induction. This is supported by data from the Raeppli flies which shows that *apterous* is induced separately in several cells of the wing disc in the early stages of expression since several clones expressing different combinations of fluorescent proteins exist (see Fig. 42). The Raeppli data also shows that

clones in the notum are larger and oftentimes longitudinal, comparable in shape to the single cell clone in Fig. 44. This could indicate that once all the cells of the notum express *apterous*, the further pattern in the notum is determined solely by cell division. Depending on the exact time point of *apterous* induction, there would be a larger or smaller number of clones of more or less longitudinal shape, under the assumption that the orientation of the cell divisions is given by the longitudinal stresses on the wing disc due to *twist*-expressing cells and/or tracheal growth.

In the hinge and dorsal wing pouch, the pattern of *apterous* expression is also determined by both induction and division. Since the clones are smaller in size, induction may play a role for a longer period of time, compared to the notum. The data shown in Figs. 37 and 39 shows that the area of the *apterous*-expressing region increases faster than the area of the entire wing disc in the second instar. This either means that the dorsal hinge grows faster than the entire wing disc, which indeed it appears to [25], and/or necessitates the induction of *apterous* in further cells. Since the clones in the hinge are smaller and more numerous than the clones in the notum, despite both regions increasing in area by a similar factor, *apterous* must be induced for longer in the hinge. Taking into account a possible decrease in clone size in the direction of the DV boundary, and that Serrate expression is gradually confined to cells near the DV boundary in the early third instar [55], it might be speculated that the induction of *apterous* is linked to the expression of Serrate/dLMO. This would support the idea that the DV boundary is not established as a smooth boundary until the early third instar, in accordance with [34, 36, 58], and might explain why single dorsal cells which did not belong to a clone were occasionally found near the compartment boundary surrounded by clone cells in [40].

McClure et al. published data showing *apterous* expression in about 40 cells in the posterior peripodial membrane [20], which also appears to be recognizable in Figs. 1E and F of [77]. This region at the edge of the wing disc borders on the NW boundary and the wing blade of the disc proper, so that it could be speculated that it arises when the muscle fiber begins to pull on the wing disc, possibly

pulling the posterior disc proper 'up and over' into the peripodial membrane. The pull of the muscle fiber could also play a part in the squamous morphogenesis which takes place in the peripodial membrane around the time of the second molt and leads to the anterior shift in the AP boundary mentioned earlier. This process has been linked to the expression of *hedgehog* and *dpp*, but since both are present prior to squamous morphogenesis, an additional factor must play a part at this time. Ecdysone has been excluded as a direct factor but it is conceivable that, if it plays a role in the contraction of the muscle fiber, it could act as an indirect factor [20].

The data from the Raeppli flies in Fig. 42 questions the idea that cells can cross the NW boundary by changing their fate [62, 81]. Clones do not appear to cross the NW boundary and, under the assumption that a change in cell fate should not lead to a change in the fluorescent proteins a cell is expressing, this indicates that the NW boundary might be some sort of boundary after all. A possibly divergent behavior of *apterous*-expressing cells on either side of the NW boundary is also indicated by the fact that stains for *apterous* lead to areas of different staining intensities, divided by the NW boundary [82]. The possibility that the NW boundary is an actual boundary in the sense of a 'weak' lineage restriction is also supported by the growth trails found for the single cell clones, which tend to remain on one side of the NW boundary from at least the second instar on. Interestingly, experiments with clones that could not receive Dpp, which plays a role in defining the notum by repressing Iro-C expression, showed a normal Iro-C border in the anterior compartment. This indicates that additional factors must play a role in maintaining the NW boundary [66] in the anterior compartment. One of these factors may be mechanical stress (see below).

6.3 Growth Anisotropies

Several results discussed above, as well as published findings, indicate that the wing disc does not only grow inhomogeneously in time, but also in space [11, 84, 85]. In order to quantify how wing disc growth changes as a function of time and location in the wing disc, the development of single cell clones was

observed.

By the time the clones in the wing pouch were well-recognizable in the second instar, they were already longitudinal in shape (see Fig. 43), in agreement with [11, 32, 91], indicating a preferred orientation of cell divisions [11, 87], possibly due to mechanical stresses. In the notum, second instar wing discs also showed longitudinal clones - the disc proper clone in Fig. 44 even appeared to be a line of single cells [87]. These results speak against earlier research which showed that clones induced in the notum early in development were generally more isodiametric [91], with cell divisions showing no preferential orientation [87]. This may be explained by considering that the wing discs assessed were dissected in the later third instar, by which point in time the notum had grown substantially in width (see below), so that clones which might have been longitudinal before the third instar looked more isodiametric.

Upon growing mainly along the proximal-distal axis during most of the second instar, the wing disc begins to grow in a different direction distal of the WN boundary in the late second instar, as was discussed above. Clones which are above or below the WN boundary at this time stay above or below it, respectively, throughout the rest of larval development. In Fig. 43, it appears that, in the second half of the second instar, the dorsal hinge increases in area faster than the entire wing disc. Accordingly, the ratio of notum to wing disc area decreases at this time, as is shown in Fig. 48.

In the third instar, the notum grows at about the same rate as the entire wing disc, whereby a substantial amount of growth appears to take place parallel to the DV boundary at this time, especially in the anterior compartment, as can be seen in Figs. 45, 46 and 30. Beginning in the early third instar, the wing pouch and the ventral hinge begin to grow substantially in area (see Fig. 49), whereby the wing pouch grows in a radial fashion. This is hard to see in Figs. 43 and 49) but can be recognized in Fig. 2D in [113].

6.4 External Stresses

Several different sources of external stress have been seen to act upon the wing disc in certain regions and at distinct times. These are discussed in this section.

Throughout all of larval development the wing disc is attached to a certain part of the second thoracic lateral tracheal branch (see Fig. 50). In this context, it can only be said that the wing disc is permanently attached to the tracheal branch at the knee by fibers, as was shown in Fig. 55B, and is likely also permanently attached to the trachea by *twist*-expressing cells at its proximal end (see Fig. 51). The rest of the tracheal branch appears to be in permanent contact with the wing disc, but considering how its relative position in respect to the wing disc changes from the outer posterior compartment to the mid-anterior during development, this attachment appears to be of a more transient nature.

In the first and second instars, the wing imaginal disc is stretched along the proximal-distal axis, probably by a combination of tracheal growth and being stretched by the *twist*-expressing cells. This is underlined by the oval shape of the wing disc and the apical cell outlines at this time, as well as by the fact that early wing discs become round upon dissection (see Fig. 52). These external stresses may lead to cell divisions which are oriented along the proximal-distal axis, which would explain the longitudinal shapes of clones at this time.

One, or more, fibers anchor the wing disc to parts of the cuticle, as was shown in Fig. 53, spanning it. Around the time of the second molt, a muscle fiber which attaches the wing disc to the leg and haltere discs [99], begins to exert a visible pulling force in a direction roughly perpendicular to the tracheal branch the wing disc is attached to (see Fig. 54). The fact that this muscle fiber, which was not observed during the first instar, becomes noticeable in the second instar may be due to leg disc growth, which may change the position of the fiber in the larva, whereby the growth of the leg disc itself might be due to the contraction of the muscle fiber. The contraction of this muscle fiber can be observed in and ex vivo and may play a role in the change in direction of wing disc growth at this time

and in the, possibly consequential, formation of the kink in the *engrailed* expression pattern. It should be mentioned that the in-vivo imaging process necessarily looks at the larva at its most stretched out. During normal larval development, the contraction of the muscle fiber is most likely superimposed by the crawling and feeding motions of the larva.

Mini threads have also been observed to pull on the wing disc, although the role they play is not clear. The pulling forces they exert only appear to affect single cells. It is conceivable that they might help to span the wing disc and may even play a role in the induction of *apterous*.

6.5 Summary

In this summary the experimental results, which were discussed separately above, will be brought together in an attempt to give a unified picture of wing disc development. The figures are only intended to clarify the general ideas and are thus merely sketches and not to scale.

A sketch of a first instar wing disc (light gray), including the trachea (thick black lines) it is attached to, is shown in Fig. 62. In this, as well as the following images, the posterior compartment is shown in yellow and the WN boundary represented by a dashed gray line. External mechanical stresses are indicated by red arrows, points at which the wing disc is fixed to the trachea are indicated by red crosses.

In the first larval instar, the wing disc grows only due to an increase in cell volume. At this time, the apical wing disc is an ellipsoid, likely due to being stretched along the proximal-distal axis by a combination of tracheal growth and a pulling force exerted by *twist*-expressing cells (red arrow) at the proximal end of the wing disc. This stretching can also be seen in oval apical cell outlines. The *engrailed* pattern is smooth, *apterous* may be expressed in single cells near the time of the first molt (see below).

After the first molt, cells begin to divide exponentially and the average apical

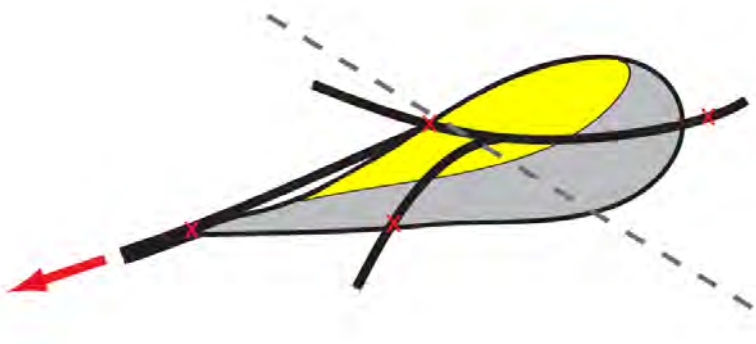

Figure 62: Illustration of a first instar wing disc connected to trachea. External stresses are indicated by the red arrows, fixpoints by the red crosses. The posterior compartment is yellow. The dashed gray line indicates the WN boundary.

cell area decreases, while the variance in apical cell areas increases, possibly as a consequence of the mitoses - these may also be induced by the ecdysone pulse in late first instar [115]. Growth appears to be oriented mainly along the proximal-distal axis, yet divided by the NW boundary, possibly due to cell divisions oriented by the external stresses of tracheal growth and *twist*-expressing cells. The inhomogeneous distribution of stress might also be a reason why the variance in apical cell areas become larger in the second instar.

Apterous is induced in single cells when the wing disc has reached a certain size, independent of the instar the larva is in. First expression is oftentimes found in a characteristic region and possibly due to mechanical stress. *Apterous* expression is illustrated in blue in Fig. 63; the dotted line indicates a fiber connecting the wing disc to the cuticle while the outgrowth in the lower right-hand corner is the muscle fiber. Thereupon, *apterous* expression is induced in all the cells of the notum, as well as in some hinge cells. The wing disc hence grows through cell proliferation, especially in the hinge, possibly due to a combination of stresses and the expression of *dpp* (orange line in Fig. 63) in this area. At the same time, *apterous* may be continuously induced at the border between the dorsal and ventral cells. Also around this time, the wing disc becomes flatter, possibly in connection with the formation of the peripodial membrane.

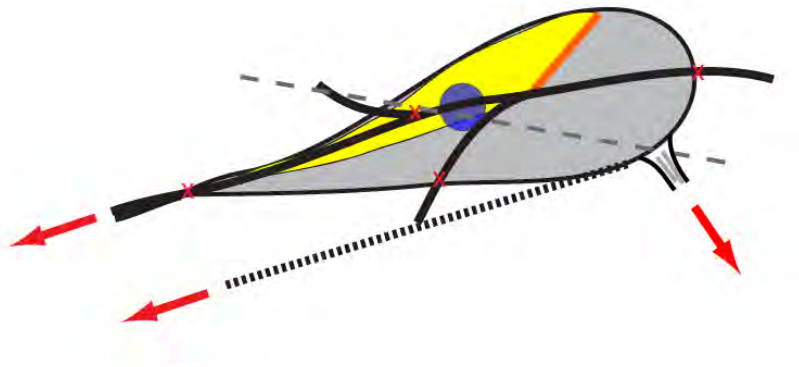

Figure 63: Illustration of a second instar wing disc and trachea. *Apterous* expression is shown in blue, *dpp* in orange.

The muscle fiber, which connects the wing disc to the leg and haltere discs, visibly begins to stretch the disc around the time of the second molt. The angle at which it pulls on the wing disc changes over time, possibly due to leg disc growth. The muscle fiber thus appears to tip the distal region of the wing disc away from the trachea, although this change in shape may also be a consequence of the location of the stripe of *dpp* expression. One, or both, of these factors likely lead to the kink in the *engrailed* expression pattern.

At this time, the dorsal hinge is significantly larger in area than either the ventral hinge or the wing pouch. This could indicate higher growth rates in this region, where stresses and the growth factor Dpp both have positive effects in the second instar, as opposed to the notum, where Dpp is lacking, and the ventral wing pouch, which appears to lack stresses [66]. The pattern of the strain ellipses may help to explain the boundary qualities of the NW boundary, under the assumption that cell divisions are oriented in the direction of stress, which basically radiates out from the attachment point of the muscle fiber, as can be seen in Figs. 45 and 46. In the third instar, the anterior region of the notum appears to grow in width more than the posterior compartment (see Fig. 30). Although the anterior notum does show more stress in the early third instar, as expected considering the positions of the attachment points of the *twist*-expressing cells and the muscle fiber, the development of the clone in Fig. 44, as well as the general growth of the notum, argue for spatially uniform growth during most of the third instar so that a

role for external forces at this time is probably negligible.

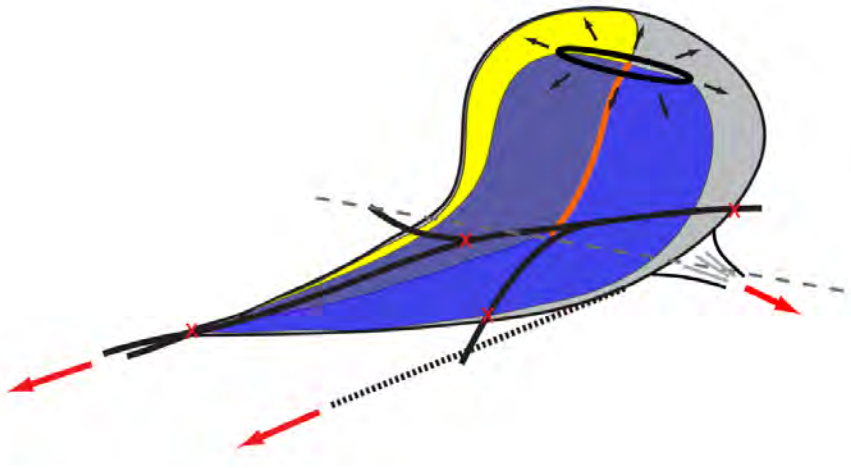

Figure 64: Illustration of a early third instar wing disc and trachea. The black oval indicates the wing pouch.

Once *apterous* is expressed by about 60% of the cells, at the beginning of the third instar, the wing pouch and ventral compartments begin to increase in area. It can be speculated that signaling at the DV boundary begins at this point and the radial growth of the wing pouch shown in Fig. 64 is thus linked to the expression of *wingless* and *vestigial* [116]. As the wing pouch grows, compression begins to build up in the center of the wing disc [6, 97]. From this point on, growth regulation by internal mechanical forces plays an ever larger role, while the effects of external mechanical forces become smaller. The effects of internal mechanical forces also become visible in the distribution of average apical cell areas. Growth regulation leads cells to become more similar in size and, preferably, hexagonal [103], in the interest of densest packing.

Compression in the wing disc might also lead to the formation of the characteristic folds shown in Fig. 65, as the tissue buckles to relieve stress. It may be speculated that the muscle fiber plays a part in generating the fold at the NW boundary, while preventing folds from forming in the notum.

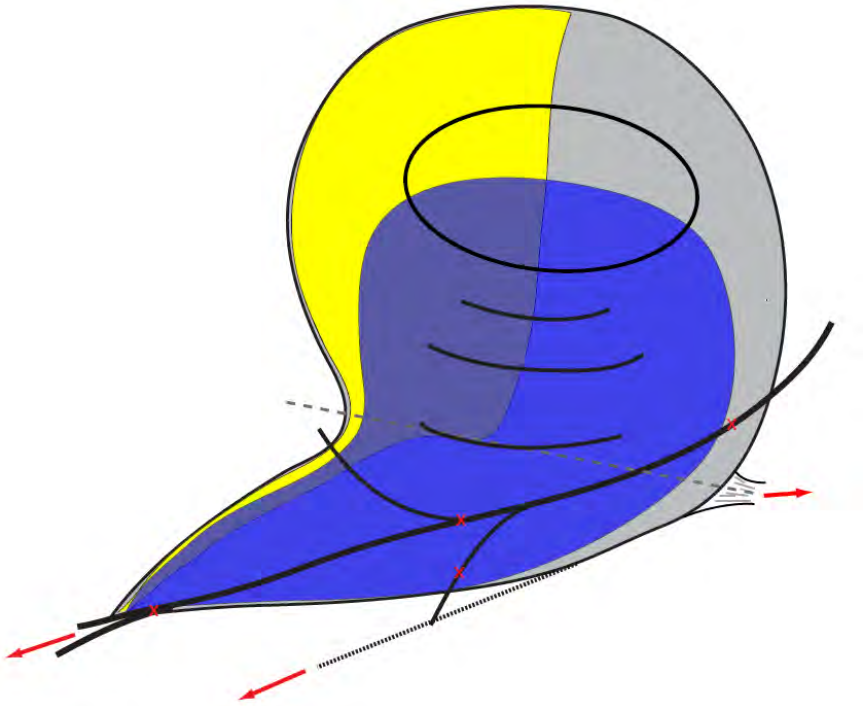

Figure 65: Illustration of a late third instar wing disc and trachea.

In summary, a case can be made for a role for external mechanical forces in wing disc growth and patterning, yet it is as of now difficult to say whether there is actually a causal relationship. The attachment point of the muscle fiber appears to introduce a certain asymmetry to the wing disc, and yet it is also possible that the asymmetry is inherent to the wing disc and the muscle fiber forms at the future NW boundary. In order to substantiate some of the research presented here, further work needs to be done. A short list of possible experiments is given in the following, final chapter.

7 Outlook

The research presented in this thesis leaves some loose ends. Several of the conclusions drawn need to be confirmed by further experiments, some of which are listed in the following.

- Above all, it would be intriguing to be able to remove or cut the muscle fiber during early development, for example by using laser ablation or gene manipulation, in order to assess how this affects the further development of the wing disc. Although this has been attempted manually, the larva in question did not develop normally. The wing disc did appear to grow slightly along trachea in a usually not observed way, supporting some of the ideas above, but also indicating that the muscle fiber may play such a fundamental role that removing it inhibits further larval development.

  In this context, it would also be interesting to study whether the contraction of the muscle fiber is (inter-)connected with:

  - ecdysone levels (which peak in the middle of the second instar [115] and appear to be essential for survival [117] at this time)
  - the expression of *dpp* and the columnarization of disc proper cells
  - the development of the peripodial membrane
  - larval movement
  - the level of *twist* expressed, in analogy to [96]

  It may be possible to do similar experiments using *Musca domestica* larvae, which are significantly larger, making manual manipulation of the muscle fiber, if it exists, easier.

- Additional single cell clone wing discs need to be imaged to verify the data shown, especially regarding the asymmetry in growth at the WN boundary. It would also be good to better quantify the growth rates in the different regions of the wing disc by imaging wing discs, in which these are labeled fluorescently, in-vivo.

- The Raeppli larvae should be imaged in-vivo, once the instruments available allow it, in order to follow the development of the dorsal compartment as a function of time and region in the wing disc. The results attained might illuminate some of the ideas proposed in the discussion section.
- The experiments which led to an increase in fluorescence upon stretching ought to be repeated in a culture medium [118].
- The role of the peripodial membrane, which was largely ignored in this work, could also be studied. It is conceivable that it plays a role in stabilizing the form of the wing disc.
- Bate et al. [98] described persistent *twist*-expressing cells, which are muscle precursor cells. These may be identical to the *twist*-expressing cells and muscle fiber described here. It might be interesting to take a closer look at the possible connections between these cells, *apterous* expression and the formation of the direct and indirect flight muscles [119].

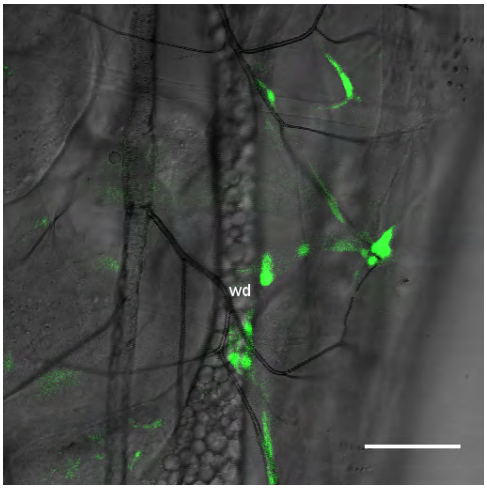

Figure 66: *Twist*-expressing cells connect the wing disc to the cuticle and possibly to the leg and haltere discs. The scale bar is 50 µm.

Bibliography

[1] A. García-Bellido, "Genetic control of wing disc development in Drosophila," *Ciba Found Symp.*, vol. 0, pp. 161–182, 1975.

[2] G. Morata and P. Ripoll, "Minutes: Mutants of Drosophila autonomously affecting cell division rate," *Developmental Biology*, vol. 42, no. 2, pp. 211 – 221, 1975.

[3] D. P. Kiehart, C. G. Galbraith, K. A. Edwards, W. L. Rickoll, and R. A. Montaguea, "Multiple forces contribute to cell sheet morphogenesis for dorsal closure in Drosophila," *J Cell Biol.*, vol. 149, pp. 471–490, 2000.

[4] E. Williams-Masson, A. Malik, and J. Hardin, "An actin-mediated two-step mechanism is required for ventral enclosure of the C. elegans hypodermis," *Development*, vol. 124, pp. 2889–2901, Aug. 1997.

[5] M. Köppen, B. G. Fernández, L. Carvalho, A. Jacinto, and C.-P. Heisenberg, "Coordinated cell-shape changes control epithelial movement in zebrafish and Drosophila," *Development*, vol. 133, pp. 2671–2681, July 2006.

[6] T. Aegerter-Wilmsen, C. M. Aegerter, E. Hafen, and K. Basler, "Model for the regulation of size in the wing imaginal disc of Drosophila," *Mechanisms of Development*, vol. 124, no. 4, pp. 318 – 326, 2007.

[7] L. Hufnagel, A. A. Teleman, H. Rouault, S. M. Cohen, and B. I. Shraiman, "On the mechanism of wing size determination in fly development," *Proceedings of the National Academy of Sciences*, vol. 104, no. 10, pp. 3835–3840, 2007.

[8] U. Nienhaus, T. Aegerter-Wilmsen, and C. M. Aegerter, "Determination of mechanical stress distribution in Drosophila wing discs using photoelasticity," *Mechanisms of Development*, vol. 126, pp. 942 – 949, 2009.

[9] T. Schluck, U. Nienhaus, T. Aegerter-Wilmsen, and C. M. Aegerter, "Mechanical control of organ size in the development of the Drosophila wing disc." PLOS ONE, in press.

[10] L. Wolpert, R. Beddington, T. Jessel, P. Lawrence, E. Meyerowitz, and J. Smith, *Principles of Development*. Oxford University Press, 2002.

[11] P. J. Bryant, "Cell lineage relationships in the imaginal wing disc of Drosophila melanogaster," *Developmental Biology*, vol. 22, no. 3, pp. 389 – 411, 1970.

[12] "http://www.pearsonhighered.com/mathews/ch28/fi28p45.htm," (25.09.2013).

[13] P. J. Bryant and P. Levinson, "Intrinsic growth control in the imaginal primordia of Drosophila, and the autonomous action of a lethal mutation causing overgrowth," *Developmental Biology*, vol. 107, no. 2, pp. 355 – 363, 1985.

[14] M. J. Butler, T. L. Jacobsen, D. M. Cain, M. G. Jarman, M. Hubank, J. R. S. Whittle, R. Phillips, and A. Simcox, "Discovery of genes with highly restricted expression patterns in the," *Development*, vol. 130, pp. 659–670, Feb. 2003.

[15] M. Bate and A. Arias, "The embryonic origin of imaginal discs in Drosophila," *Development*, vol. 112, pp. 755–761, July 1991.

[16] M. Mandaravally Madhavan and H. A. Schneiderman, "Histological analysis of the dynamics of growth of imaginal discs and histoblast nests during the larval development of *Drosophila melanogaster*," *Development Genes and Evolution*, vol. 183, pp. 269–305, 1977. 10.1007/BF00848459.

[17] J. Zeitlinger and D. Bohmann, "Thorax closure in Drosophila: involvement of Fos and the JNK pathway," *Development*, vol. 126, pp. 3947–3956, Sept. 1999.

[18] T. J. Widmann and C. Dahmann, "Dpp signaling promotes the cuboidal-to-columnar shape transition of Drosophila wing disc epithelia by regulating Rho1," *Journal of Cell Science*, vol. 122, pp. 1362–1373, May 2009.

[19] S. K. Pallavi and L. S. Shashidhara, "Egfr/Ras pathway mediates interactions between peripodial and disc proper cells in Drosophila wing discs," *Development*, vol. 130, pp. 4931–4941, Oct. 2003.

[20] K. D. McClure and G. Schubiger, "Developmental analysis and squamous morphogenesis of the peripodial epithelium in Drosophila imaginal discs," *Development*, vol. 132, pp. 5033–5042, Nov. 2005.

[21] F. A. Martín, S. C. Herrera, and G. Morata, "Cell competition, growth and size control in the Drosophila wing imaginal disc," *Development*, vol. 136, pp. 3747–3756, Nov. 2009.

[22] T. P. Neufeld, A. F. A. de la Cruz, L. A. Johnston, and B. A. Edgar, "Coordination of growth and cell division in the Drosophila wing," *Cell*, vol. 93, no. 7, pp. 1183 – 1193, 1998.

[23] P. Lawrence and G. Morata, "Compartments in the wing of Drosophila: A study of the engrailed gene," *Developmental Biology*, vol. 50, no. 2, pp. 321 – 337, 1976.

[24] D. A. O'Brochta and P. J. Bryant, "A zone of non-proliferating cells at a lineage restriction boundary in Drosophila," *Nature*, vol. 313, pp. 138–141, Jan. 1985.

[25] L. Johnston and A. Sanders, "Wingless promotes cell survival but constrains growth during Drosophila wing development," *Nature Cell Biology*, vol. 5, pp. 827–833, 2003.

[26] L. A. Johnston and B. A. Edgar, "Wingless and Notch regulate cell-cycle arrest in the developing Drosophila wing," *Nature*, vol. 394, pp. 82–84, July 1998.

[27] P. A. Lawrence and G. Struhl, "Morphogens, compartments, and pattern: Lessons from Drosophila?," *Cell*, vol. 85, no. 7, pp. 951 – 961, 1996.

[28] J. T. Patterson, "The production of mutations in somatic cells of Drosophila melanogaster by means of x-rays," *Journal of Experimental Zoology*, vol. 53, no. 3, pp. 327–372, 1929.

[29] J. Patterson, "Somatic segregation produced by x-rays in Drosophila melanogaster," *Proc Natl Acad Sci U S A*, vol. 16, pp. 109–111, 1930.

[30] C. Stern, "Somatic crossing over and segregation in Drosophila melanogaster," *Genetics*, vol. 21, pp. 625–730, Nov. 1936.

[31] F. Crick and P. Lawrence, "Compartments and polyclones in insect development," *Science*, vol. 189, pp. 340–347, Aug. 1975.

[32] A. Garcia-Bellido and J. Merriam, "Parameters of the wing imaginal disc development of Drosophila melanogaster," *Developmental Biology*, vol. 24, no. 1, pp. 61 – 87, 1971.

[33] A. Garcia-Bellido, P. Ripoll, and G. Morata, "Developmental compartmentalisation of the wing disk of Drosophila," *Nature New Biology*, vol. 245, pp. 251–253, 1973.

[34] D. Brower, "The sequential compartmentalization of Drosophila segments revisited," *Cell*, vol. 41, pp. 361–364, 1985.

[35] J. Szabad, P. Simpson, and R. Nöthiger, "Regeneration and compartments in Drosophila," *Journal of Embryology and Experimental Morphology*, vol. 49, pp. 229–241, Jan. 1979.

[36] A. Garcia-Bellido, P. Ripoll, and G. Morata, "Developmental compartmentalization in the dorsal mesothoracic disc of Drosophila," *Developmental Biology*, vol. 48, no. 1, pp. 132 – 147, 1976.

[37] G. Morata and P. A. Lawrence, "Control of compartment development by the engrailed gene in Drosophila," *Nature*, vol. 255, pp. 614–617, June 1975.

[38] D. Brower, P. Lawrence, and M. Wilcox, "Clonal analysis of the undifferentiated wing disk of Drosophila," *Developmental Biology*, vol. 86, no. 2, pp. 448 – 455, 1981.

[39] P. J. Bryant, "Pattern formation in the imaginal wing disc of Drosophila melanogaster: Fate map, regeneration and duplication," *Journal of Experimental Zoology*, vol. 193, no. 1, pp. 49–77, 1975.

[40] F. J. Diaz-Benjumea and S. M. Cohen, "Interaction between dorsal and ventral cells in the imaginal disc directs wing development in Drosophila," *Cell*, vol. 75, no. 4, pp. 741 – 752, 1993.

[41] P. A. Lawrence, "A general cell marker for clonal analysis of Drosophila development," *Journal of Embryology and Experimental Morphology*, vol. 64, pp. 321–332, Aug. 1981.

[42] D. L. Brower, R. J. Smith, and M. Wilcox, "A monoclonal antibody specific for diploid epithelial cells in Drosophila," *Nature*, vol. 285, pp. 403–405, June 1980.

[43] M. Chalfie, Y. Tu, G. Euskirchen, W. Ward, and D. Prasher, "Green fluorescent protein as a marker for gene expression," *Science*, vol. 263, pp. 802–805, Feb. 1994.

[44] B. Cohen, E. A. Wimmer, and S. M. Cohen, "Early development of leg and wing primordia in the Drosophila embryo," *Mechanisms of Development*, vol. 33, no. 3, pp. 229 – 240, 1991.

[45] P. A. Lawrence and G. Morata, "The early development of mesothoracic compartments in Drosophila: An analysis of cell lineage and fate mapping and an assessment of methods," *Developmental Biology*, vol. 56, pp. 40–51, Mar. 1977.

[46] D. Brower, "Ultrabithorax gene expression in Drosophila imaginal discs and larval nervous system," *Development*, vol. 101, pp. 83–92, Sept. 1987.

[47] "http://www.mun.ca/biology/desmid/brian/biol3530/db_02/fig2_28.jpg," (25.09.2013).

[48] C. Dahmann and K. Basler, "Compartment boundaries: at the edge of development," *Trends in Genetics*, vol. 15, no. 8, pp. 320 – 326, 1999.

[49] R. Burke and K. Basler, "Dpp receptors are autonomously required for cell proliferation in the entire developing Drosophila wing," *Development*, vol. 122, pp. 2261–2269, July 1996.

[50] D. Nellen, R. Burke, G. Struhl, and K. Basler, "Direct and long-range action of a DPP morphogen gradient," *Cell*, vol. 85, no. 3, pp. 357 – 368, 1996.

[51] M. Zecca, K. Basler, and G. Struhl, "Sequential organizing activities of engrailed, hedgehog and decapentaplegic in the Drosophila wing," *Development*, vol. 121, pp. 2265–2278, 1995.

[52] S. Blair, D. Brower, J. Thomas, and M. Zavortink, "The role of apterous in the control of dorsoventral compartmentalization and PS integrin gene expression in the developing wing of Drosophila," *Development*, vol. 120, pp. 1805–1815, July 1994.

[53] J. Williams, S. Paddock, and S. Carroll, "Pattern formation in a secondary field: a hierarchy of regulatory genes subdivides the developing Drosophila wing disc into discrete subregions," *Development*, vol. 117, pp. 571–584, Feb. 1993.

[54] L. Paul, S. Wang, S. Manivannan, L. Bonanno, S. Lewis, C. Austin, and A. Simcox, "Dpp-induced Egfr signaling triggers postembryonic wing development in Drosophila," *Proc Natl Acad Sci U S A*, vol. 110, pp. 5058–5063, 2013.

[55] M. Milan and S. Cohen, "Temporal regulation of apterous activity during development of the Drosophila wing," *Development*, vol. 127, pp. 3069–3078, 2000.

[56] M. Wilcox, A. DiAntonio, and M. Leptin, "The function of PS integrins in Drosophila wing morphogenesis," *Development*, vol. 107, pp. 891–897, Dec. 1989.

[57] E. Steiner, "Establishment of compartments in the developing leg imaginal discs of Drosophila melanogaster," *Wilhelm Roux's Archives*, vol. 180, no. 1, pp. 9–30, 1976.

[58] G. Morata and P. A. Lawrence, "Development of the eye-antenna imaginal disc of Drosophila," *Developmental Biology*, vol. 70, no. 2, pp. 355 – 371, 1979.

[59] M. Aliee, J.-C. Röper, K. Landsberg, C. Pentzold, T. J. Widmann, F. Jülicher, and C. Dahmann, "Physical mechanisms shaping the Drosophila dorsoventral compartment boundary," *Current Biology*, vol. 22, no. 11, pp. 967 – 976, 2012.

[60] U. Nienhaus, T. Aegerter-Wilmsen, and C. M. Aegerter, "In-vivo imaging of the Drosophila wing imaginal disc over time: Novel insights on growth and boundary formation," *PLoS ONE*, vol. 7, p. e47594, 10 2012.

[61] S.-H. Wang, A. Simcox, and G. Campbell, "Dual role for Drosophila epidermal growth factor receptor signaling in early wing disc development," *Genes & Development*, vol. 14, no. 18, pp. 2271–2276, 2000.

[62] M. Zecca and G. Struhl, "Subdivision of the Drosophila wing imaginal disc by EGFR-mediated signaling," *Development*, vol. 129, no. 6, pp. 1357–1368, 2002.

[63] M. Zecca and G. Struhl, "Control of growth and patterning of the Drosophila wing imaginal disc by EGFR-mediated signaling," *Development*, vol. 129, no. 6, pp. 1369–1376, 2002.

[64] J. Couso, M. Bate, and A. Martinez-Arias, "A wingless-dependent polar coordinate system in Drosophila imaginal discs," *Science*, vol. 259, pp. 484–489, Jan. 1993.

[65] M. Ng, F. J. Diaz-Benjumea, J.-P. Vincent, J. Wu, and S. M. Cohen, "Specification of the wing by localized expression of wingless protein," *Nature*, vol. 381, pp. 316–318, May 1996.

[66] F. Cavodeassi, I. Rodríguez, and J. Modolell, "Dpp signalling is a key effector of the wing-body wall subdivision of the Drosophila mesothorax," *Development*, vol. 129, pp. 3815–3823, Aug. 2002.

[67] A. Baonza, F. Roch, and E. Martín-Blanco, "DER signaling restricts the boundaries of the wing field during Drosophila development," *Proceedings of the National Academy of Sciences*, vol. 97, pp. 7331–7335, June 2000.

[68] K. D. Irvine and E. Wieschaus, "fringe, a boundary-specific signaling molecule, mediates interactions between dorsal and ventral cells during Drosophila wing development," *Cell*, vol. 79, no. 4, pp. 595 – 606, 1994.

[69] S. Speicher, U. Thomas, U. Hinz, and E. Knust, "The Serrate locus of Drosophila and its role in morphogenesis of the wing imaginal discs: control of cell proliferation," *Development*, vol. 120, pp. 535–544, Mar. 1994.

[70] J. Kim, K. D. Irvine, and S. B. Carroll, "Cell recognition, signal induction, and symmetrical gene activation at the dorsal-ventral boundary of the developing drosophila wing," *Cell*, vol. 82, no. 5, pp. 795 – 802, 1995.

[71] I. Rebay, R. J. Fleming, R. G. Fehon, L. Cherbas, P. Cherbas, and S. Artavanis-Tsakonas, "Specific EGF repeats of Notch mediate interactions with Delta and serrate: Implications for notch as a multifunctional receptor," *Cell*, vol. 67, no. 4, pp. 687 – 699, 1991.

[72] J. de Celis, A. Garcia-Bellido, and S. Bray, "Activation and function of Notch at the dorsal-ventral boundary of the wing imaginal disc," *Development*, vol. 122, pp. 359–369, Jan. 1996.

[73] D. Doherty, G. Feger, S. Younger-Shepherd, L. Y. Jan, and Y. N. Jan, "Delta is a ventral to dorsal signal complementary to Serrate, another Notch ligand, in Drosophila wing formation.," *Genes & Development*, vol. 10, pp. 421–434, Feb. 1996.

[74] V. M. Panin, V. Papayannopoulos, R. Wilson, and K. D. Irvine, "Fringe modulates Notch-ligand interactions," *Nature*, vol. 387, pp. 908–912, June 1997.

[75] J. Celis de and S. Bray, "Feed-back mechanisms affecting Notch activation at the dorsoventral boundary in the Drosophila wing," *Development*, vol. 124, pp. 3241–3251, Sept. 1997.

[76] M. Milán and S. M. Cohen, "A re-evaluation of the contributions of Apterous and Notch to the dorsoventral lineage restriction boundary in the Drosophila wing," *Development*, vol. 130, pp. 553–562, Feb. 2003.

[77] M. Milán, F. J. Diaz-Benjumea, and S. M. Cohen, "Beadex encodes an LMO protein that regulates Apterous LIM-homeodomain activity in Drosophila wing development: a model for LMO oncogene function," *Genes Dev.*, vol. 12, pp. 2912–2920, 1998.

[78] F. Diaz-Benjumea and S. Cohen, "Serrate signals through Notch to establish a Wingless-dependent organizer at the dorsal/ventral compartment boundary of the Drosophila wing," *Development*, vol. 121, pp. 4215–4225, Dec. 1995.

[79] M. Zecca and G. Struhl, "Control of Drosophila wing growth by the vestigial quadrant enhancer," *Development*, vol. 134, pp. 3011–3020, Aug. 2007.

[80] E. Villa-Cuesta and J. Modolell, "Mutual repression between msh and Iro-c is an essential component of the boundary between body wall and wing in drosophila," *Development*, vol. 132, pp. 4087–4096, Sept. 2005.

[81] R. D. del Corral, P. Aroca, J. L. G mez Skarmeta, F. Cavodeassi, and J. Modolell, "The Iroquois homeodomain proteins are required to specify body wall identity in Drosophila," *Genes & Development*, vol. 13, pp. 1754–1761, July 1999.

[82] B. Cohen, M. E. McGuffin, C. Pfeifle, D. Segal, and S. M. Cohen, "apterous, a gene required for imaginal disc development in Drosophila encodes a member of the LIM family of developmental regulatory proteins.," *Genes & Development*, vol. 6, pp. 715–729, May 1992.

[83] P. Fernandez-Funez, C.-H. Lu, D. E. Rincon-Limas, A. Garcia-Bellido, and J. Botas, "The relative expression amounts of apterous and its cofactor dldb/Chip are critical for dorso-ventral compartmentalization in the Drosophila wing," *EMBO J*, vol. 17, pp. 6846–6853, Dec. 1998.

[84] T. Bittig, O. Wartlick, M. González-Gaitán, and F. Jülicher, "Quantification of growth asymmetries in developing epithelia," *The European Physical Journal E: Soft Matter and Biological Physics*, vol. 30, pp. 93–99, 2009.

[85] D. L. Brower, R. J. Smith, and M. Wilcox, "Cell shapes on the surface of the Drosophila wing imaginal disc," *Journal of Embryology and Experimental Morphology*, vol. 67, pp. 137–151, Feb. 1982.

[86] T. Lecuit and L. Le Goff, "Orchestrating size and shape during morphogenesis," *Nature*, vol. 450, pp. 189–192, Nov. 2007.

[87] L. A. Baena-López, A. Baonza, and A. García-Bellido, "The orientation of cell divisions determines the shape of Drosophila organs," *Current Biology*, vol. 15, no. 18, pp. 1640 – 1644, 2005.

[88] S. M. da Silva and J.-P. Vincent, "Oriented cell divisions in the extending germband of Drosophila," *Development*, vol. 134, pp. 3049–3054, Sept. 2007.

[89] Y. Gong, C. Mo, and S. E. Fraser, "Planar cell polarity signalling controls cell division orientation during zebrafish gastrulation," *Nature*, vol. 430, pp. 689–693, Aug. 2004.

[90] I. Castanon and M. González-Gaitán, "Oriented cell division in vertebrate embryogenesis," *Current Opinion in Cell Biology*, vol. 23, no. 6, pp. 697 – 704, 2011.

[91] J. Resino, P. Salama-Cohen, and A. García-Bellido, "Determining the role of patterned cell proliferation in the shape and size of the Drosophila wing," *Proc Natl Acad Sci U S A*, vol. 99, pp. 7502–7507, 2002.

[92] Y. Mao, A. L. Tournier, P. A. Bates, J. E. Gale, N. Tapon, and B. J. Thompson, "Planar polarization of the atypical myosin Dachs orients cell divisions in Drosophila," *Genes & Development*, vol. 25, pp. 131–136, Jan. 2011.

[93] M. Rauzi and T. Lecuit, "Closing in on mechanisms of tissue morphogenesis," *Cell*, vol. 137, no. 7, pp. 1183 – 1185, 2009.

[94] S. Woolner and P. Martin, "Embryo morphogenesis and the role of the actin cytoskeleton," in *Aspects of the Cytoskeleton* (E. E. Bittar and S. Khurana, eds.), vol. 37 of *Advances in Molecular and Cell Biology*, pp. 251 – 283, Elsevier, 2006.

[95] B. I. Shraiman, "Mechanical feedback as a possible regulator of tissue growth," *Proceedings of the National Academy of Sciences of the United States of America*, vol. 102, no. 9, pp. 3318–3323, 2005.

[96] E. Farge, "Mechanical induction of twist in the Drosophila foregut/stomodeal primordium," *Current Biology*, vol. 13, no. 16, pp. 1365 – 1377, 2003.

[97] T. Aegerter-Wilmsen, M. B. Heimlicher, A. C. Smith, P. B. de Reuille, R. S. Smith, C. M. Aegerter, and K. Basler, "Integrating force-sensing and signaling pathways in a model for the regulation of wing imaginal disc size," *Development*, vol. 139, pp. 3221–3231, Sept. 2012.

[98] M. Bate, E. Rushton, and D. Currie, "Cells with persistent twist expression are the embryonic precursors of adult muscles in Drosophila," *Development*, vol. 113, pp. 79–89, 1991.

[99] C. Dambly-Chaudière, A. Ghysen, Y. Jan, and L. Jan, "Muscle connections between imaginal discs in Drosophila," *Developmental Biology*, vol. 113, no. 2, pp. 288 – 294, 1986.

[100] M. Minsky, "Microscopy apparatus," 1961.

[101] F. Hamaratoglu, A. M. de Lachapelle, G. Pyrowolakis, S. Bergmann, and M. Affolter, "Dpp signaling activity requires pentagone to scale with tissue size in the growing *Drosophila* wing imaginal disc," *PLoS Biol*, vol. 9, p. e1001182, 10 2011.

[102] S. Aldaz, L. M. Escudero, and M. Freeman, "Live imaging of Drosophila imaginal disc development," *Proceedings of the National Academy of Sciences*, vol. 107, pp. 14217–14222, Aug. 2010.

[103] M. C. Gibson, A. B. Patel, R. Nagpal, and N. Perrimon, "The emergence of geometric order in proliferating metazoan epithelia," *Nature*, vol. 442, pp. 1038–1041, Aug. 2006.

[104] J. B. Duffy, "GAL4 system in drosophila: A fly geneticist's swiss army knife," *genesis*, vol. 34, no. 1-2, pp. 1–15, 2002.

[105] A. Brand and N. Perrimon, "Targeted gene expression as a means of altering cell fates and generating dominant phenotypes," *Development*, vol. 118, pp. 401–415, June 1993.

[106] H. Oda and S. Tsukita, "Real-time imaging of cell-cell adherens junctions reveals that Drosophila mesoderm invagination begins with two phases of apical constriction of cells," *Journal of Cell Science*, vol. 114, pp. 493–501, Feb. 2001.

[107] R. Lattao, S. Bonaccorsi, X. Guan, S. Wasserman, and M. Gatti, "Tubby-tagged balancers for the Drosophila x and second chromosomes," *Fly (Austin)*, vol. 5, pp. 369–70, 2011.

[108] K. Shim, K. J. Blake, J. Jack, and M. A. Krasnow, "The Drosophila ribbon gene encodes a nuclear BTB domain protein that promotes epithelial migration and morphogenesis," *Development*, vol. 128, pp. 4923–4933, Dec. 2001.

[109] P. Thevenaz, U. E. Ruttimann, and M. Unser, "A pyramid approach to subpixel registration based on intensity," *Image Processing, IEEE Transactions on*, vol. 7, no. 1, pp. 27–41, 1998.

[110] R. Farhadifar, J.-C. Röper, B. Aigouy, S. Eaton, and F. Jülicher, "The influence of cell mechanics, cell-cell interactions, and proliferation on epithelial packing," *Current Biology*, vol. 17, no. 24, pp. 2095 – 2104, 2007.

[111] M. Asipauskas, M. Aubouy, J. A. Glazier, F. Graner, and Y. Jiang, "A texture tensor to quantify deformations: the example of two-dimensional flowing foams," *Granular Matter*, vol. 5, no. 2, pp. 71–74, 2003.

[112] M. Tuceryan and A. K. Jain, *The Handbook of Pattern Recognition and Computer Vision (2nd Edition), by C. H. Chen, L. F. Pau, P. S. P. Wang (eds.)*. World Scientific Publishing Co., 1998.

[113] M. I. Worley, L. Setiawan, and I. K. Hariharan, "TIE-DYE: a combinatorial marking system to visualize and genetically manipulate clones during development in Drosophila melanogaster," *Development*, vol. 140, pp. 3275–3284, June 2013.

[114] S. Ishihara and K. Sugimura, "Bayesian inference of force dynamics during morphogenesis," *Journal of Theoretical Biology*, vol. 313, pp. 201–211, Nov. 2012.

[115] C. S. Thummel, "Molecular mechanisms of developmental timing in C. elegans and Drosophila," *Developmental Cell*, vol. 1, no. 4, pp. 453 – 465, 2001.

[116] J. Couso, E. Knust, and A. M. Arias, "Serrate and wingless cooperate to induce vestigial gene expression and wing formation in Drosophila," *Current Biology*, vol. 5, no. 12, pp. 1437 – 1448, 1995.

[117] A. Garen, L. Kauvar, and J.-A. Lepesant, "Roles of ecdysone in Drosophila development," *Proceedings of the National Academy of Sciences*, vol. 74, pp. 5099–5103, Nov. 1977.

[118] J. Zartman, S. Restrepo, and K. Basler, "A high-throughput template for optimizing Drosophila organ culture with response-surface methods," *Development*, vol. 140, pp. 667–674, Feb. 2013.

[119] A. Ghazi, S. Anant, and K. Vijay Raghavan, "Apterous mediates development of direct flight muscles autonomously and indirect flight muscles through epidermal cues," *Development*, vol. 127, pp. 5309–5318, Dec. 2000.